Characterization of electrically insulating coatings for soft magnetic composite materials by means of surface sensitive analytical techniques

by

DIMITRIS NIKAS

Diploma work No. 114/2013
Department of Materials and Manufacturing Technology
CHALMERS UNIVERSITY OF TECHNOLOGY
Gothenburg, Sweden

Diploma work in the Master programme Materials Engineering

Performed at: Department of Materials and Manufacturing Technology
Chalmers University of Technology
SE-412 96 Gothenburg

Supervisor(s): **MSc.** Christos Oikonomou
Department of Materials and Manufacturing Technology
Chalmers University of Technology
SE-412 96 Gothenburg

Examiner: **Professor** Lars Nyborg
Department of Materials and Manufacturing Technology
Chalmers University of Technology,
SE - 412 96 Gothenburg

DIMITRIS NIKAS

© DIMITRIS NIKAS

Diploma work no 114/2013
Department of Materials and Manufacturing Technology
Chalmers University of Technology
SE-412 96 Gothenburg
Sweden
Telephone + 46 (0)31-772 1000

Reproservice
Gothenburg, Sweden 2013

Characterization of electrically insulating coatings for soft magnetic composite materials by means of surface sensitive analytical techniques

DIMITRIS NIKAS
Department of Materials and Manufacturing Technology
Chalmers University of Technology

Abstract

Powder metallurgy (PM) is a cost effective and efficient process for producing net-shaped parts of high tolerances and homogeneous properties in large production volumes. These are few of the reasons why this technique is preferred in manufacturing soft magnetic composite (SMC) materials for electromagnetic applications. The concept of SMC consists of encapsulating pure iron particles with an electrically insulating coating which yields compacts of high bulk resistivity and isotropic magnetic behaviour. Such materials provide great freedom in design and exhibit improved magnetic performance compared to more traditional laminated steels and ferrites for a wide range of frequency applications.

In the present thesis, surface characterization of such type of composite powder in as-received state was performed using surface sensitive analytical techniques. Information regarding the nature of the surface layer is important in designing the process and tailoring the properties of a product towards a desired application. The material under examination was commercially available phosphated iron grade which was analyzed using X-ray photoelectron spectroscopy (XPS) and high resolution scanning electron microscopy (HR SEM) coupled with energy dispersive X-ray analysis (EDX). Based on these techniques, thickness estimation, morphology, coverage, chemical state and compositional depth profile analysis of the insulating coating was conducted.

The aim of this investigation was to evaluate the effect of the surface characteristics and geometry of powder on such type of analyses. For this purpose, gas and water atomized high purity iron grades, having spherical and irregular shape respectively, were used. Both kinds of powder were covered with uniform oxides layers of different thicknesses and they were both divided into different particle size fractions. Furthermore, standards and flat samples of similar composition to the metal powders were prepared and evaluated accordingly using additional thermoanalytical and X-ray diffraction (XRD) techniques in order to acquire reference values.

The results showed that the as-received state appears to have a greater contribution of oxide thickness than when it is fractioned. This is supposed to be a result of the fact that the unsieved powder has a significant difference in the particle size and this can cause more shading effects during the XPS analysis.Moreover, the SMC powder exhibited a complex surface layer structure consisting of a mixture of iron oxide and iron phosphate compounds of the order of few nanometres.

Keywords: Powder Metallurgy, soft magnetic composites (SMC), gas and water atomized iron powder, surface oxides, phosphate coating, XPS, HR SEM, EDX

Acknowledgements

This master degree project was done from January 2013 to June 2013 at Department of Materials and Manufacturing Technology at Chalmers University of Technology.

At the end of this work I would like to thanks Höganäs AB for providing the powder materials studied at this project.

I would like to thank my supervisor Christos Oikonomou for the support and guidance during the entire six month period.

I would also like to thanks my examiner Prof. Lars Nyborg for the useful feedback and Assoc. Prof. Eduard Hryha for the interesting discussions we had during this project

Finally I would like to thank all the people in the department that helped me during this time, especially Urban Jelvestam for the help with XPS, Dr. Yiming Yao for the help with use of SEM, Dr. Kumar Babu Surreddi and MSc. Julio Maistro for the XRD tests and Dr. Raquel De Oro Calderon and Eduard Hryha for the help with the TGA analysis.

Also many thanks to my classmates for the help and long discussions we had almost every day at the department during this period that helped me with the present work.

Gothenburg, December 2013

Dimitris Nikas

Table of Contents

Chapter 1..... 1

Introduction 1

Chapter 2..... 3

Theoretical background..... 3

2.1 Powder metallurgy.....2
2.2 Soft magnetic composites powders.....4
2.2.1 Iron core losses in electromagnetic applications.....5
2.2.2 Advantages and Properties of soft magnetic composites.....6
2.3 Phosphating process.....7
2.3.1 *Kinetics of the phosphating process*.....9
2.4 X-Ray photoelectron spectroscopy (XPS).....9
2.5 Scanning electron microscopy (SEM) and Energy dispersive X-ray spectroscopy (EDX).....11
2.6 X-ray diffraction (XRD).....13
2.7 Thermogravimetry (TG).....15

Chapter 3.....17

Materials and Experimental procedures 17

Chapter 4.....19

Results.....19

4.1 Analysis of the iron oxide standards.....18
4.2 Analysis of the ABC100.30 powder.....25
4.3 Analysis of the Gas atomized powder.....40
4.4 Analysis of the phosphate standards.....57
4.5 Analysis of the Somaloy 500 powder..... ...62

Chapter 5.....75

Discussion.....75

5.1 Pure iron powders and standards.....76
5.2 Somaloy powder and phosphate standards.....78

Chapter 6.....80

Conclusions and future work.....83

References 82

Chapter 1

Introduction

Soft Magnetic Composite (SMC) materials designed for electromagnetic applications are being produced based on traditional Powder Metallurgical (PM) techniques. The latter provide profitable and sustainable production routes that yield net-shaped parts, minimizing thus the required post treatment steps. The concept of SMC technology is based on encapsulating each individual iron particle with a thin, in the order of nanometres, electrically insulating surface layer and subsequently pressing them together in a three dimensional array form of a finished compact. In this manner, uniform and isotropic 3D magnetic properties are acquired that offer design freedom in creating unique and innovative application concepts

The SMC products exhibit improved magnetic performance for a wide range of frequency applications as opposed to more traditional laminated steels and ferrites. This is due to the fact that they offer higher bulk electrical resistivity by effectively confining the deleterious effects of eddy currents, especially at high frequency applications. As opposed to more conventional PM techniques, production of SMC parts does not require sintering since that would compromise the viability of the insulating coating. Conversely, a heat treatment at lower temperatures is performed in order to relax any stresses introduced during compaction, improving thus the magnetic induction of the part and promoting curing of the surface layer for mechanical strengthening. Additionally, it is possible by changing the thickness of the layer and the particle size distribution of the SMC powder to essentially tailor the magnetic properties of a compact towards a desired application.

From the above, it is obvious that the insulating coating is the paramount feature of the SMC technology and thorough investigations of its nature and behaviour are required to improve and tailor the process in producing parts of desired properties. The objective of this thesis work was to implement techniques and methods that would provide valid information on the surface chemistry and characteristics of the surface layer. Surface sensitive analytical techniques, namely X-ray photoelectron spectroscopy (XPS) and high resolution scanning electron microscopy (HR SEM) combined with energy dispersive X-ray analysis (EDX) are traditionally used in material science to investigate, characterize and model surface reactions.

The aim of the current experimental investigations, based on the aforementioned techniques, was to determine the morphology, homogeneity, chemical composition, thickness and cohesion of the insulating layer to the iron particles. For this reason, standards were acquired and analysed in order to accurately determine the chemical composition and state of the material of interest. Additionally, thermodynamic considerations regarding the composition and stability of the insulating coating were addressed and compared with the experimental findings. Furthermore, the contribution from factors related to particles geometric characteristics, as size, shape, surface area and morphology, on the analysis of the surface layer were also evaluated based on a theoretical model. The SMC grade was divided into different size fractions and compared to metal powders of similar sizes and various surface characteristics in order to quantify those effects.

Chapter 2

Theoretical background

2.1 *Powder metallurgy*

Powder metallurgy (PM) refers to the processing science of manufacturing complex shaped parts of high tolerances in large quantities and having low production cost. In conventional press and sinter PM process this is done by using metal powder as base material which is then densified to parts of the desired shape through custom made dies at high pressures. These so called "green bodies" are subsequently sintered at high temperatures, below the melting point of the material, in order to promote bonding between the metal particles and thus improve the mechanical properties. Prealloyed powder allows processing below melting temperature and sometimes even at solid state, thus avoiding problems like segregation or shrinkage during solidification in castings.

The PM technology has many advantages over other manufacturing techniques such as: material saving (around 95% of the material is used), energy per time saving (i.e. lowest energy consumption per kilogram of finished part), complex shapes, high reproducibility, wide range of properties and uniqueness in certain fields (e.g. it is the only process that allows manufacture of cemented carbides, CMCs/MMCs, refractory metals, structural ceramics, etc). Some of these advantages emerge from the fact that PM yields the possibility to manufacture more complex microstructures where porosity or oxide dispersion and homogeneity required are superior as compared to the results of other processes. Many methods exist for producing PM parts such as hot or cold isostatic pressing, metal injection molding, powder forging, solid state sintering, liquid phase sintering, etc. The whole tree of the powder metallurgy processing appears from the illustration below (Fig 2.1).

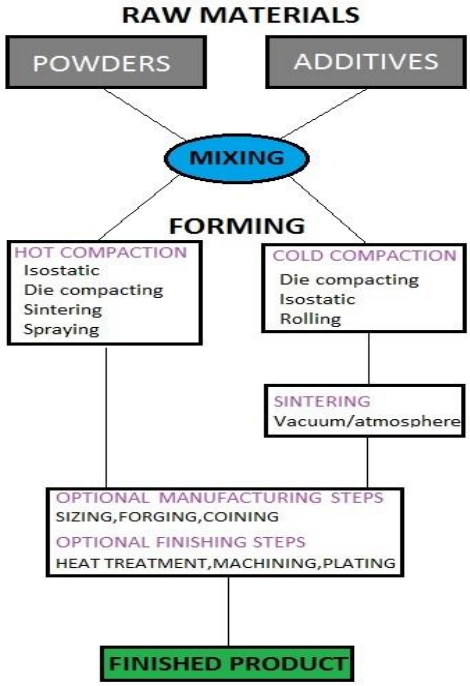

Figure 2.1: PM process route (author illustration redrawn from [2]).

Fields of application of PM include 1) applications with high cost savings where complex shapes, small parts or large series are generated 2) applications where improved properties for better performance are needed and 3) applications where PM is the unique way as mentioned above.

Powder characterization

All of the above mentioned processes start with a powder therefore it is important to understand the nature of the material to be able to evaluate the process and the final product properties. A powder consists of particles, which are defined as the smallest units of powder that cannot be subdivided further. Typical sizes in metal powder are between 1μm-0.1mm (smaller than sand). The main attributes of a powder that need to be considered and are studied in this report are:

1) particle size/distribution
2) particle shape
3) surface area
4) surface characteristics
5) composition, homogeneity and contamination

Also to fully characterize a powder it is necessary to describe how it is manufactured and understand the various parameters in every step of the process [1].

Manufacturing of iron powders

The main categories of manufacturing techniques are:

- Mechanical Fabrication
- Electrolytic fabrication
- Chemical fabrication
- Atomization fabrication

Mechanical alloying involves fracturing and shearing powdering material in order to achieve very small particles and then mixing them mechanically by milling using hard balls in a large jar. In electrolytic fabrication, powder is precipitated at the cathode of an electrolytic cell whereas in chemical techniques thermal decomposition or precipitation from a liquid is mostly used.

Since the metal powders studied in the present thesis are manufactured by either gas or water atomization techniques, a more detailed description of their production route is given below. The main feature of atomization techniques is that a jet stream of gas or water of high pressure is directed against the molten metal that is fed as shown in Fig. 2.2,which gives rapid cooling.

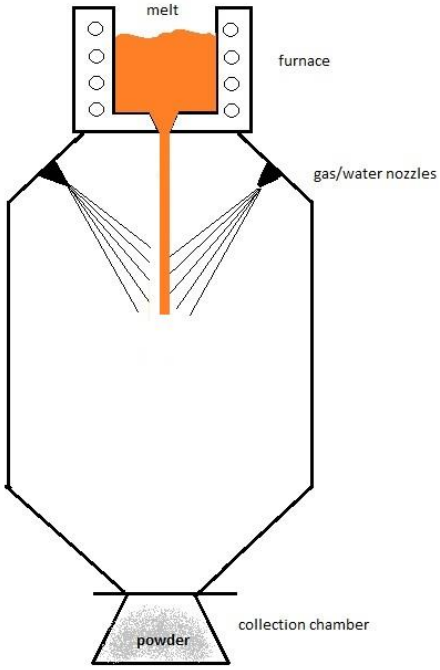

Figure 2.2: Simplified schematic of a vertical atomizer.

The main difference in the two types of powder is the shape of the particles. Gas atomized powder has spherical particles while water atomized has irregularly shaped particles. This affects the surface roughness of the powder and thus the compaction capabilities later in the process to produce the final parts.

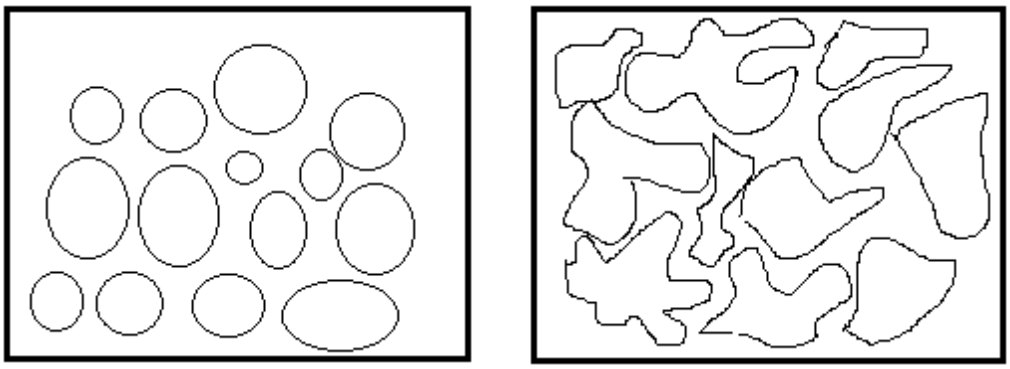

Figure 2.3: Drawing of gas atomized (left) and water atomized (right) powder particles.

Moreover, water atomization oxidizes the powder significantly more than gas atomization, affecting in this way its sintering capabilities and mechanical properties. For this reason, a deoxidation process step is highly necessary after powder production by heating in hydrogen [3].

2.2 *Soft magnetic composites powders*

Soft magnetic composite (SMC) powder consists of ferromagnetic particles that are encapsulated with an electrically insulating thin surface layer. This type of composite is used primarily for electromagnetic applications. They are typically manufactured from normal PM techniques under die compaction of the powder mix to the desired compact shape followed by heat treatment at low temperatures. No sintering step is

required since the formation of necks between the particles would damage the function of the insulating coating.

Thus, preparation of an SMC finished compact includes the following parts:
a) High purity iron powder, produced by water atomization, is preferred as base material due to its excellent magnetic properties (e.g. magnetic permeability and induction) and suitable mechanical properties (e.g. higher green strength due to the mechanical interlocking between the irregular shaped particles). b) Coating of the iron particles with an electrically insulating layer making sure that good adhesion and coverage between the particles surface and the layer is achieved.
c) Mixing insulated particles with a lubricant in order to reduce interparticle and particles to die wall friction.
d) Compacting the powder by conventional die compaction to form the green body
e) Heat treating the green body to a temperature regime between 400-700°C in order to relax stresses introduced during compaction (i.e. to reduce hysteresis core losses) and to promote a curing operation that yields mechanical strength to the part.

The schematic below shows how the coated iron particles appear in a soft magnetic composite (Fig 2.4) [5].

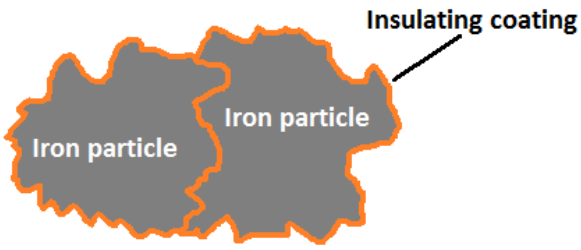

Figure 2.5: Schematic of SMC particles.

2.2.1 *Iron core losses in electromagnetic applications*

Magnetic properties of the material comprise the most important part when it comes to electromagnetic applications. There are two main characteristics of an iron core component. These are its core loss properties and magnetic permeability.

There are three main contributions to the dissipation in magnetic materials:

1) Hysteresis loss;
2) Eddy current loss;
3) Residual loss.

Residual losses are only important in low induction and high frequency levels and can be ignored for power applications.
Eddy current losses within an iron core occur due to electrical resistance losses that the alternating electric field creates. Two main effects are observed in materials when eddy currents are induced: incomplete magnetization of the material and increase in core losses. One way to minimize core losses is by using thin laminated materials and confining in this way the circulation of eddy currents within each laminate.

The SMC concept uses composite iron powder which due to its insulating surface layer allows eddy currents to travel only inside each particle, thus giving relatively high bulk resistivity. The small non-magnetic distances between every particle also act as air gaps which decrease the permeability of the bulk material.
As opposed to eddy current losses which are more prominent with increasing application frequency, hysteresis losses are the main factor in low frequencies and can be reduced by:
a) Large particle size;
b) High purity iron;
c) Stress relieve annealing step that follows the compaction step.

2.2.2 *Advantages and Properties of soft magnetic composites*

Soft magnetic composites(SMC) have many advantages over laminated steels that are generally used today. The most important one is that they exhibit magnetic and thermal isotropy that yields three dimensional magnetic flux path capabilities. Furthermore, net shape parts can be produced even in complex configurations using conventional powder metallurgy compaction processes at a relatively lower cost. The SMC have similar magnetic saturation induction values to those of wrought steel laminates and also lower eddy current losses at higher frequencies for a wider range due to the presence of the insulating coating. Because of these advantages lately they are preferred as alternative to steel laminates for new electric designs such as electric motors, fast switching actuators and pulse transformers [6].

As mentioned above, SMC material exhibits significant advantages that make it appealing for electromagnetic applications due to their properties. Some of these are:

- magnetic and thermal isotropy;
- very low eddy current loss and relatively low total core loss from low to high frequencies;
- high magnetic permeability at high fields;
- high remanent magnetization;
- high resistivity;
- reduction in size and weight;
- large anisotropy constant;
- low coercivity;
- high Curie temperature.

Additionally, one of the advantages of the SMC technique is the fact that it is possible to tailor the properties of a component to a desired application. These can be achieved by changing the particles size distribution or the coating thickness and composition in order to affect the permeability or core-loss characteristics of the part.

2.3 The phosphating process [22]

Phosphating is a well-known metal conversion treatment especially in automotive industry. It is used to provide the material with a thin layer of a phosphate coating that gives anticorrosion and wear resistance properties to the surface. It is also used as a pretreatment procedure to parts that are going to be painted afterwards.
Furthermore, it has been shown that such a coating provides insulation if used on iron powder thus greatly improving its magnetic properties [11].

Stages of general phosphating process

The stages of the phosphating process are as follows:

- Cleaning. The surface that is to be coated is mechanically cleaned and degreased usually in an alkaline solution (e.g. this step can be avoided as acetone is used as solvent).
- Rinsing the material in hot water.
- Cleaning of the surface with an acid (pickling). The acid dissolves possible oxide films and rust stains that might be present.
- Another step of water rinsing.
- Phosphating either by immersing the material in a phosphate bath or by spraying.
- Water rinsing.
- Drying.

Phosphating chemistry

The main components of a conventional phosphating solution are:

- Water or acetone as the main solvent
- Phosphoric acid (H_3PO_4)
- Ions (typically cations) of bivalent metals such as Zn^{2+}, Fe^{2+}, Mn^{2+}.
- Accelerator- This substance is needed to increase the coating process rate and reduce the grain size of the deposited coating. It is usually an oxidizing reagent such as nitrate, nitrite or peroxide.

When a metallic material, for instance iron, is immersed into a phosphate solution the iron ions are being provided by the dissolving substrate and a top chemical reaction takes place on the surface. There the iron dissolution is initiated at the micro anodes present on the substrate by the free phosphoric acid present in the bath. Hydrogen evolution occurs at the microcathodic sites [12] according to the following equations:

$$\mathbf{3Fe + 6H^{+} + 2PO_4^{3-} = 3Fe^{2+} + 2PO_4^{3-} + 3H_2} \quad \mathbf{(1)}$$

$$\mathbf{Fe \rightarrow Fe^{2+} + 2e^{-}} \quad \mathbf{(2)}$$

$$\mathbf{2H^{+} + 2e^{-} \rightarrow H_2} \quad \mathbf{(3)}$$

As these reactions proceed, the pH is locally lowered at the surface. Then, the metal surface becomes first covered by a thin layer of primary ferrous phosphate which is water soluble and then a thicker insoluble secondary and tertiary ferrous phosphate given by the reactions below:

Primary ferrous phosphate (soluble): $Fe + 2H_3PO_4 = \mathbf{Fe(H_2PO_4)_2} + H_2$ **(4)**

Secondary ferrous phosphate (insoluble): $Fe(H_2PO_4)_2 + Fe = 2\mathbf{FeHPO_4} + H_2$ **(5)**

Tertiary ferrous phosphate (insoluble): $3Fe^{2+} + 2PO_4^{3-} = \mathbf{Fe_3(PO_4)_2}$ **(6)**

A simplified schematic of the phosphating process is shown in Figure 5.

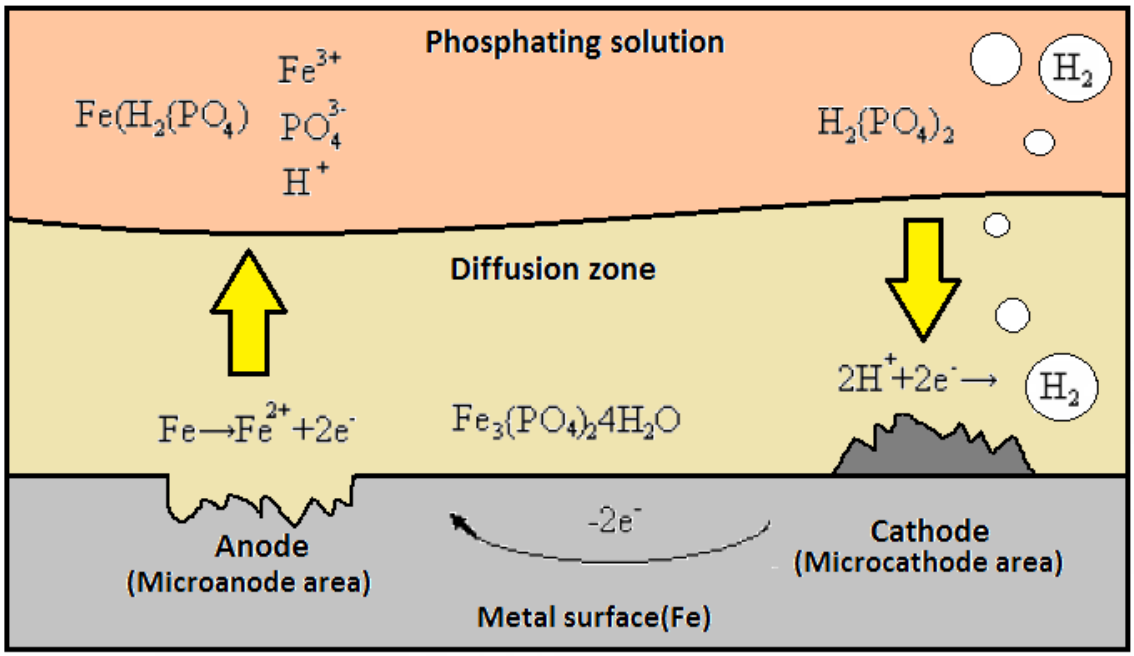

Figure 2.5: Schematic of the phosphating process.

The existing ions are hydrogen anions shown in Figure 5 and the resultant coating is iron-phosphate as indicated by the chemical reactions. The treatment is carried out by stirring the iron powder continuously in the solution bath in order to expose each particle [13].

During the process a very small amount of metal is removed from the surface and then re-deposited in an irregular fashion. However, this etching also has the side effect of permanently removing some of the metal, since not all of it is re-deposited. The key parameters that must be controlled to achieve a quality phosphate coating are concentration, temperature, pH, and dwell time. These parameters also affect the coating thickness which in turn affects the degree of crystallinity of the coating. Thinner coatings show an amorphous structure whereas thicker ones tend to give more crystal structure [14].

During the formation of ferrous phosphate the solution suffers a depletion of the free acid concentration and as a result the pH in metal/solution interface rises. As indicated already above, such rise of the pH affects the hydrolytic equilibrium of soluble primary phosphates and insoluble tertiary phosphates in the solution. Phosphoric acid should always be added in the solution in order to keep the bath stable and make it effective for deposition of the phosphate at the microcathodic sites

2.3.1 *Kinetics of the phosphating process*

Several studies of the phosphating kinetics have shown that the formation of the coating follows four stages, namely:

a) Induction stage
b) Initiation of film growth
c) Exponential main growth stage
d) Linear growth increase

In the induction stage, the surface oxide layer is removed. The initiation happens when the first nuclei start to form and thus rate of nucleation increases fast. This also depends on the phosphate bath conditions, the oxidizing agents and the pretreatment process that the surface has undertaken [22]. Most important part of growth is the exponential stage.
By using accelerators in the phosphating bath reduction of the induction period and extension of the linear stage is achieved. It has been reported that the rate of phosphating is defined by the diffusion of Fe^{2+} from the substrate to the coating/solution interface [15]. The rate of phosphating reaction is a function of microanodes on the surface:

$$\frac{-dFA}{dt} = K \cdot FA \cdot dt \quad \textbf{(7)}$$

where *dt* is the change in time, *FA* the surface area of anodes in micro cells and *K* the reaction rate constant. The latter reflects the influence of other factors on the process such as temperature, surface conditions, etc. which can additionally vary [15]. This was shown elsewere for carbonyl iron powder expressing the variation of the rate constant according to:

$$K = 143.4 \exp(-\frac{4745}{RT}) sec^{-1} \quad \textbf{(8)}$$

in which E = 4745 cal/mol is the activation energy of the phosphatizing reaction and k = 143.4 the rate constant coefficient [22].

2.4 X-Ray photoelectron spectroscopy (XPS)

X-Ray Photoelectron Spectroscopy (XPS) is a versatile, well established and widely applicable spectroscopic technique for studying surfaces [7]. It can be used to acquire chemical composition and state of the elements present in a material surface, as well as the surface layer thickness when combined with sputtering operations through ion gun technique. Its basic principle involves the ejection of a photoelectron from a core level inside an atom by an X-ray photon of specific energy (Fig 2.6)[8].

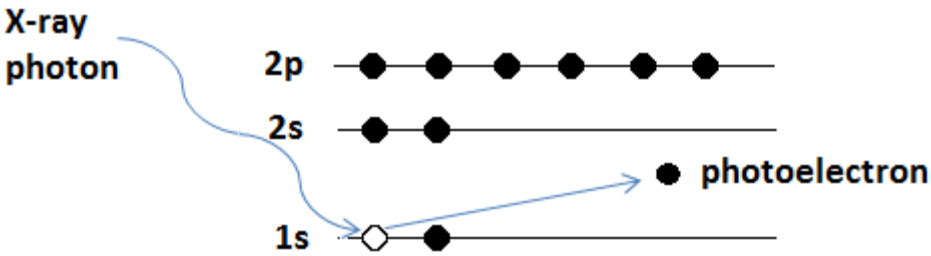

Figure 2.6: Schematic of the XPS photoemission of a 1s electron.

The instrument is measuring the kinetic energy (E_K) of these photoelectrons which depends on the energy of the X-ray photon (hv). The property that identifies the parent element and the atomic energy level is the binding energy (E_B) of the photoelectron which is calculated from the above energies using the formula below:

$$E_B = hv - E_K - \varphi \quad \textbf{(9)}$$

where φ is the work function of the spectrometer and is characteristic of its experimental configuration [9].The main components of an XPS system are the X-ray source, the stage, the lens system, the analyzer and the detector. These components are enclosed in an ultra-high vacuum chamber. A schematic of the instrument is shown in Figure 6.

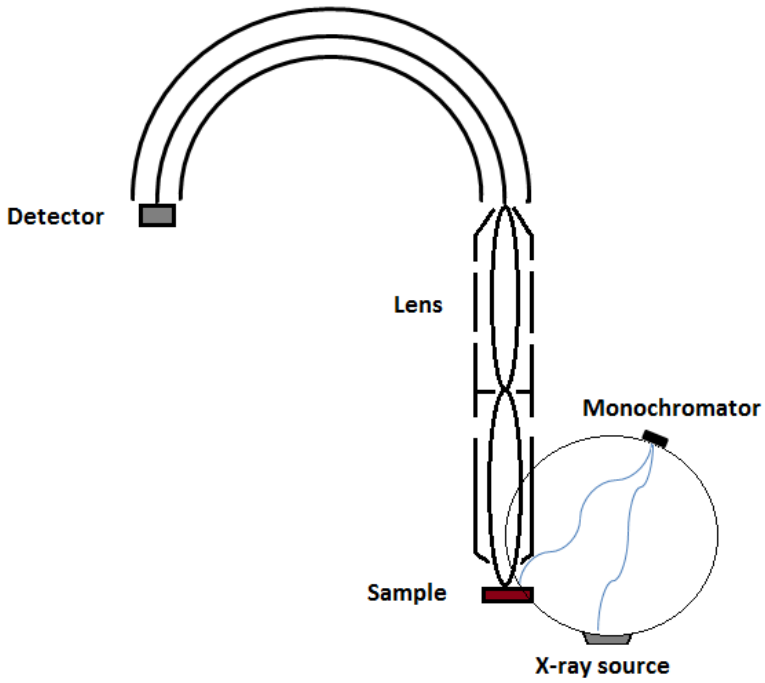

Figure 2.7: Schematic of the XPS instrument.

The requirement for the vacuum arises for two reasons: firstly electrons that travel towards the analyzer should encounter as few gas molecules as possible otherwise they will be scattered and will not reach the detector, while secondly the technique itself is sensitive to surface contamination. The electrons are focused through a hemispherical analyzer of a constant voltage by an electrostatic lens. The energy discrimination of the electrons is done by controlling the pass energy and sweeping the potential in the lens [10].

In the above configuration an argon ion gun can also be used if depth profiling is needed. This involves the bombardment of the sample with heavy ions. The most common gas that is used is argon. After ion etching the sample with the Ar^+ ions in specific intervals a small eroded area is created. By analyzing the surface after every interval and plotting the intensity versus the etching depth the thickness of oxides or coatings can be determined.

A typical XPS spectrum consists of a set of sharp peaks and a background, both emerging from the elements present on the surface of the sample. The axes depict binding energies versus number of electron counts which represents the intensity of a given element in the sample. The peaks originate from core or Auger electrons that escape the material without energy loss whereas the background comes from electrons that have suffered inelastic scattering and thus energy loss. A typical spectrum appears in Figure 2.8. The notation that is used in XPS uses the electron orbitals nl_j, i.e. $1s_{1/2}$, $2s_{1/2}$, $2p_{1/2}$, $2p_{3/2}$, etc. Different electron spin is depicted with a different peak in the spectrum.

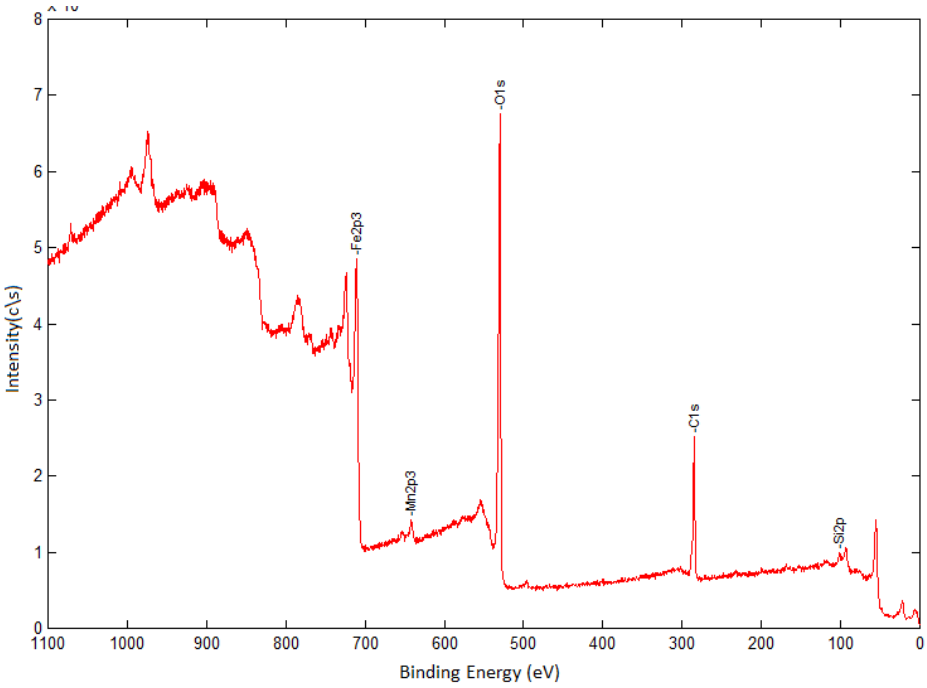

Figure 2.8: XPS survey spectrum of Fe-powder in the as received state.

2.5 *Scanning electron microscopy (SEM) and energy dispersive X-ray spectroscopy (EDX)*

Scanning electron microscopy (SEM) is one of the most commonly used microscopic techniques when it comes to materials characterization. The main advantage is its high resolution and depth of focus that provide very detailed topographic contrast. The basic principle of this method is bombarding the sample with a beam of accelerated electrons and detecting the various signals that are emitted from the sample area that is irradiated. The source of electrons is usually a bent tungsten filament which has to be heated in order to emit electrons Using high voltage of up to 30 keV electrons are accelerated and directed towards the sample. Magnetic lenses and apertures are also used for controling the diameter of the beam and to focus it over the sample. The

beam scans the surface under examination in a raster scan manner. The instrument operates under high vacuum conditions so interactions between electrons and gas molecules are avoided. A schematic of a SEM instrument is shown in Figure 2.9.

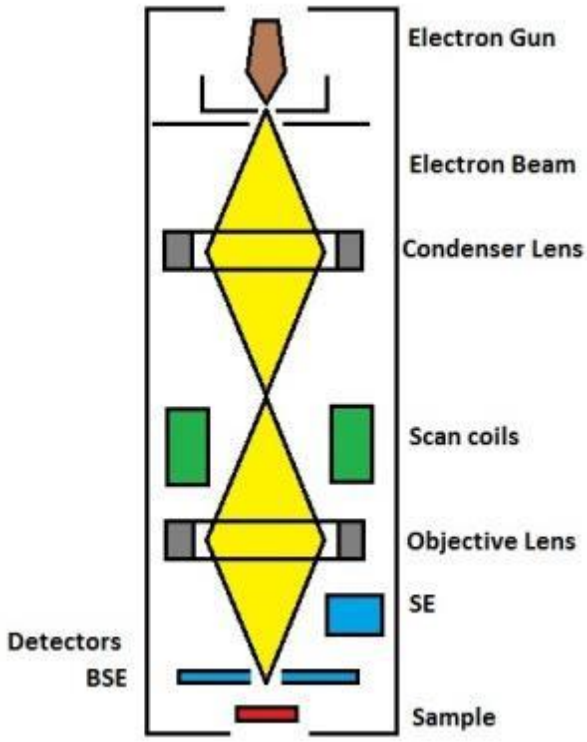

Figure 2.9: Schematic of SEM instrument.

There are many different ways that the sample can interact with the electron beam depending on the penetrating depth (fig 2.10). Different kinds of detectors help collect the various sample responses and through computer software the respective image on the screen is provided. Advanced microscopes are also equipped with a Field Emission Gun (FEG) that yields high quality imaging at low acceleration voltages combined with higher resolution and brightness.

For normal imaging purposes secondary (SE) or backscattered electrons (BSE) are most commonly used. Secondary electrons offer a) higher resolution b) higher signal-to-noise ratio which gives better quality images with good topographic contrast, while the backscatter electrons provide enhanced elemental contrast. An SEM can also be equipped with special inlens detector for improved topographical contrast at close working distances by collecting secondary electron from small angles close to the beam column [16].

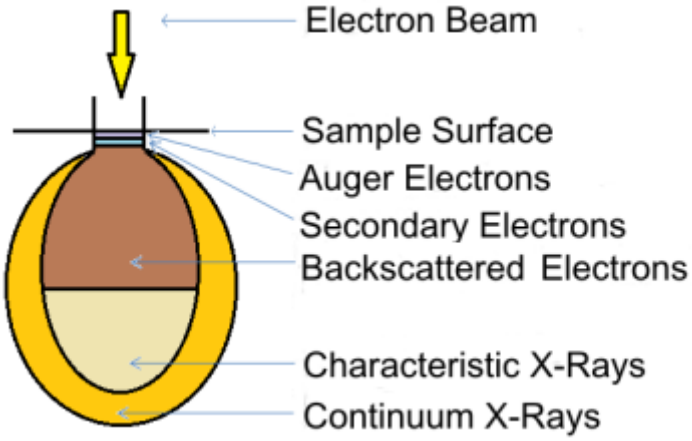

Figure 2.10: Interaction volume of sample for various types of signals.

Another possibility within the SEM is to use X-ray spectroscopy. High energy electrons from the beam have the ability to knock out a core electron from the sample atoms thus leaving a vacancy to be filled by higher energy electrons. The transition from a higher energy state to a core level happens with the simultaneous emission of an X-ray which is characteristic of the atom and the atomic transition. Using the X-ray spectroscope that is attached to the SEM one can detect such X-rays and the result is an X-ray spectrum of the area investigated (Fig 11) [16].

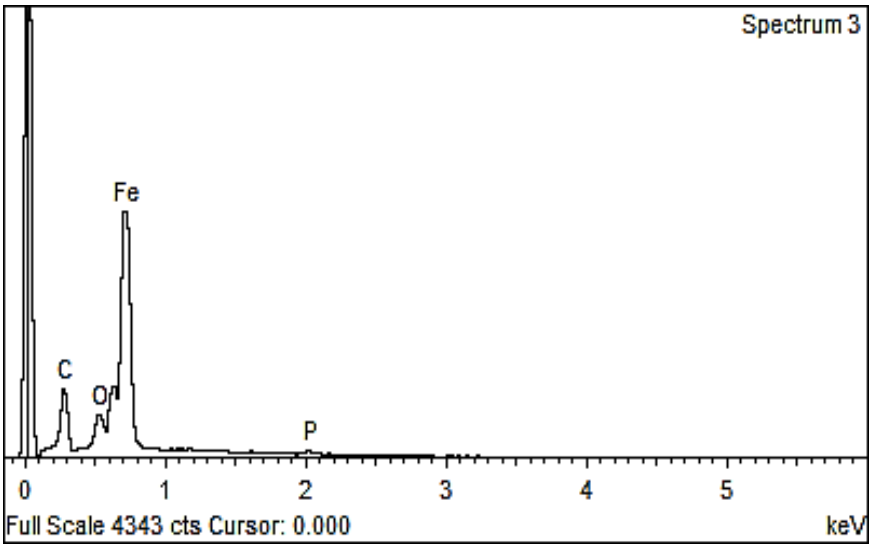

Figure 2.11: EDX spectrum of Somaloy 500.

2.6 *X-ray diffraction (XRD)*

The X-ray diffraction is an analytical technique that helps us to understand how the atoms or molecules are structured within a crystal. In this technique an X-ray beam is targeted towards the sample and is diffracted by the atoms into various specific directions. A detector is measuring the angles and intensities of these beams and the output is a 3D representation of the crystal electron density. In this manner, information such as unit cell dimensions, crystalline order, phase identification,

residual stresses in the material, among other types of analyses can be performed. In an X-ray diffraction measurement, the material investigated is mounted on the stage of the instrument and gradually rotated while the X-ray source is also moving at specified angle intervals. X-rays are scattered elastically inside the material and while most of them cancel one another as they add destructively some add constructively following Braggs law:

$$2d\sin\theta = n\lambda \qquad (10)$$

where d is the spacing between diffracting planes, ϑ is the incident angle, n is any integer and λ is the wavelength of the beam [23].

The diffracted x-rays produce a pattern and since most materials have unique structure, compounds can be identified using already known patterns from available databases. A typical XRD patterns is shown below:

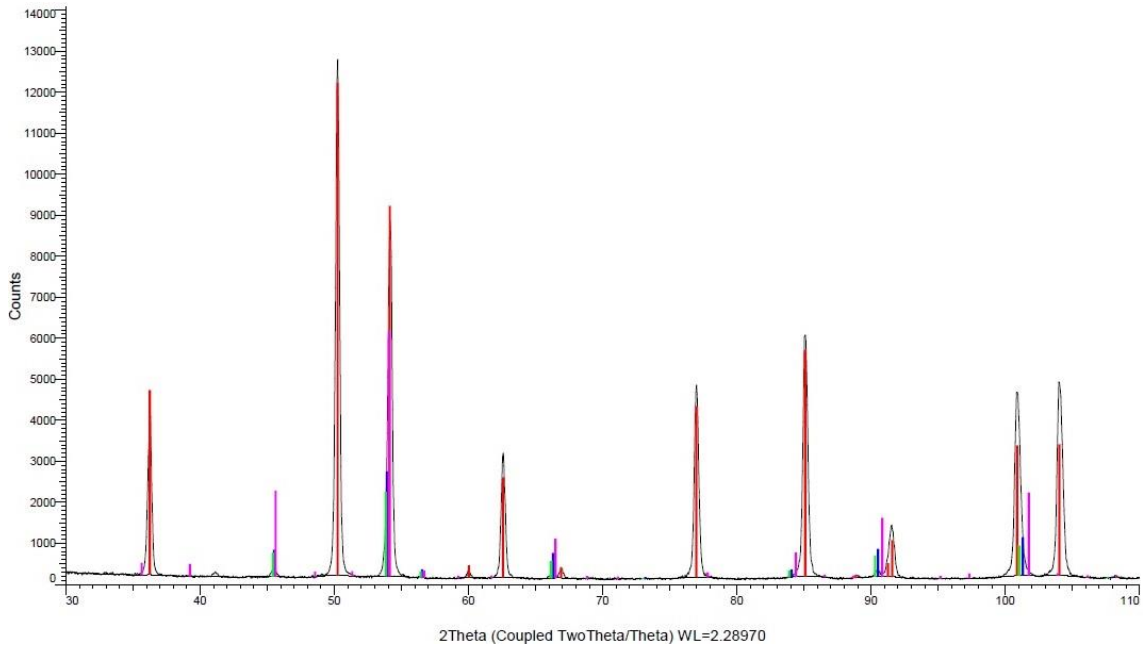

Figure 2.12: XRD pattern with the database fitting lines present.

A powder X-ray diffractometer consists of an X-ray source (usually an X-ray tube), a sample stage, a detector and a way to vary the incident angle. The X-ray is focused on the sample at some angle θ, while the detector opposite the source reads the intensity of the X-ray it receives at *2*θ away from the source path. The incident angle is then increased over time at a desired step interval while the detector angle always remains 2θ above the source path (Figure 2.13).

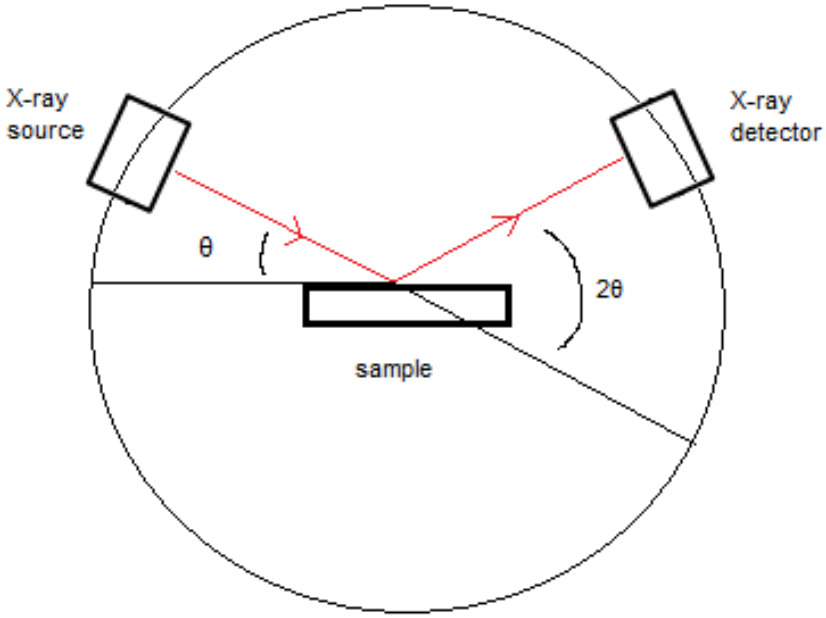

Figure 2.13: Schematic of a difractometer.

2.7 Thermogravimetry (TG)

Thermogravimetric analysis is the technique that measures the change in mass of a sample as a function of temperature in a predefined temperature program. Temperature is then first slowly increased then followed by an isothermal plateau for a specified time and then a faster cooling down of the sample is performed. The weight of the sample is measured before the procedure and compared to the weight change that is happened during the temperature increase. From this data a weight loss curve is generated. The instrument consists of a sample holder, a high resolution balance and the furnace all inside a vacuum chamber with possibility to also have a gas atmosphere. [26]

Chapter 3

Materials and Experimental procedures

Materials under examination

In this thesis three types of powder were studied and they were all provided by Höganas AB, Sweden:

- Commercially available ABC100.30 powder, produced by water atomization
- High purity Fe powder, produced by a pilot gas atomizer
- Commercially available Somaloy 500® soft magnetic composite powder

Additionally, an iron foil, 1mm in thickness, of 99,5% purity and chemical composition shown in Table 1 produced by Goodfellow Cambridge Ltd. was used for standard calibration measurements after fine polishing to 1 µm. The samples prepared from the foil were 0.85mm x 0.85mm in dimensions and they were subsequently annealed at a maximum temperature of 500 ^{0}C for 15 min with a rate of 10^{0}C/min in argon 50% / nitrogen 50% atmosphere. Furthermore, additional samples were also treated under the same coating process as the soft magnetic composite powder grade.

Table 1: Fe foil composition

Element	Fe	Mn	Si	C	P	S
Content (wt%)	99.5	0.3	0.1	<0.08	<0.4	<0.05

To accurately perform curve fitting operations on the samples under investigation and assess the effect of the sputtering operations on the compounds present on the surfaces, measurements were conducted for chemical standards. These included iron oxides Fe_2O_3 and Fe_3O_4 (Sigma-Aldrich) along with iron (III) phosphate dihydrate ($FePO_42H_2O$) and in dehydrated ($FePO_4$) state after heat treatment, all in powder form.

Sieving

To investigate the effect of particle morphology and geometry, all three types of powder were sieved using the same sieve sizes which were chosen according to their particle size distributions specifications as received from the manufacturer. The sample size for every sieving process was 25g and was conducted with the octagon 2000 Digital Sieve Shaker from Endecotts using the 106µm and 53µm aperture size sieve grids also from Endecotts. Because of the powder fine nature, each sieve operation lasted 15min under the alternate mode where the apparatus first shakes and then stops the sieve to leave the particles some time to settle through the meshes. After

sieving every powder grade, the samples were categorized in three particle size fractions:

- 106µm and higher
- Between 106 µm and 53 µm
- 53 µm and below

Equipment and powder preparation

Measurements were done for each of the three kinds of powder in their "as-received" state as well for each of the powder size fractions after sieving.
Surface analysis of powder was done at Chalmers University of Technology with X-ray photoelectron spectroscopy (XPS) using the PHI 5500 instrument.
The XPS samples were prepared by using double sided adhesive conductive carbon tape as this method allows the particles to stick on the tape without deformation and alterations of the microstructure.
Along with the XPS measurements, ion etching was also performed on every sample to get the composition depth profile of each powder. Based on this method it was possible to estimate the oxide and phosphate thicknesses according to a theoretical model described earlier by Nyborg et al. [18].. The PHI MULTIPACK software (PERKIN ELMER, Eden Prairie, Minnesota, USA) was used for the XPS curve fitting analysis.

To characterize the morphology of the metal particles a FEG SEM LEO Gemini 1550 (CARL ZEISS - LEO electron microscopy, GmbH, Germany) was used while chemical micro analysis on the powder surfaces was conducted using EDX spectroscopy (INCA Energy) (Oxford Instruments, High Wycombe, England).
For the SEM analyses the samples were prepared by placing small amount of powder between two soft aluminum plates and pressing at low pressures of 1-2 MPa to "mechanically" interlock the particles on the plate surfaces. The samples were then mechanically mounted on a specific holder providing good conductivity for the sample and then analyzed.

For the XRD analyses the instrument from "BRUKER ANALYTICAL X-RAY SYSTEMS (AXS)" was used. The source was Cr Ka at 2.29Å wavelength. Scans were performed from 20° to 120° with 0.05^o step and 5 sec/step

The TG instrument used in the present work is a simultaneous TG/DTA/DSC thermal analyzer STA 449 F1 Jupiter equipped with a high resolution system both in weight and temperature measurement.

Iron oxides – iron phosphate

The oxides (Fe_2O_3, Fe_3O_4) that were used as standards were also mounted on carbon tape for the XPS analysis whereas the iron phosphate standard ($FePO_4$) was compacted and placed in the XPS as a compact using a specific holder. For two of these materials (Fe_2O_3 and $FePO_4$) electron neutralizer had to be used due to their insulating nature charging effects.
Samples were also prepared from all the chemical standards for XRD measurements in order to define their crystalline state and purity.

Chapter 4

Results

4.1 Analysis of the iron oxide standards

- Iron(III) oxide (Fe_2O_3)

The XPS spectrum of the iron (III) oxide gives a clear oxidic peak and the Fe^{3+} satellite peak is also visible, see Figure 4.1.

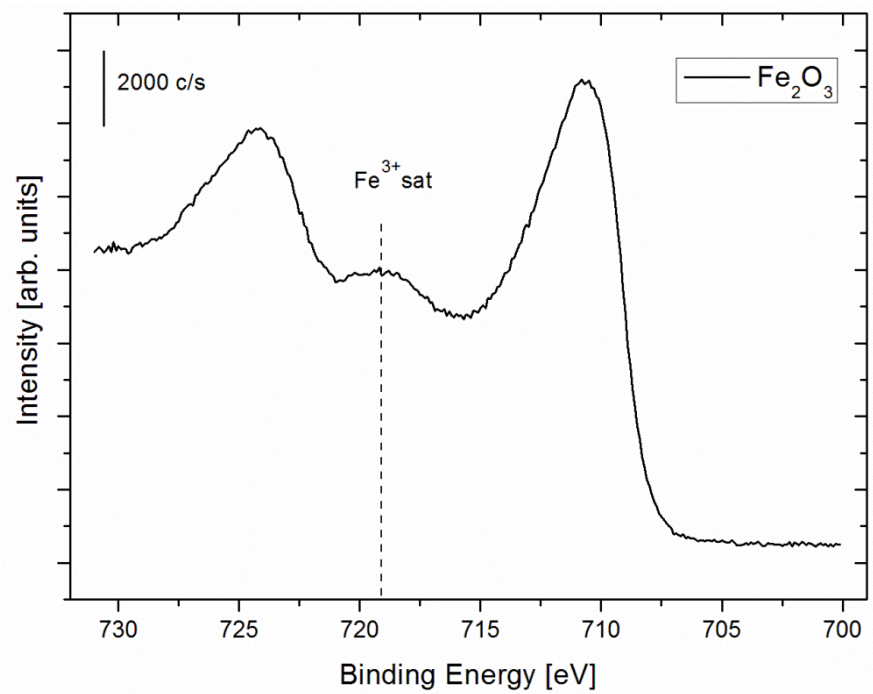

Figure 4.1: XPS high resolution spectrum of the iron Fe2p3 peaks for Fe_2O_3 at 0nm.

By using curve fitting the iron signal is analyzed to its three main contributions. As shown in Figure 4.2 the peak at 712.8 eV corresponds to the hydroxide compounds on the surface, the peak at 710.6 eV is assigned to iron in Fe^{3+} state while the peak at 709.5 eV is for iron in Fe^{2+} state. The background removal, method used in this thesis work was "iterated Shirley". Charging effects were observed in this sample and electron flood gun for charge neutralization was used. The adventitious hydrocarbon with binding energy at 285 eV was also used as reference value for additional software peak position correction. The oxygen signal shows a clear oxide peak at 529.7 eV and OH^- also present (Figure 4.2) [27].

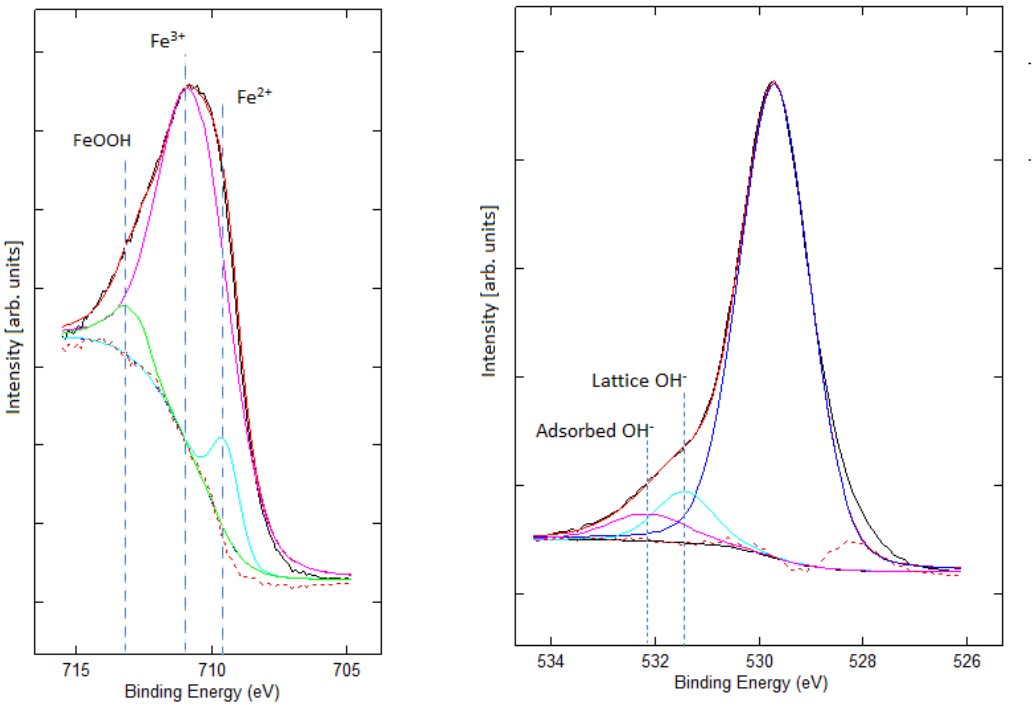

Figure 4.2: XPS analysis of chemical state of iron and oxygen peakswith the help of curve fitting in as-received state of the Fe_2O_3.

The binding energy values for the oxidized states of iron are used for the curve fitting operations on all the samples analyzed in the present study. After excessive sputtering the metallic state of iron appears (Fig 4.3).

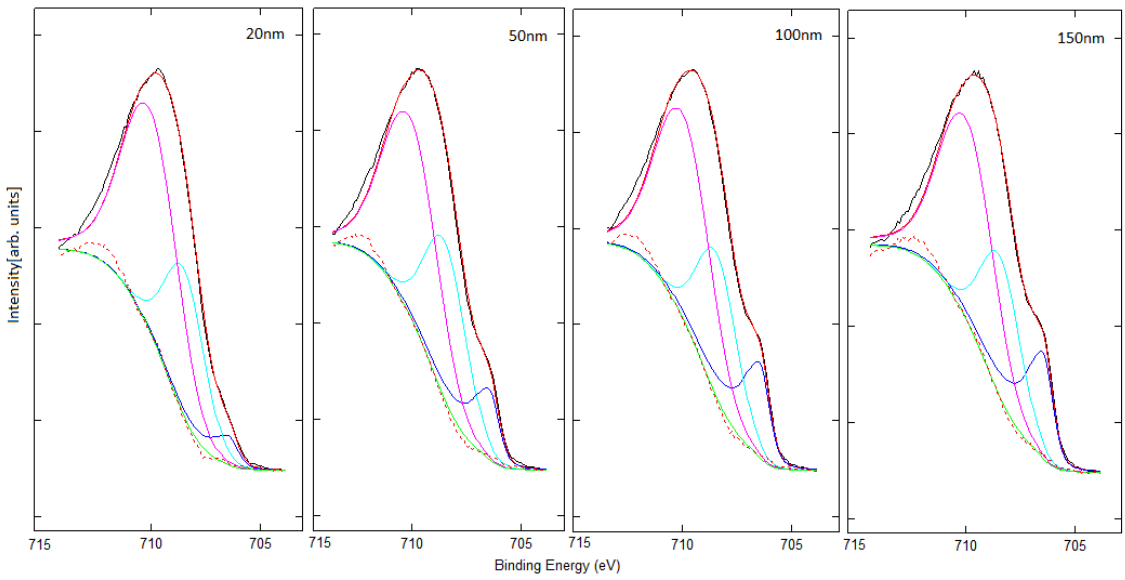

Figure 4.3: Appearance of the metallic state of iron in XPS analysis after excessive ion sputtering at Fe_2O_3 standard.

To accurately determine the chemical standard purity and composition, XRD technique was implemented. The findings are shown in Figure 4.4. It is clear that the oxide is crystalline and the semi-quantitative analysis with DIFFRAC.EVA v.3.0 from BRUKER showed

that for the case of Fe2O3 there is approximately 92.5% of rhombohedral hematite and 7.5% of orthorhombic magnetite.

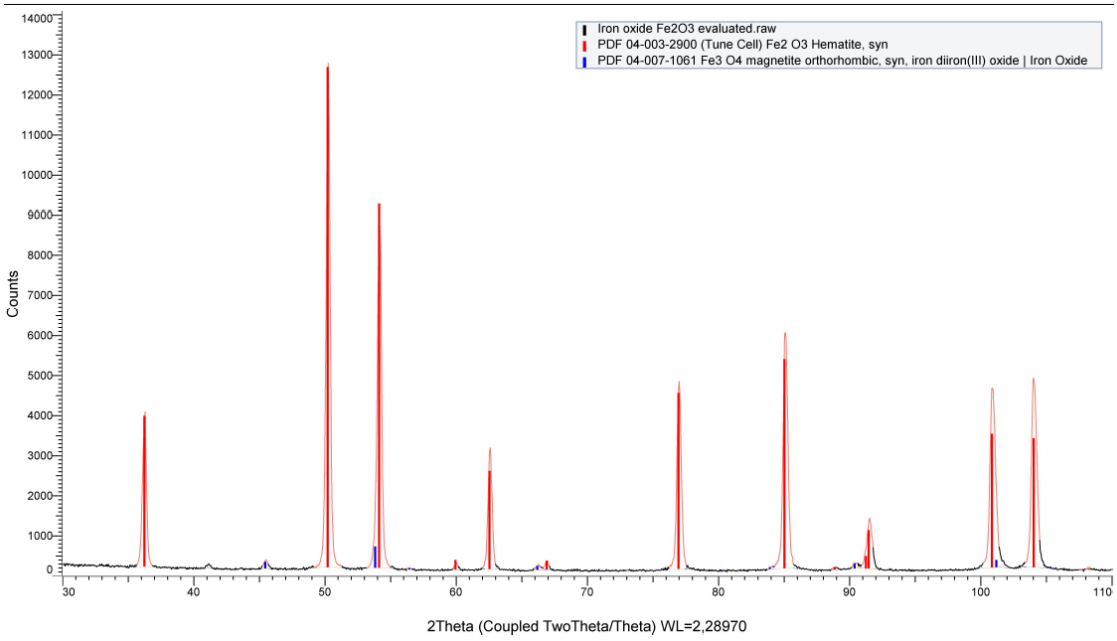

Figure 4.4: XRD spectrum of Fe_2O_3 with database references of the known phases.

- Iron(II,III) oxide (Fe_3O_4)

The second type of iron oxide standard(Fe3O4) was also examined with XPS. This oxide can also be formulated as $FeO \cdot Fe_2O_3$ and it contains both Fe^{2+} and Fe^{3+} ions in proportions 1:2. The XPS high resolution spectrum show a lower contribution of the Fe^{3+} satellite peak since Fe^{2+} is also present for this oxide (Fig 4.5).

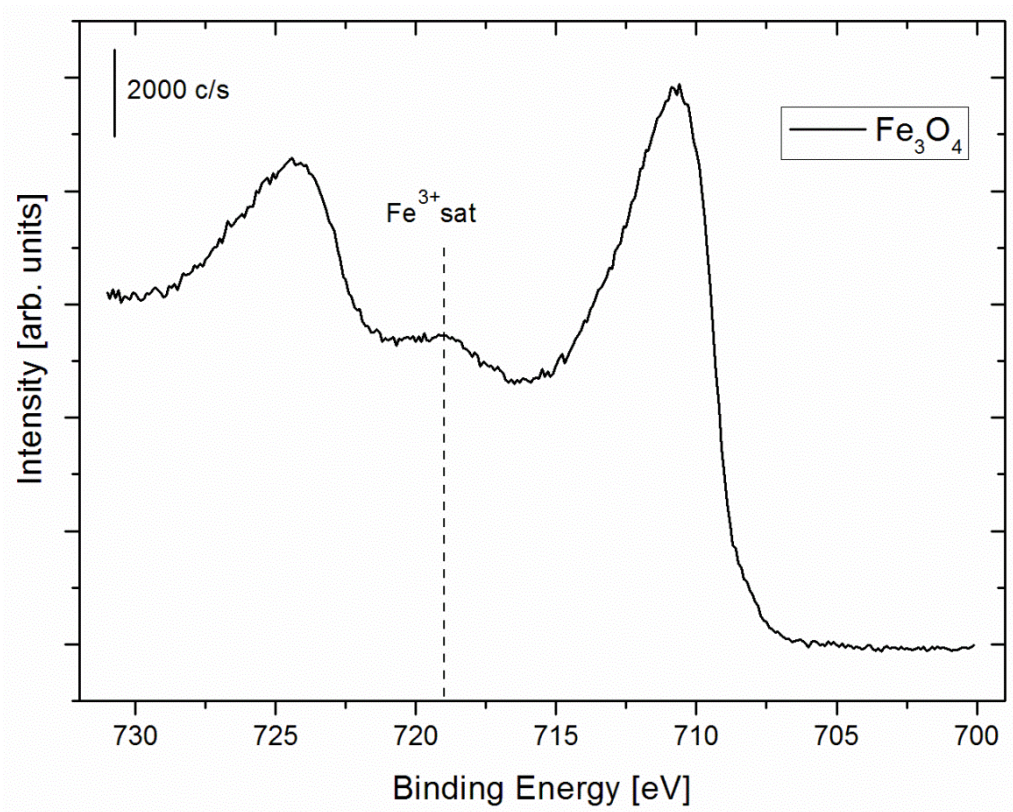

Figure 4.5: XPS high resolution spectrum of the iron Fe2p3 peaks for as-received Fe_3O_4.

By curve fitting the binding energies of these cations are confirmed as shown in Figure 4.6 below.

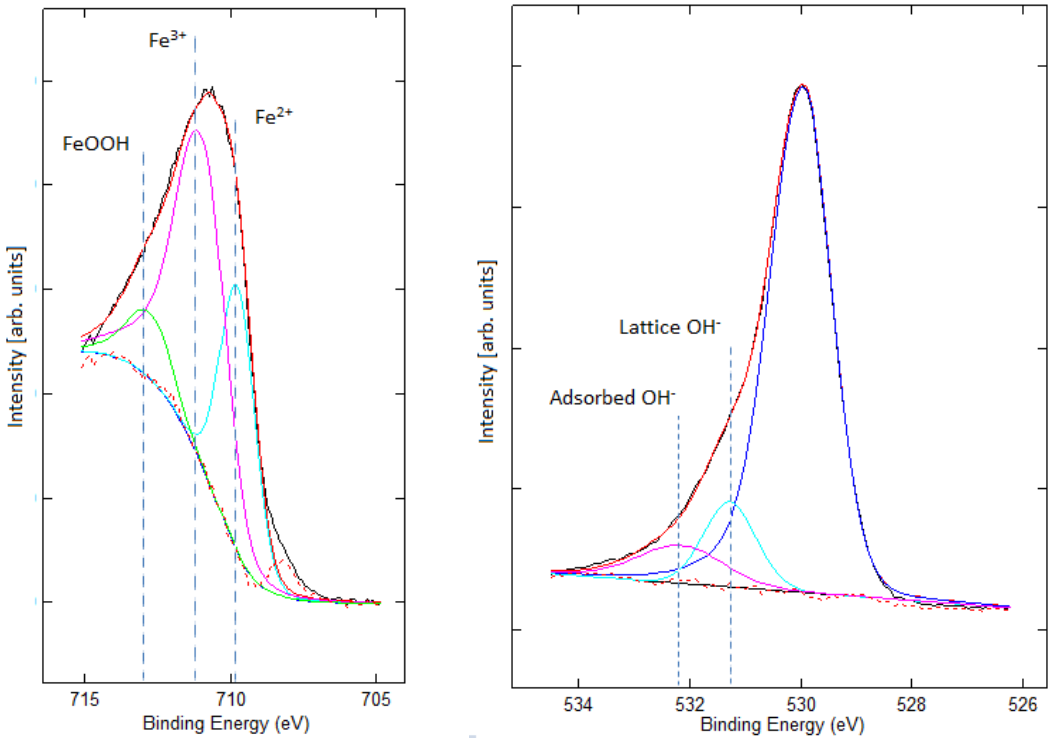

Figure 4.6: Analysis of chemical state of iron and oxygen with the help of curve fitting in as-received state of the Fe_3O_4.

The binding energy of Fe^{3+} is 710.9 eV and that of Fe^{2+} is 709.8 eV with the expected ratio 1:2 between peak areas for these two contributions. The oxygen peak is at 530 eV. No charging was observed in this oxide and the values are very close in accordance to the previous examined oxide, verifying that the charge correction on Fe_2O_3 was correct [28].

XRD was also performed on this sample for phase determination (fig. 4.7). This oxide has also crystalline structure as shown from the distinct nature of the Fe_3O_4 peaks on the spectrum with only this phase present.

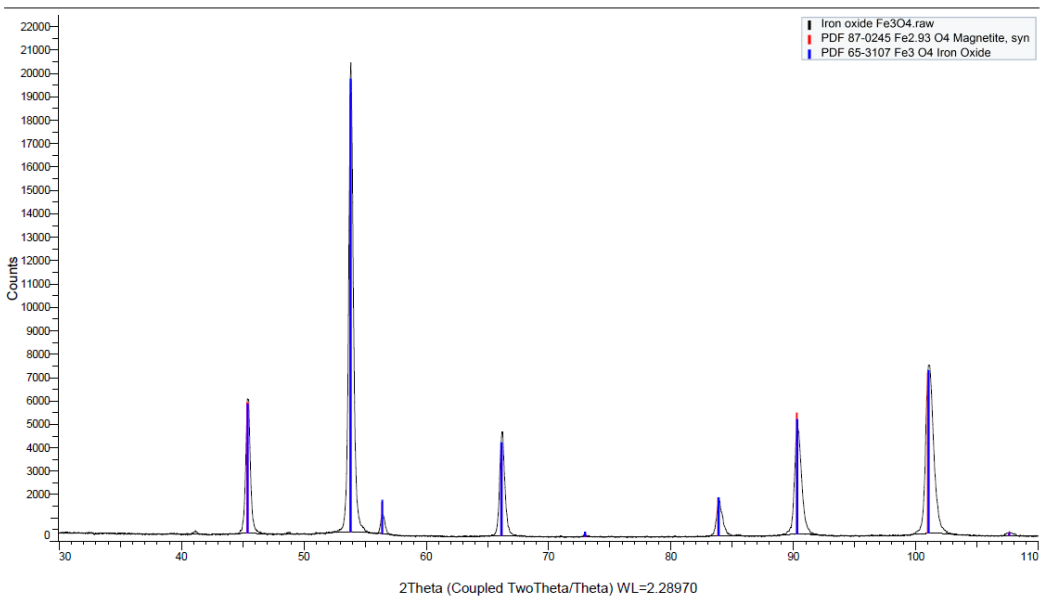

Figure 4.7: XRD spectrum of Fe_2O_3 with database references of the known phases.

- Iron foil standard

XPS analysis was performed on the iron foil in order to obtain a clear iron metal peak and use its characteristics for curve fitting of signals from the iron powder. A low resolution survey spectrum of this sample showing an overview of the elements present on its surface is depicted in Figure 4.8.

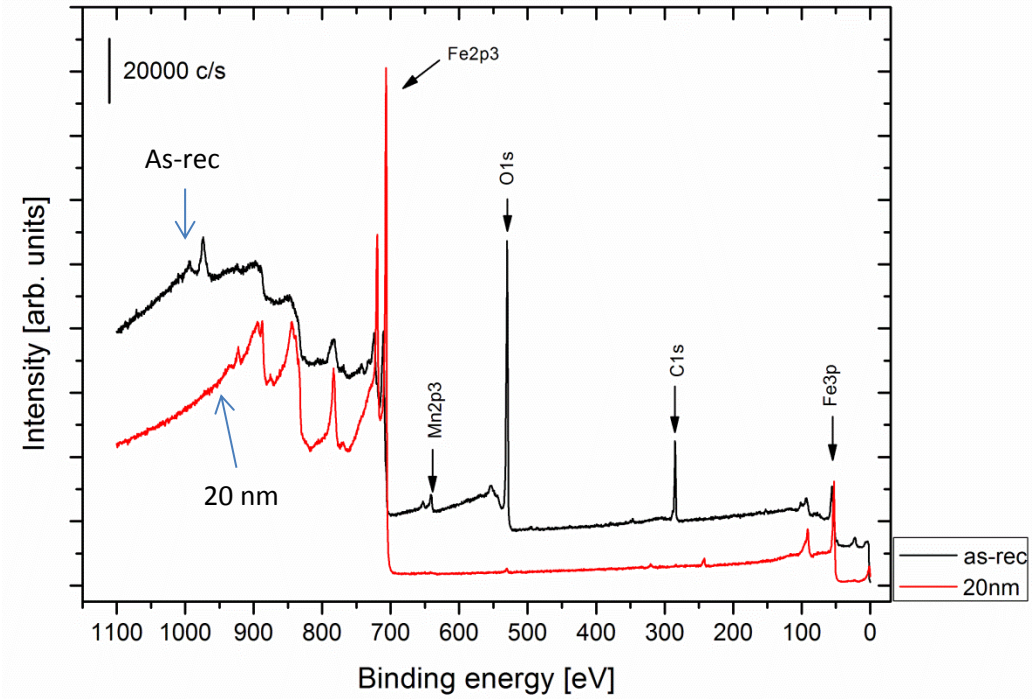

Figure 4.8: XPS survey spectra for the iron foil in as received and 20nm etched state.

As the foil was first polished and then annealed the oxide formed on top was expected to be very thin in thickness. Some impurity elements already known from the initial composition were also present on the surface. The etching steps and correspondent apparent surface composition are in Table 2.

Table 2: Element content (at%) in the surface and ion-etched state of the as-polished iron foil

Content[at%]/Element	Fe	O	C	Ca	Si	Mn
As received	23.3	53.8	18.4	0.6	1.6	1.1
Etched 1nm	44.2	54.1	-	0.43	0.6	1
2 nm	63.2	35.7	-	0.2	0.2	0.8
3 nm	85	14.4	-	-	0.3	0.4
5 nm	91.9	7.6	-	-	0.3	0.2
10 nm	93.4	6.3	-	-	-	0.3
20 nm	93.5	6.3	-	-	-	0.2

The carbon immediately disappears after the first etching step clearly indicating that its signal originates from contamination on the top layer, while silicon disappears after 1nm of sputtering. The manganese is present in oxide form within the material and exhibits a slower decrease with etch depth. The apparent concentration of iron almost reaches 94% while oxygen drops to 6.3% at 20nm etch depth. Figure 4.9 shows the progress of the elements relevant concentration.

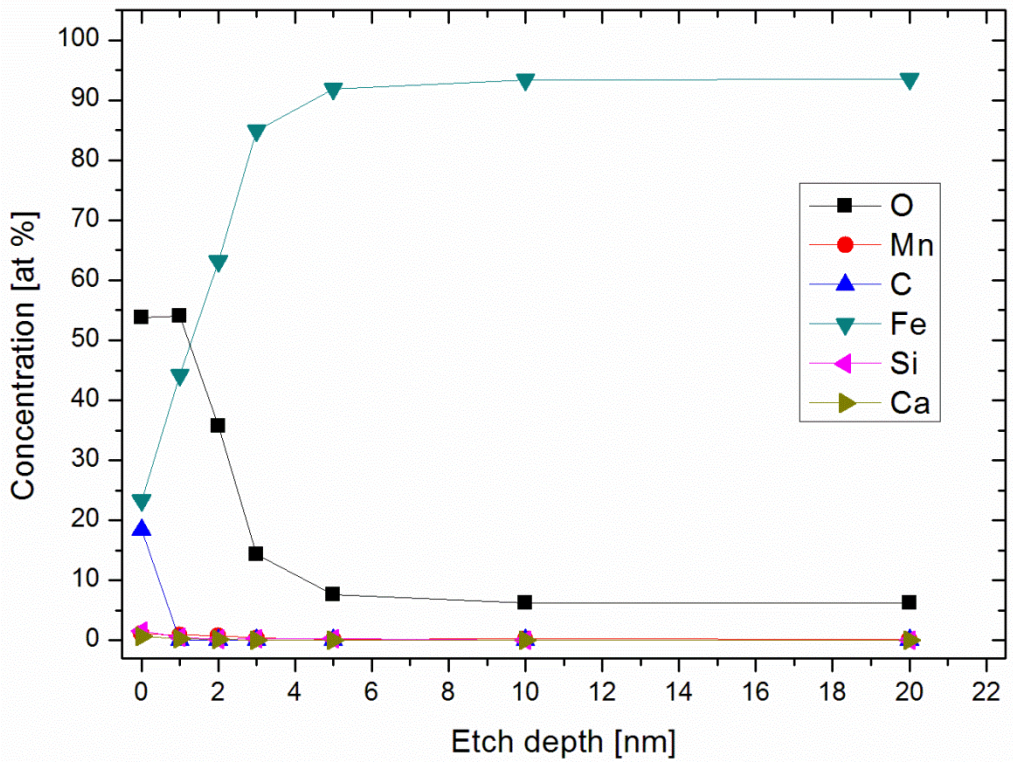

Figure 4.9: The element content over etching depth for the iron foil in the as-polished state.

The metallic peak starts to appear after the removal of the surface contamination layer which eliminates the carbon content and is very clear at 20nm etch depth. Figure 4.10 shows the high resolution XPS spectra for the iron signal at selected etch depths.

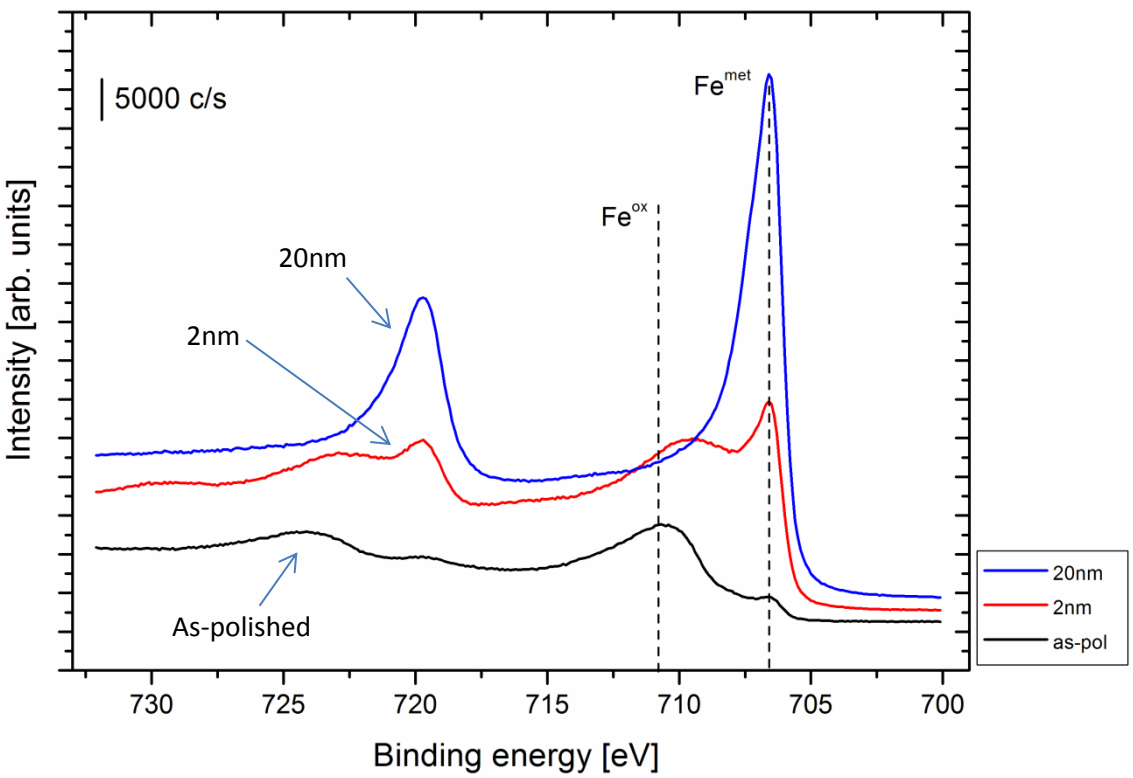

Figure 4.10: XPS spectra in the as-polished state and etching depths of 2nm and 20nm.

By using this metallic peak at 20nm all the standards needed for the curve fitting are acquired. The iron peak has an asymmetric shape and is positioned at 706.7 eV with full width at half maximum (FWHM) of 1.0eV, showing a very well defined peak (Figure 4.11).

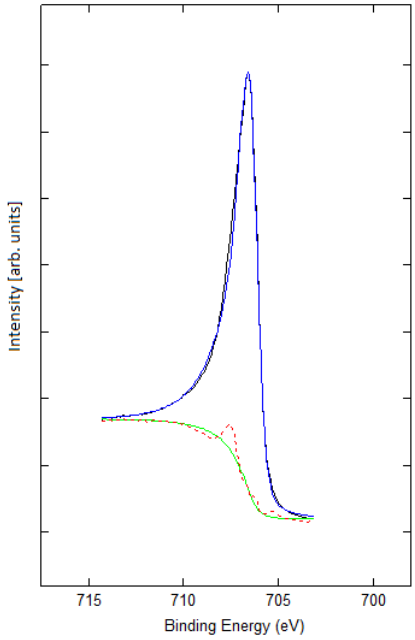

Figure 4.11: Analysis of chemical state of iron with the help of curve fitting in 20nm etching depth.

The oxide thickness for a flat specimen can be calculated using the formula below:

$$t^{ox} = \lambda^{ox} \cos\theta \, ln\left[1 + \frac{I^{ox} I_{\infty}^{ox}}{I^{m} I_{\infty}^{m}}\right]$$

where λ^{ox} is the attenuation lenght of the iron oxide (1.5nm , [17]) , θ is the angle between the normal to the surface and the electron analyser (45° for a flat surface for the instrument used) , $I_{\infty}^{m}, I_{\infty}^{ox}$ the metal and oxide intensities given from measurements on the chemical standards and I^{ox}, I^{m} the metal and oxide contribution of the iron foil at 0nm. For this foil the oxide thickness calculated with this method was 2.5nm, cf. depth profile in Fig. 4.12, which indicates a normalized Fe-metal intensity at the corresponding etch depth of ~75%

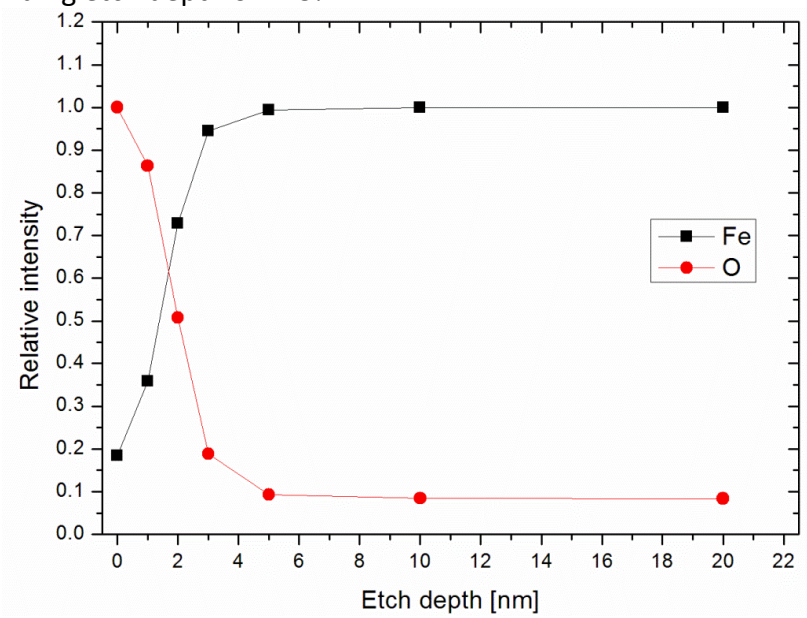

Figure 4.12: Relative intensities of Fe and O signals recorded from as-received Fe foil vs etch depth.

4.2 Analysis of the ABC100.30 powder

XPS Analysis of the as-received powder

In the XPS survey spectrum there are three main characteristic peaks. These peaks come from iron, oxygen and carbon (Figure 4.13).

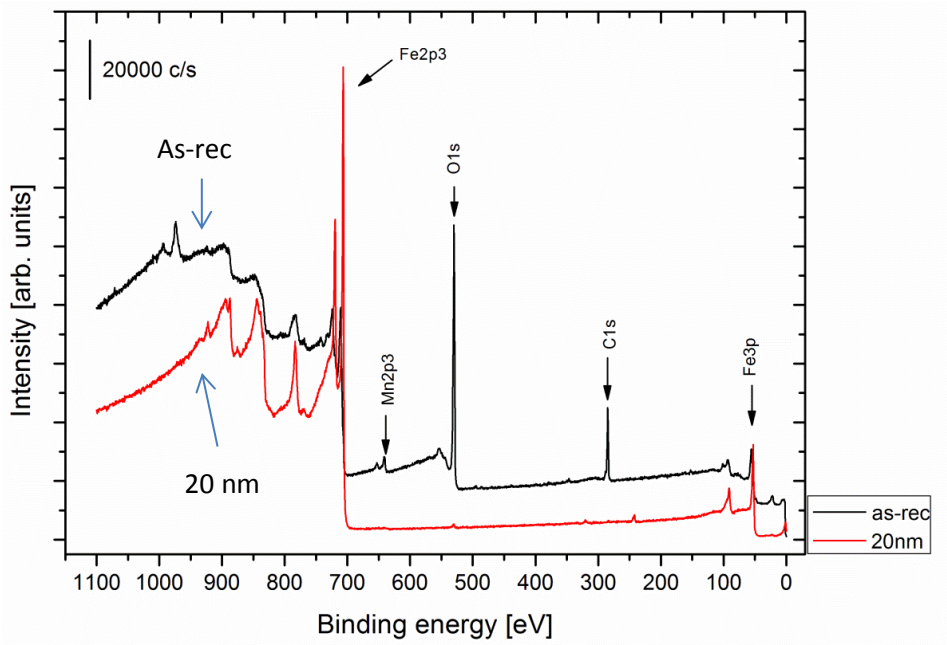

Figure 4.13: XPS survey spectrums for the iron foil in as received and 20nm etched state.

Presence of carbon is mostly due to contamination on the surface and after a couple of etching steps (2nm) the peak that remains is a result of the carbon tape onto which the powder is mounted (not of interest in the current study). Impurity content (silicon, manganese) appears to be very low. The apparent composition of this powder in the as received state is shown in Table 3.

Table 3: Element content (at%) in the surface of the as received and ion etched states of the ABC100.30 powder

Content[at%]/Element	Fe	O	C	N	Si	Mn
As received	14.9	47.3	33	1.3	1.4	2.2
Etched 1nm	34.3	59.8	3.2	-	-	2.6
2 nm	36.8	57.4	3.6	-	-	2.2
3 nm	40.8	56	0.6	-	-	2.5
4 nm	43.7	49.7	1.9	-	-	2.5
5 nm	50.4	43.3	4.1	-	-	2.2
6 nm	60.7	37.4	-	-	-	1.8
7 nm	67.8	29.7	-	-	-	2.5
8 nm	74.4	23.8	-	-	-	1.8
10 nm	81.4	16.8	-	-	-	1.9
20 nm	86.9	9.4	-	-	-	1.8
30 nm	87.8	6	-	-	-	2.4

Figure 4.14 shows the progress of the elements content as a function of the etch depth.

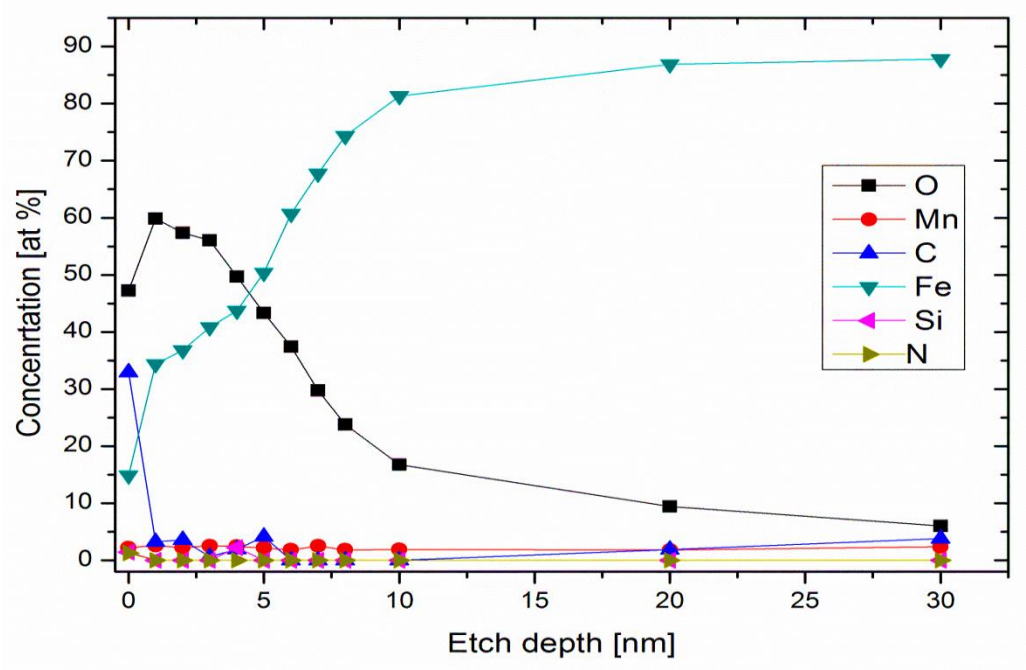

Figure 4.14: The element content over etching depth for the ABC100.30 powder in the as-received state.

As mentioned above, after 1nm of ion etching most of the surface contamination is removed as shown by the decrease in carbon content from 33% to 4%. The iron content is gradually increasing from 14.9% at the beginning to 87.8% at 30nm etch depth. Meanwhile, oxygen is decreasing from 47.3% to just 6%. Silicon and manganese impurity content is very low and thus negligible.
By performing high resolution scans in the XPS on the un-sieved sample, the following spectra are obtained at selected etch depths as shown in Figure 4.15.

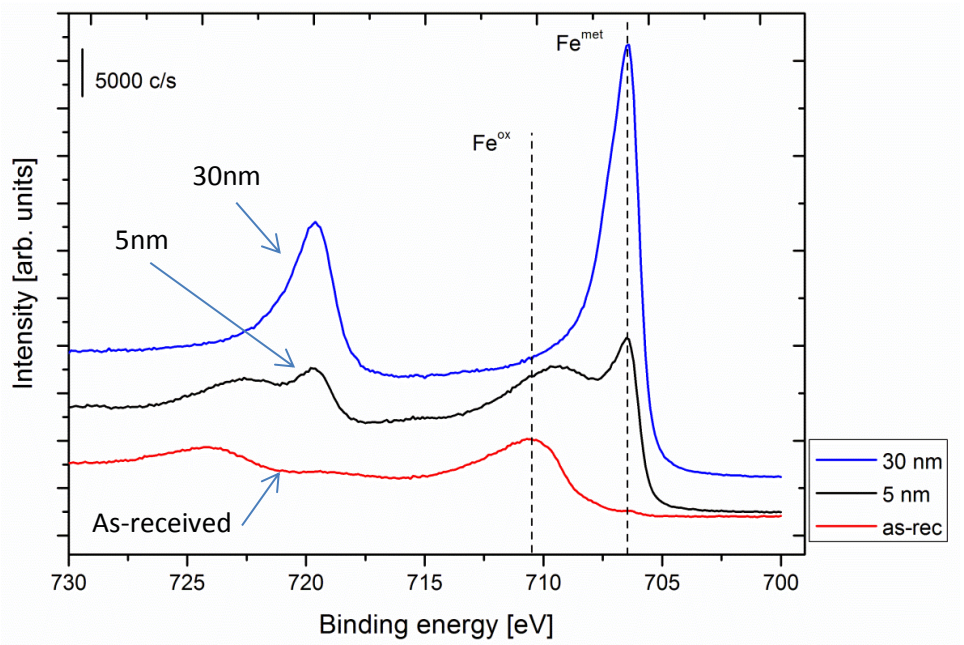

Figure 4.15 XPS spectra in as-received state and etching depths of 5nm and 30nm.

The metallic peak is not present on the as received state as it is covered by contamination and oxide layers. However, it starts to appear after a few etch steps and becomes clearly obvious after etching 30nm. The binding energy of metallic iron then is 706.5eV and the oxide which is the Fe_2O_3 is at 710.5 eV. These energies are obtained after curve fitting which allows us to distinguish the various chemical states from one another. An example of curve fitting for the iron peak is shown in Figure 4.16.

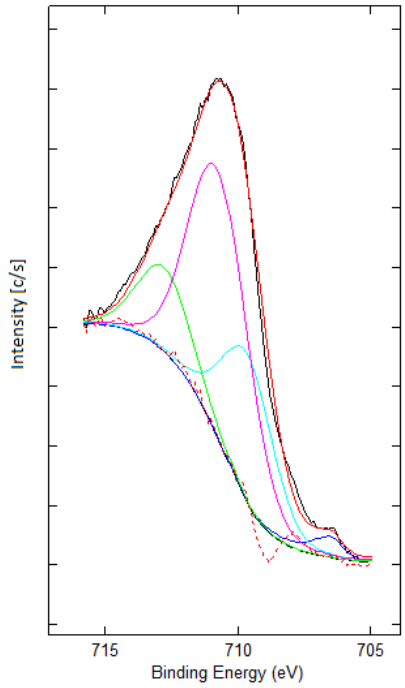

Figure 4.16 Analysis of chemical state of iron with the help of curve fitting in the as received state (0nm).

By using curve fitting the contribution of these chemical states, oxidic or metallic, can be obtained by measuring the area under each curve which depends on the amount of atoms of the specific chemical state. Due to the destructive nature of the ion etching process though, careful analysis must take place in order not to misinterpret the results. For this reason information from the measurements on the standards in respect to the effect of the ion etching on the compounds of interest is implemented.

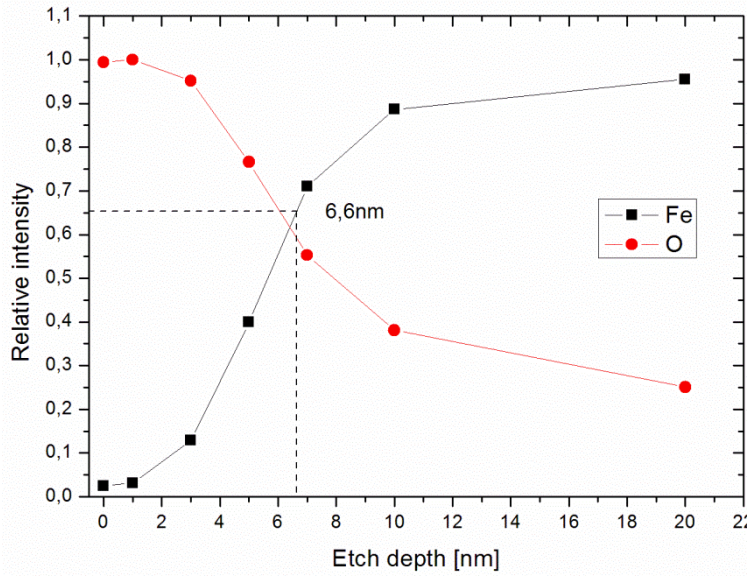

Figure 4.17: Estimation of the surface iron oxide layer using the normalized Fe-metalic(Fe2p peak) and the oxygen (O1s peak) over etch depth.

The method used in this thesis to obtain the surface layer thickness of a non-flat sample such as metal powder uses the iron normalized intensity curve. It has been shown [17] that the oxide-metal interface can be estimated by taking into account the relative intensity of the metallic signal versus the etch depth. For surface layers for which their ratio of thickness (t^{ox}) over the attenuation length (λ^{ox}) of the photoelectrons through them is $20 \geq t^{ox}/\lambda^{ox} \geq 3$, the interface can be located in the range of 60 to 72% of the relative intensity with 65% being a good estimation value for an unknown layer. When the t^{ox}/λ^{ox} is in the region $4 \geq t^{ox}/\lambda^{ox} \geq 0$ the estimation is done at 85% of the iron metallic intensity. This intensity fraction is used for the case of annealed gas atomized powder.
The relative intensity of iron and oxygen is plotted in Figure 4.17 and from that the oxide thickness can be estimated with the method described above which for this case is 6.6nm. Overall, it is shown that there is very pure iron powder, which provides a good base for evaluation and comparison with the Somaloy 500 powder later examined.

XPS Analysis of the powder fractions

After sieving, the as-received powder was divided to three size fractions and each one them was examined in the XPS. The element concentration is shown in the Tables 4 to 6 below for each fraction.

Table 4: Element content (at%) in the surface of the as received and ion etched state of the +106μm fraction of the ABC100.30 powder

Content[at%]/Element	Fe	O	C	N	Si	Mn
As received	13.2	46.5	36.7	0.3	2.2	1
Etched 1nm	23.1	51.7	23.6	-	0.7	1
2 nm	27.3	51.1	19.6	-	1.1	0.9
3 nm	28.6	49	20	-	1	1.4
4 nm	31.3	46.6	19.1	-	2	1
5 nm	34.9	42	19.3	-	2.8	1
6 nm	40.6	36.6	20	-	1.9	0.9
7 nm	44.9	31	21.2	-	2	1
8 nm	50.2	27.5	21.2	-	-	1.1
10 nm	55.4	22	21.5	-	-	1.1
20 nm	61.5	15.8	21.9	-	-	0.9
30 nm	64.7	12.7	22.3	-	-	0.2

Table 5: Element content (at%) in the surface of the as received and ion etched state of the -106/+53μm fraction of the ABC100.30 powder

Content[at%]/Element	Fe	O	C	N	Si	Mn
As received	12.2	43.3	40.5	0.7	2.4	0.9
Etched 1nm	23.6	51.1	23.1	-	1.1	1.1
2 nm	27.2	51	19.7	-	1.3	0.9
3 nm	29.5	50.1	19.1	-	0.6	0.7

4 nm	32	48	18.5	-	0.8	0.7
5 nm	36	44	18	-	1.2	0.9
6 nm	40.9	38.1	18.9	-	1.2	0.8
7 nm	46.3	32.6	19.2	-	1	0.9
8 nm	49.3	27.7	21.3	-	1.2	0.5
10 nm	56.1	21.7	21.8	-	-	0.4
20 nm	65.4	14.3	20	-	-	0.3
30 nm	64.3	13	22.5	-	-	0.1

Table 6: Element content (at%) in the surface of the as received and ion etched state of the -53µm fraction of the ABC100.30 powder

Content[at%]/Element	Fe	O	C	N	Si	Mn
As received	14.2	48.6	33	1.2	1.8	1.2
Etched 1nm	22	50.7	23.8	-	2.5	1.1
2 nm	27.2	50.3	19.6	-	2.1	0.8
3 nm	29.3	49.6	18.5	-	1.6	0.9
4 nm	31.9	48.1	17	-	2.1	0.9
5 nm	35.7	43.5	17.4	-	2.6	0.9
6 nm	40.9	38.2	18.6	-	1.7	0.7
7 nm	45.7	32.6	19.2	-	1.9	0.7
8 nm	50.2	29.5	19.6	-	-	0.8
10 nm	55.9	22.4	21	-	-	0.7
20 nm	66.1	15.2	18.1	-	-	0.7
30 nm	66.7	13.4	19.7	-	-	0.3

(a)

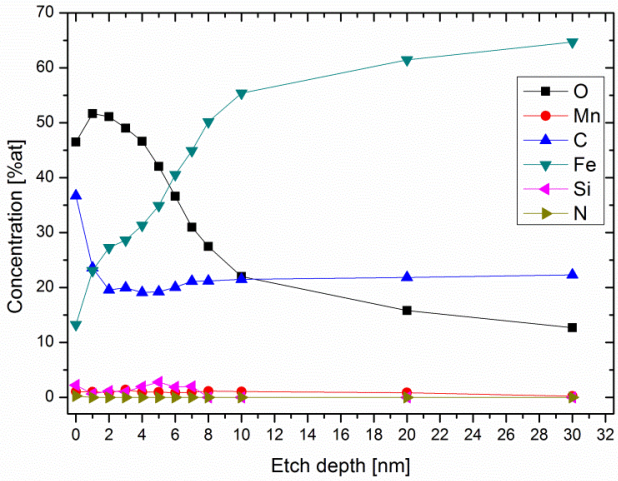

(b)

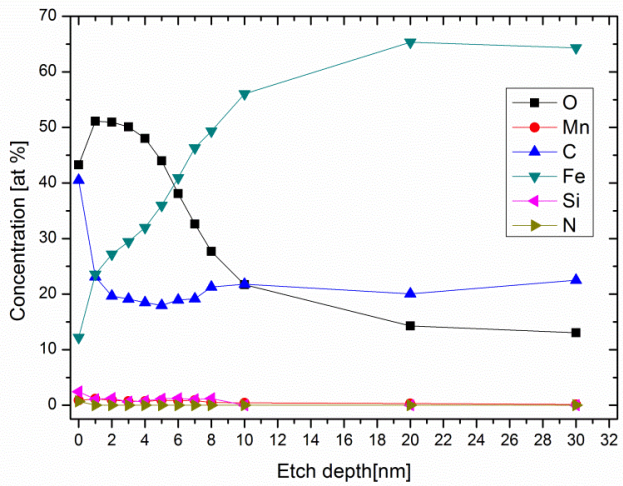

(c)

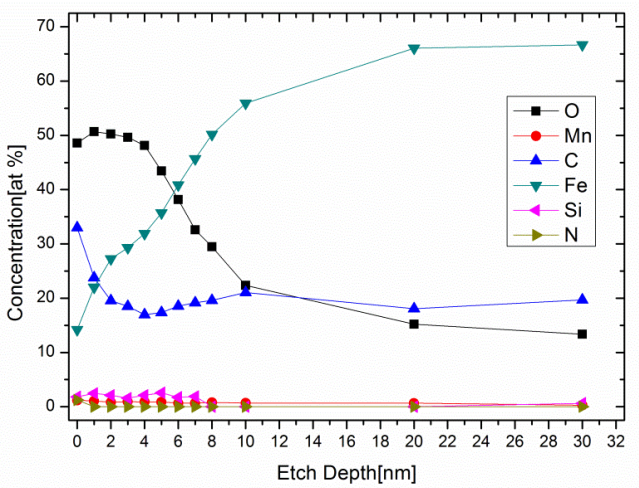

Figure 4.18: The elements content over etch depth for the ABC100.30 powder in the various fractions (a) +106µm (b)-106/+53µm(c) -53µm.

From the tables and the above graphs it is obvious that the fractions show a similar behavior in the elemental concentration profiles with the as-received unsieved powder. The oxide thickness estimations are shown in Figure 4.19.

(a)

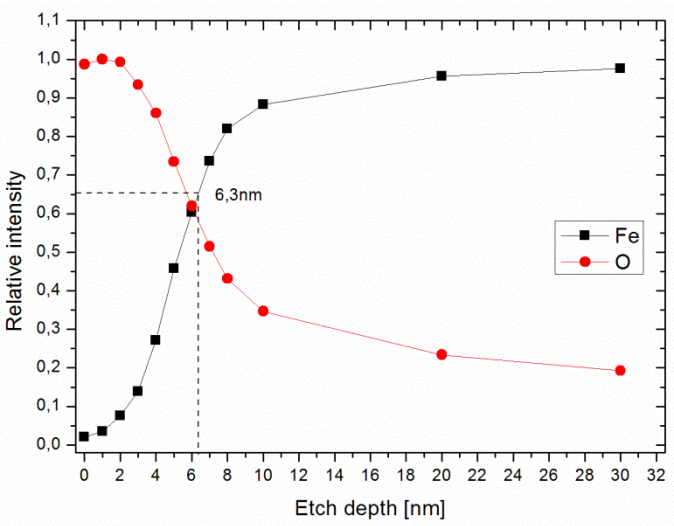

(b)

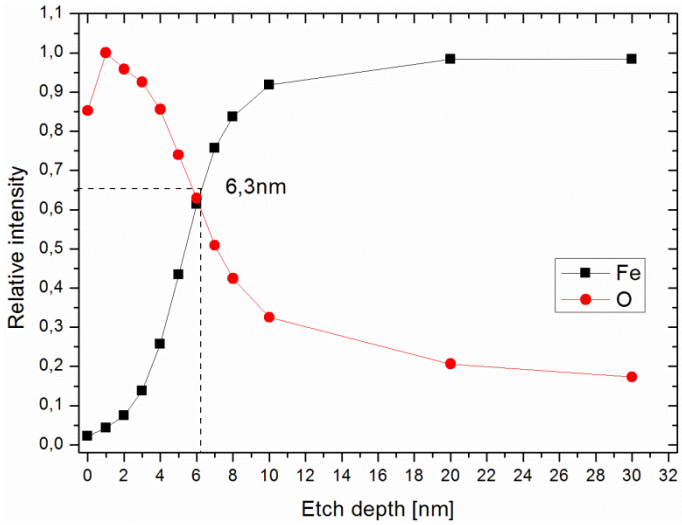

(c)

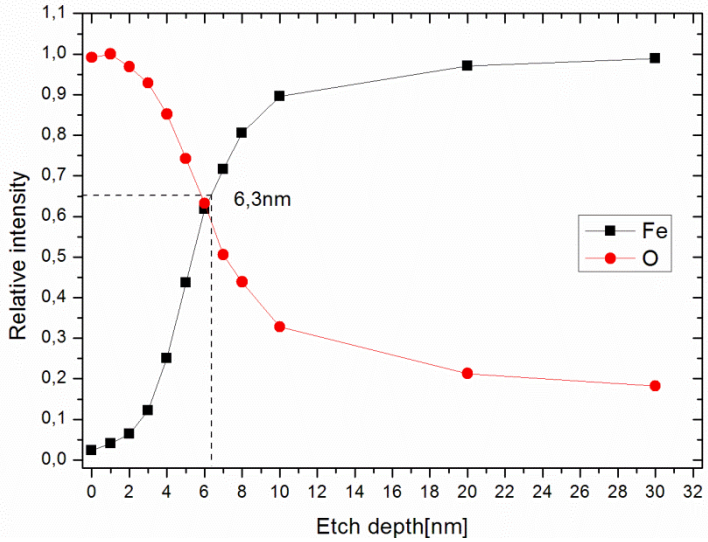

Figure 4.19: Estimation of the surface iron oxide layer using the normalized Fe-metallic (Fe2p peak) and the oxygen (O1s peak) over etch depth for the various fractions of the ABC100.30 powder (a) +106µm (b)106/+53µm(c) -53µm.

The oxide thickness is 6.3nm for all fractions. The results here show that the fractions give a lower contribution in oxide thickness than the unsieved powder which was 6.6nm.

Figure 4.20 shows a high resolution scan at 5nm of etch depth, which is near the oxide/metal interfacial region of the unsieved powder and all three fractions. The intensity is normalized so the scans can be compared without the effect of the analyzing area. The three fractions have higher metallic peaks than the unsieved powder which means lower oxide contribution. Hence, analyzing a wider size distribution means some dispersion effect regarding the thickness estimate.

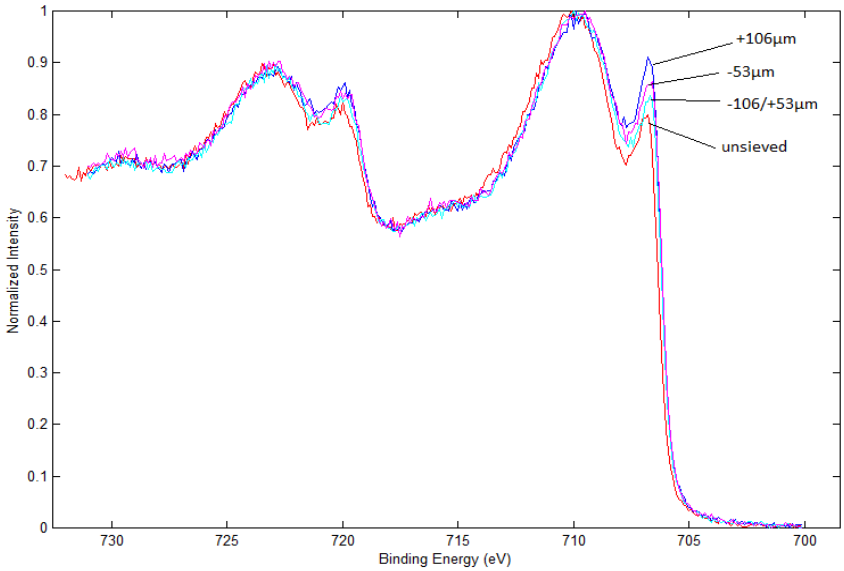

Figure 4.20: XPS high resolution surveys of the ABC100.30 fractions at 5nm etch depth.

SEM and EDX of the as-received powder

In figure 4.21 the Fe particles are displayed. The irregular shape is typical for water atomized powders. The various sizes are also visible in (a) and they range between -53µm to over 200µm (b).

(a) (b)

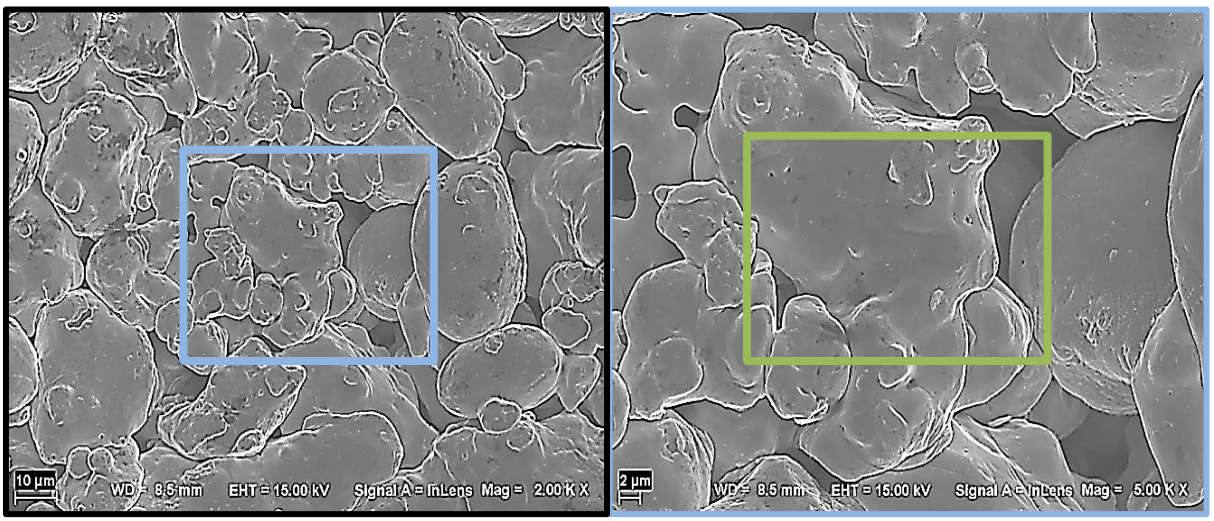

(c) (d)

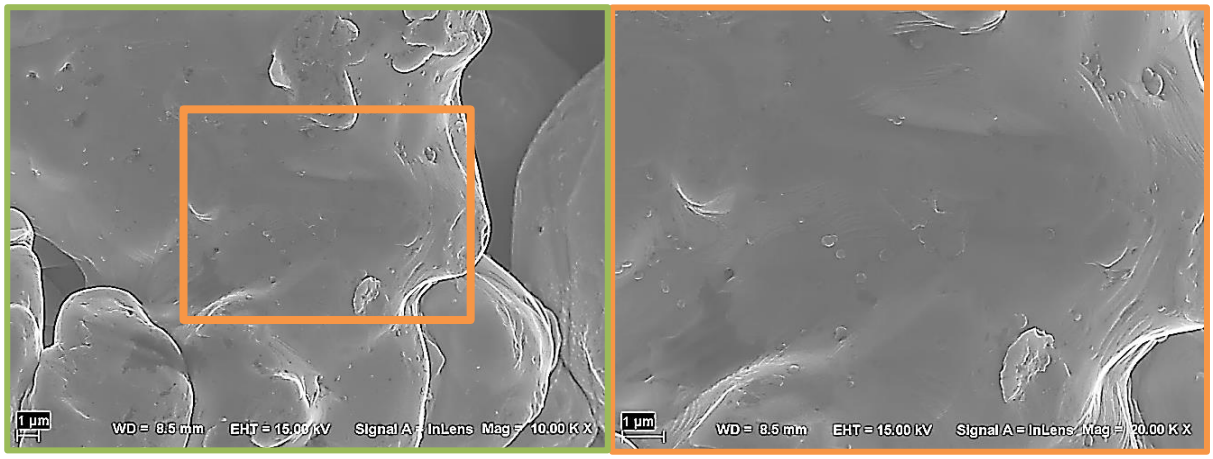

Figure 4.21: Overview of the ABC100.30 as received water atomized powder.

The surface of this powder is also visible on (c) and (d) and as expected is very clear with only some very small particulates which have been characterized in previous studies as particles with different composition [19].
Figure 4.22 shows the appearance of these particulates at higher magnification. The surface appearing on this figure is typical for this type of powder and is observed in a similar manner throughout the powder samples.

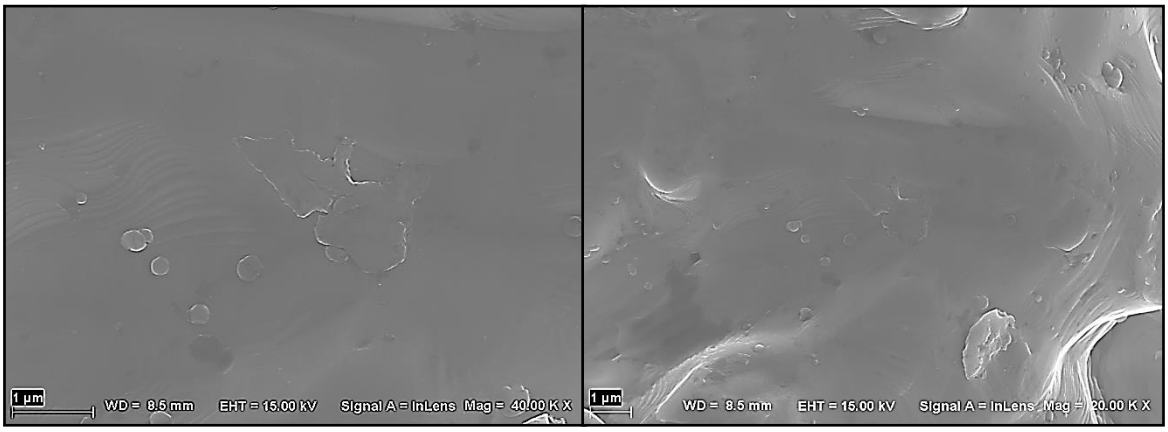

Figure 4.22: Appearance of the particulate features on the powder surface.

EDX analysis was performed to investigate the chemical composition of these particulates. This type of chemical microanalysis is regarded only quantitatively due to the large interaction volume and the geometry of the surface under examination.

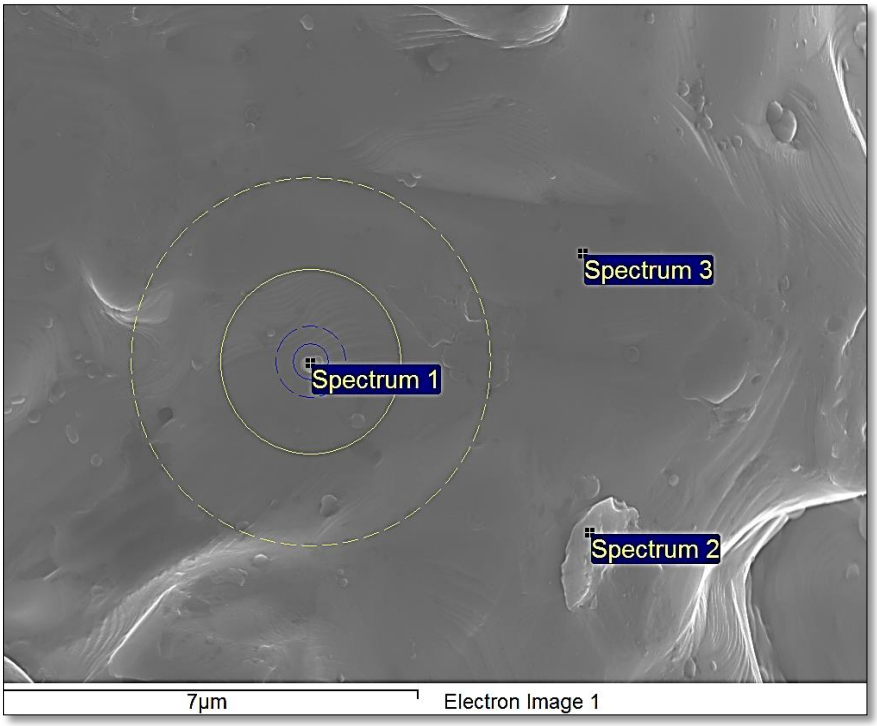

Spectrum[at%]	C	O	Al	Si	Cr	Mn	Fe
Spectrum 1	14.4	19	0.3	1.2	1.4	3.5	60.3
Spectrum 2	27.1	7.1	-	-	-	-	65.8
Spectrum 3	15.4	2.5	-	-	-	-	82.1

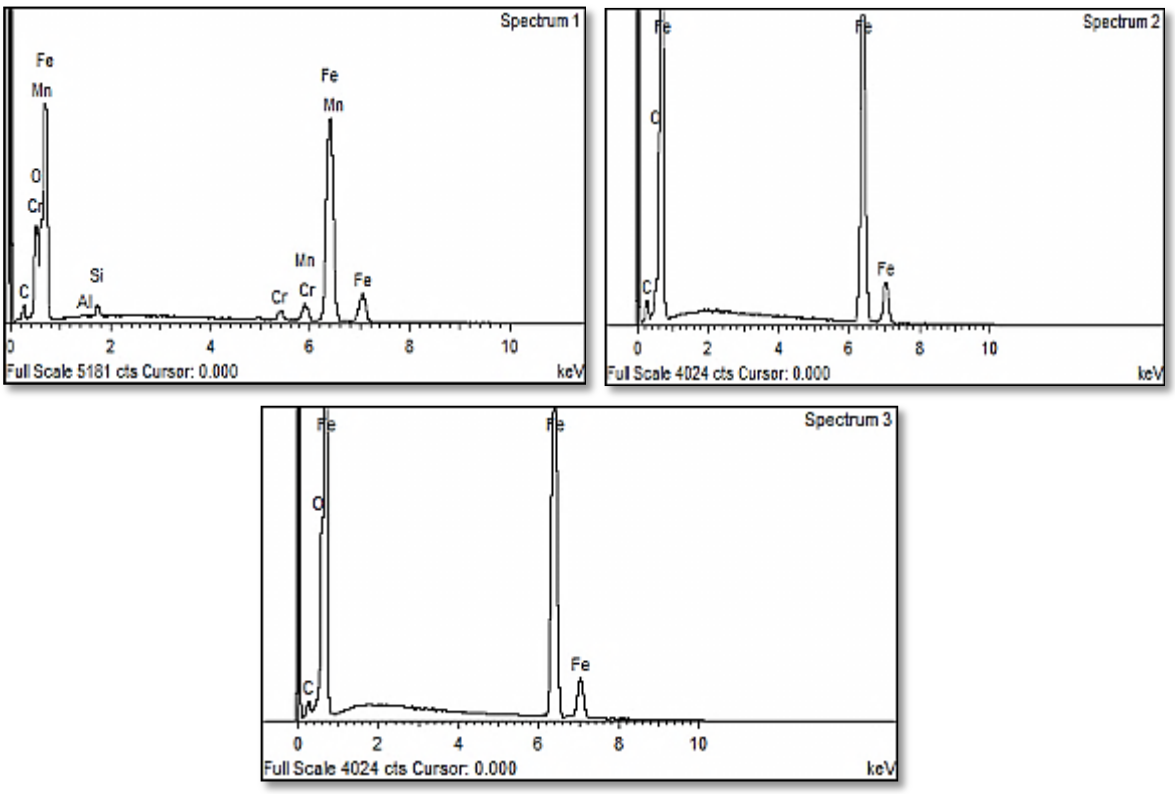

Figure 4.23: SEM image of the powder surface and results of the EDX measurements.

Figure 4.23 shows the EDX analysis performed in various points on the powder surface. The carbon signal appears to be large as a result of the surface contamination.

Spectrum 1 includes some of the small particulates in the interaction volume and it is supposed that these are mostly impurity oxides containing silicon and/or manganese. Spectrum 2 aims at a larger particulate and from the analysis it appears to be an iron oxide whereas spectrum three aim at an area where there are no particulates and the expected iron oxide layer is then detected.

SEM and EDX of the powder fractions

Figure 4.24 shows SEM images at low magnifications of the three sieved fractions at specific particles size ranges as mentioned earlier, in order to show an overview of the samples and to evaluate the quality of the sieving operation.

(a)

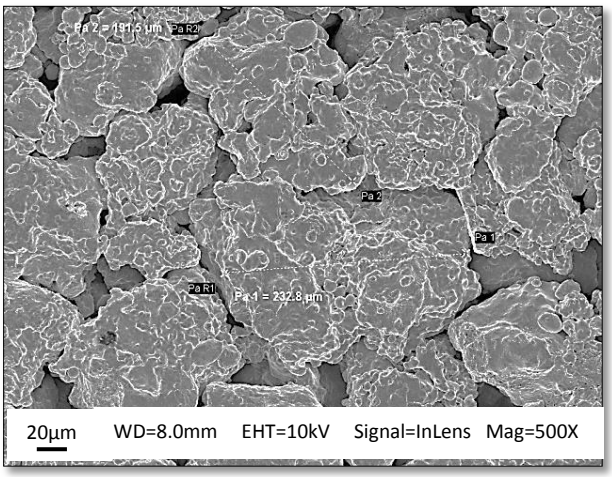

(b)

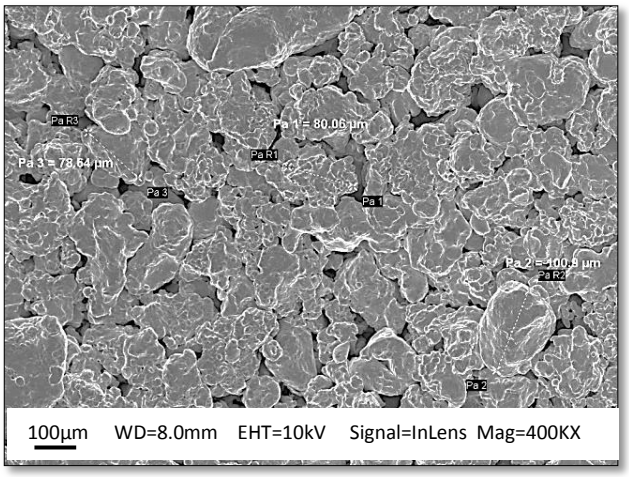

(c)

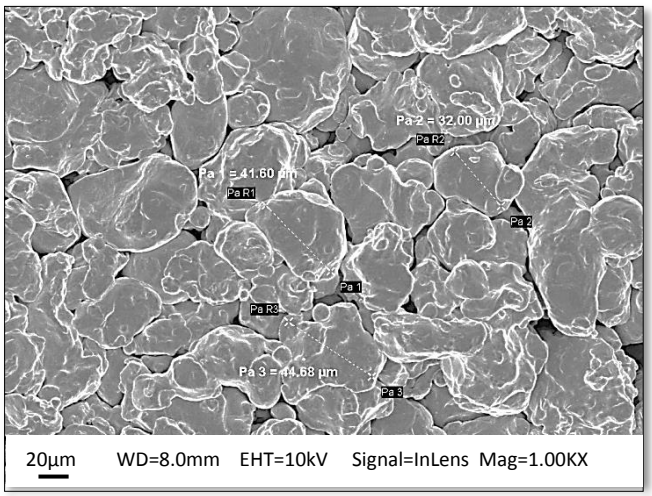

Figure 4.24: SEM overview of the of the ABC100.30 powder (a) +106µm (b)106/+53µm(c) -53µm.

- +106µm

(a) (b)

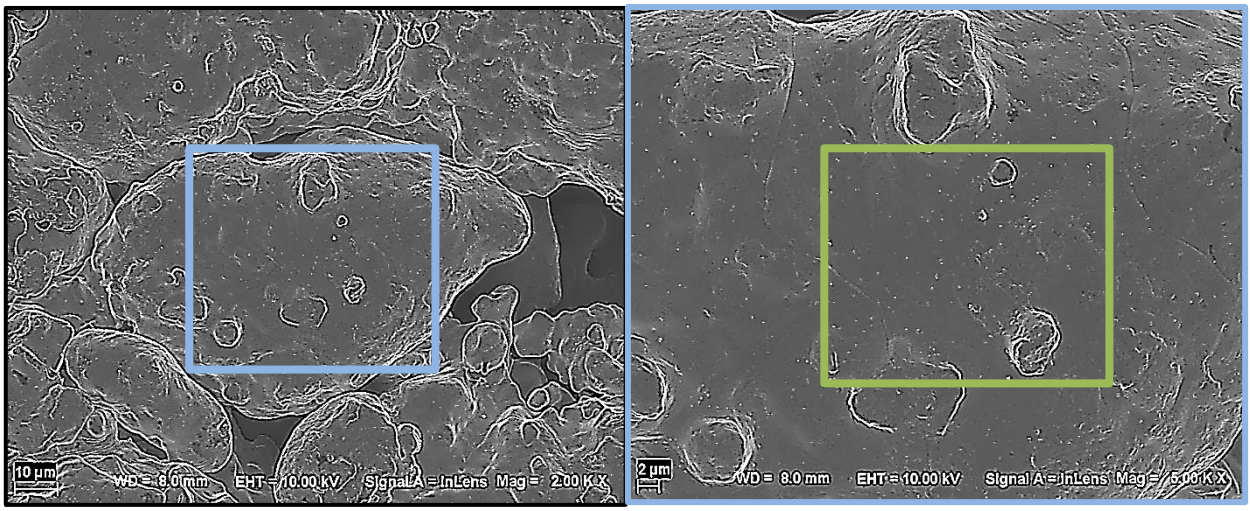

(c) (d)

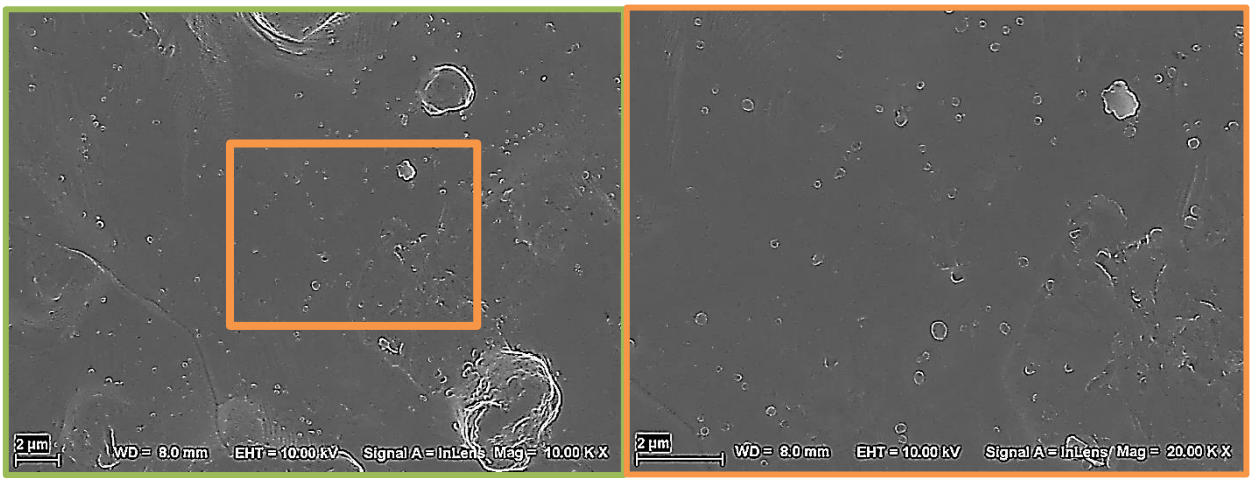

Figure 4.25: Overview of the ABC100.30 +106µm fraction.

- -106/+53µm

(a) (b)

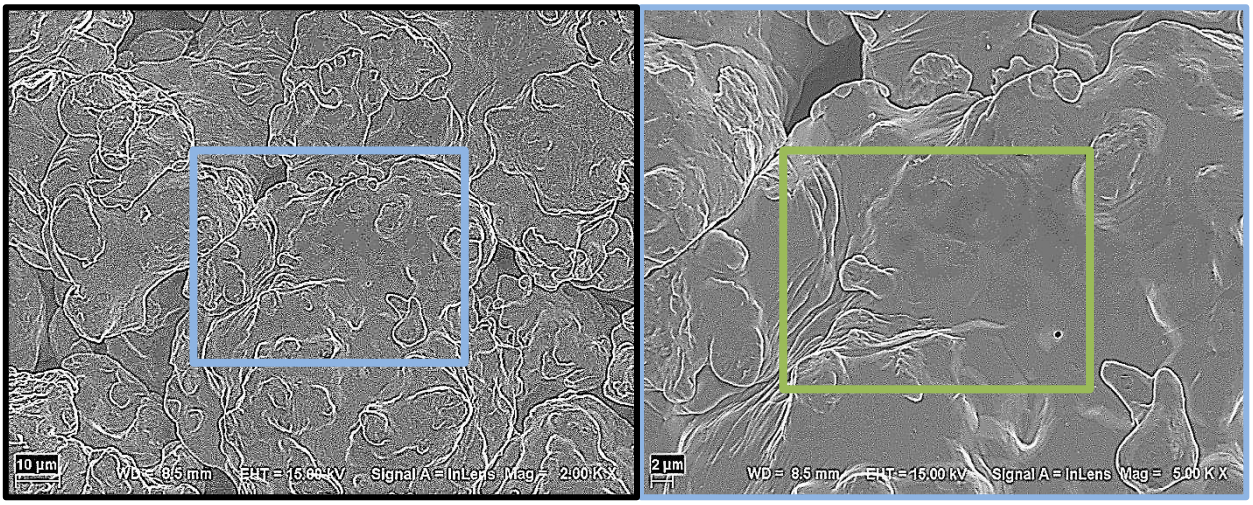

(c) (d)

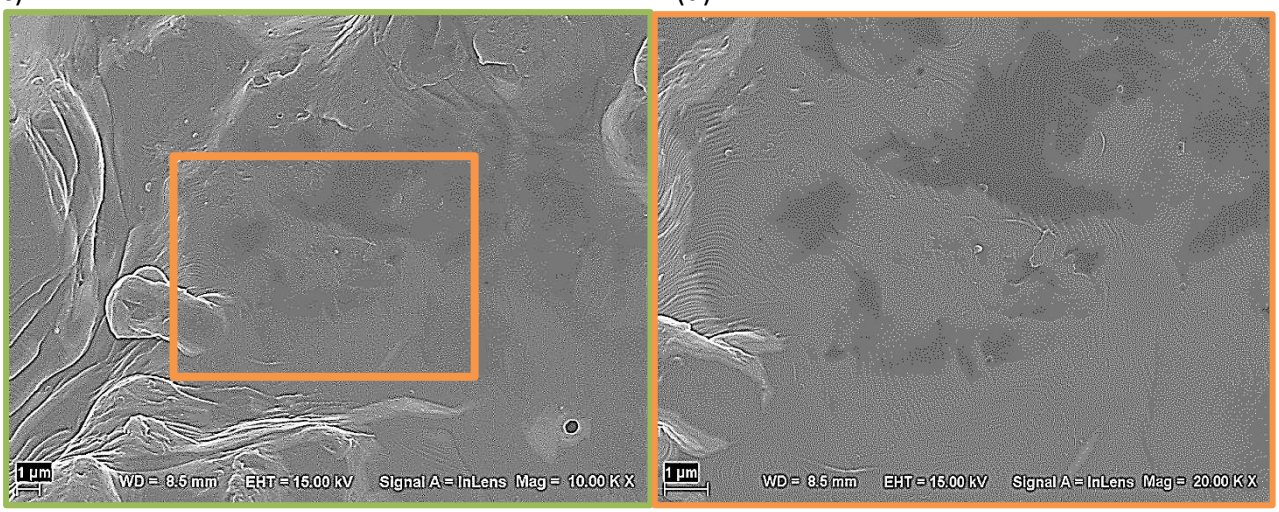

Figure 4.26: Overview of the ABC100.30 -106/+53µm fraction.

- -53µm

(a) (b)

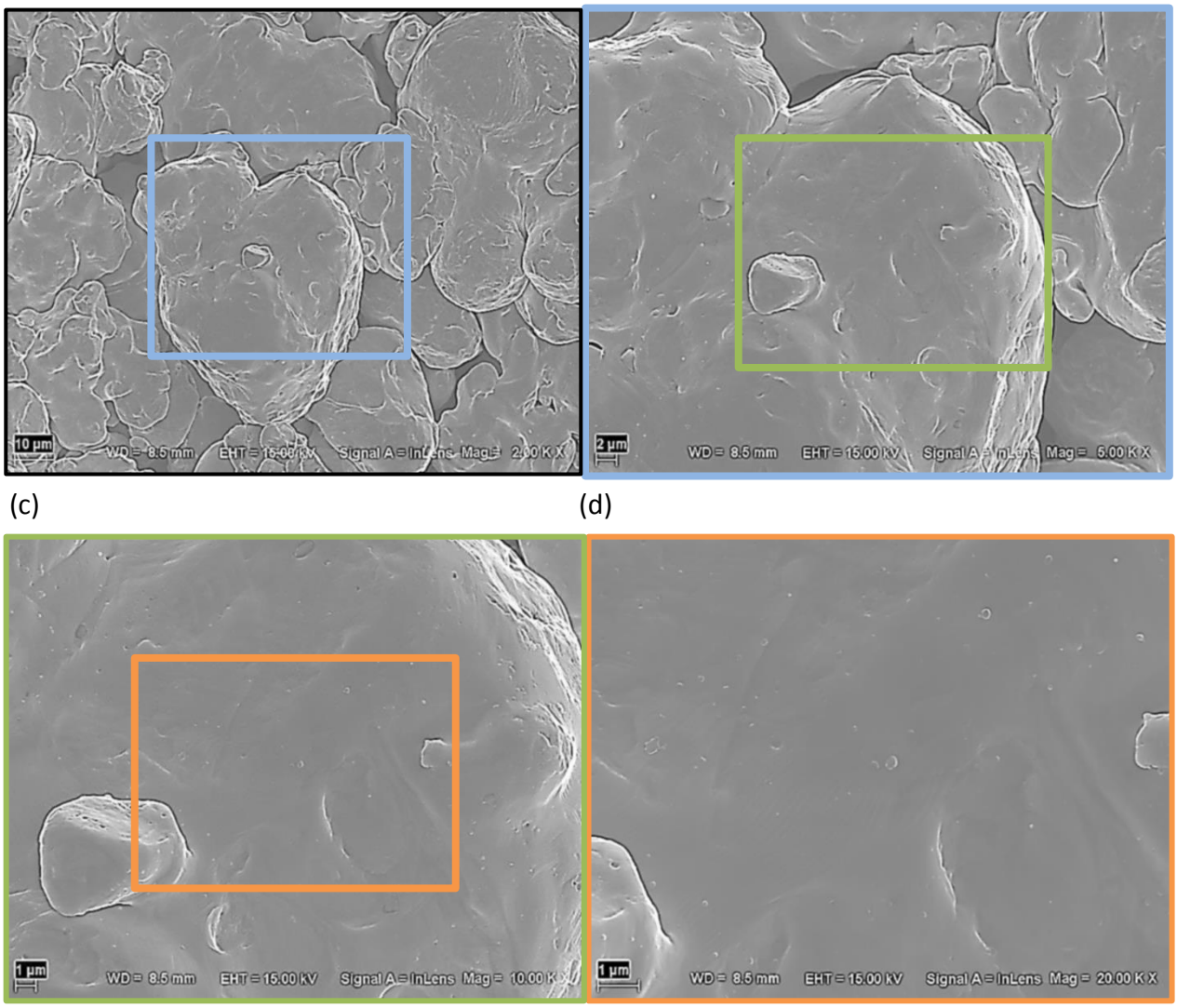

(c) (d)

Figure 4.27 Overview of the ABC100.30 -53µm fraction.

Figures 4.25, 4.26 4.27 show an overview of the ABC100.30 fractions. A smooth surface is shown with only the same small particulates appearing as before. The EDX analysis performed reveals that the particulates are silicon and manganese based oxides but most of the powder surface is ok and smooth. On those smooth surface regions the EDX chemical microanalysis shows concentration of iron, carbon as contaminant and some oxygen from surface oxides (Fig 4.28, 4.29 4.30).

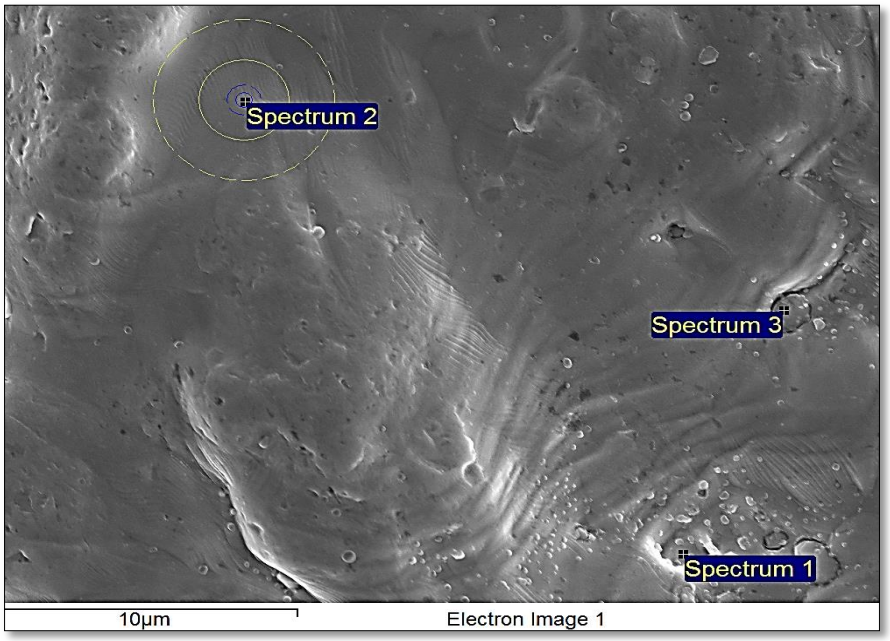

Spectrum[at%]	C	O	S	Mn	Fe
Spectrum 1	13.8	5	-	0.5	80.7
Spectrum 2	25.6	2.7	-	-	71.7
Spectrum 3	20.3	4.5	19	18.9	37.4

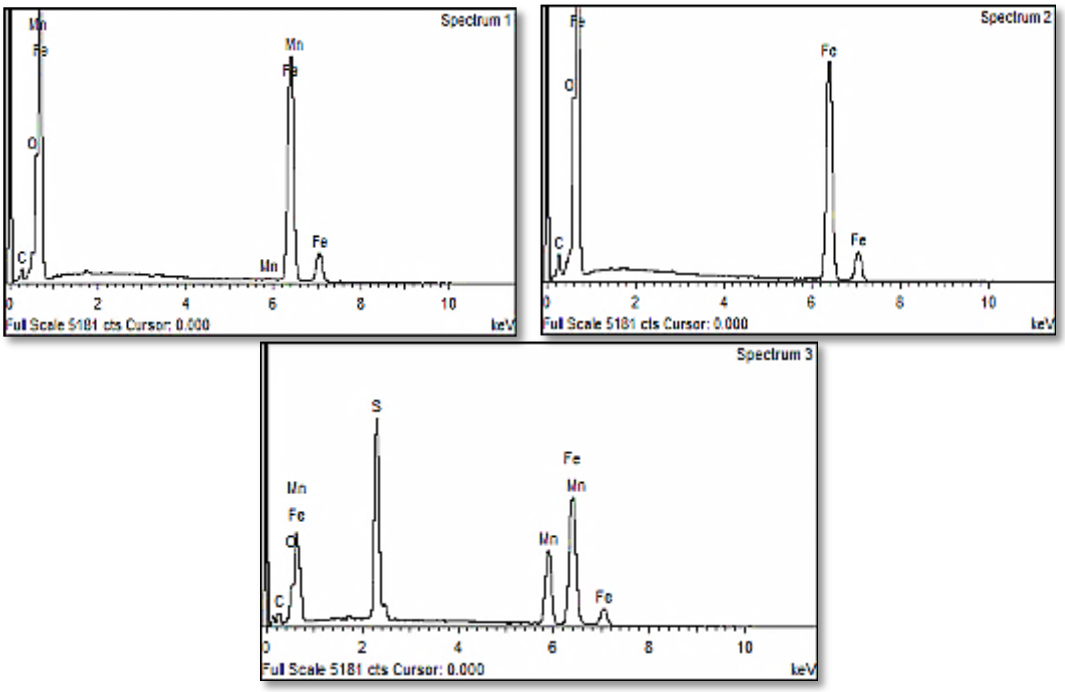

Figure 4.28: SEM image of the powder surface and results of the EDX measurements.

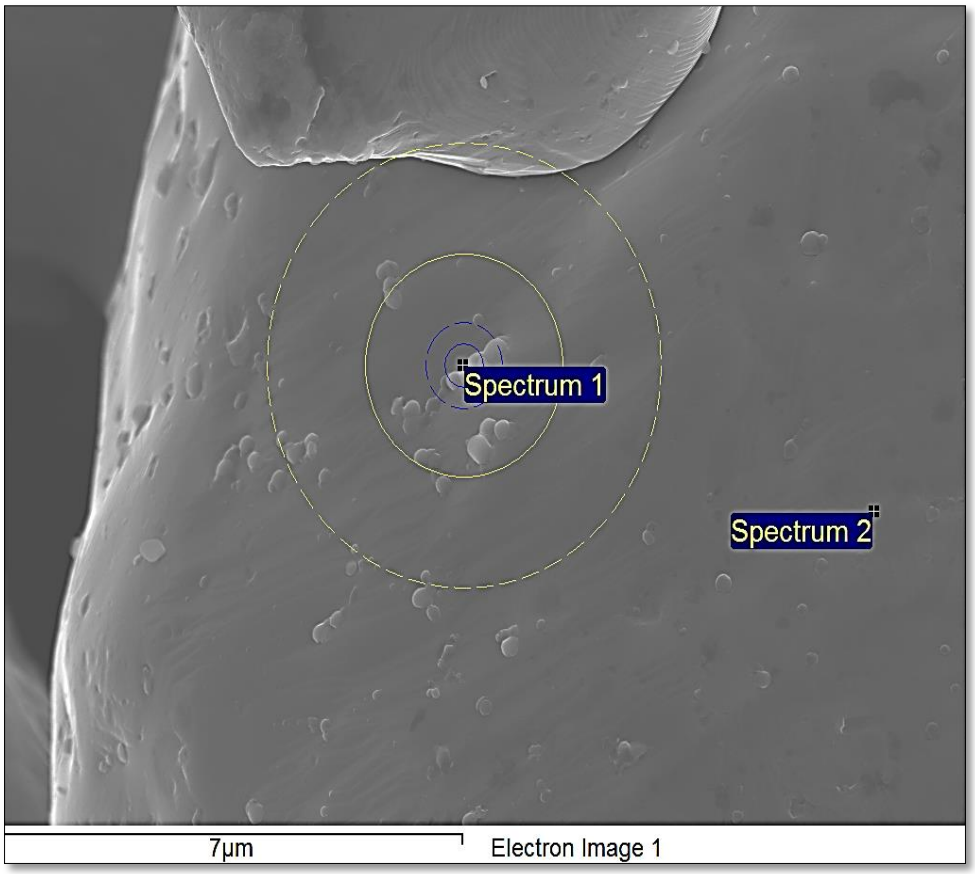

Spectrum[at%]	C	O	Mn	Fe
Spectrum 1	21	6.4	0.4	72.2
Spectrum 2	22.4	3		74.7

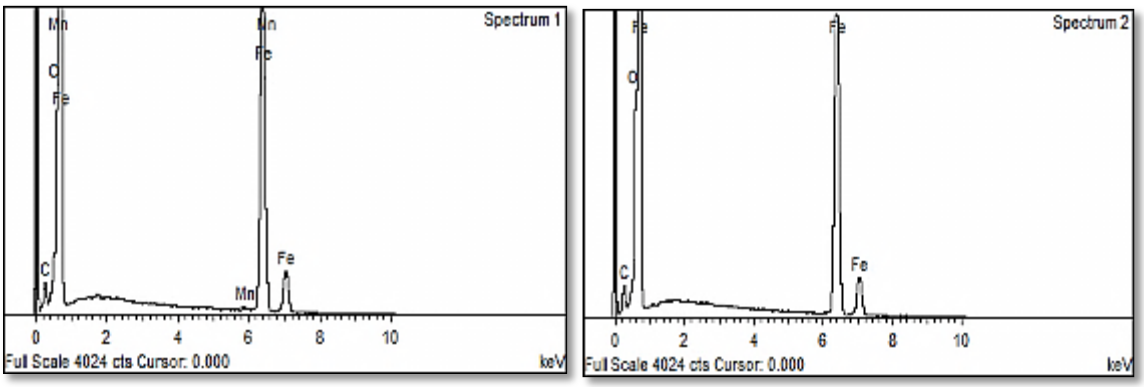

Figure 4.29: SEM image of the powder surface and results of the EDX measurements.

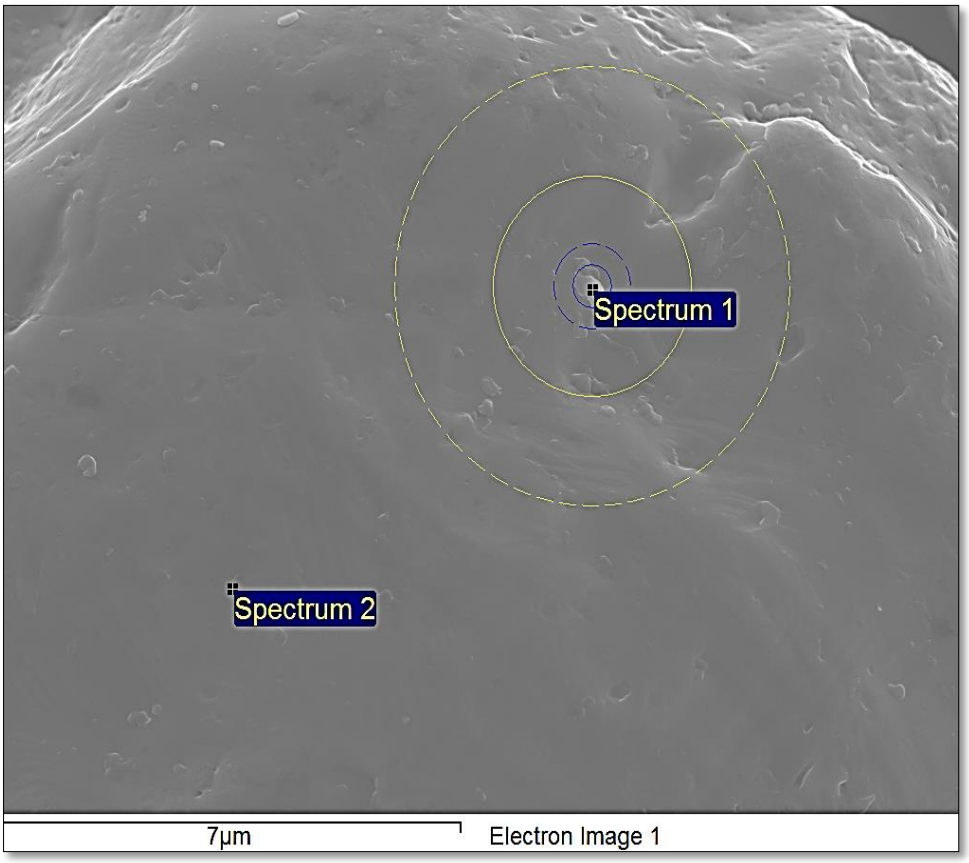

Spectrum[at%]	C	O	Mn	Fe
Spectrum 1	26	10.1	0.4	63.5
Spectrum 2	30.2	2.8	-	67

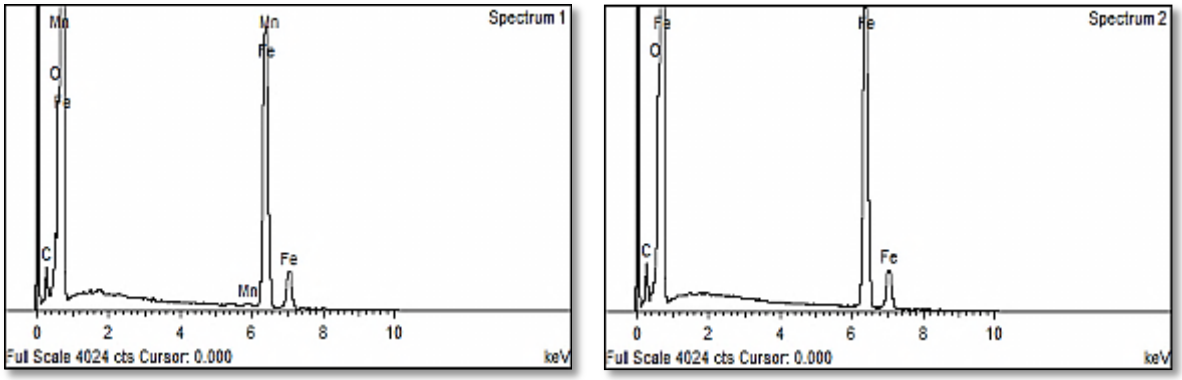

Figure 4.30: SEM image of the powder surface and results of the EDX measurements.

4.3 Analysis of the gas atomized iron powder

- As received

XPS analysis of the powder fractions

The condition of the as received powder was not suitable for examination in terms of particle size distribution, thus a high estimation error would be expected in all our analyses that would give no significant information. Hence, only the sieved fractions were examined. The composition of the grade is similar to the ABC100.30 with iron, oxygen as the main elements and some impurity elements also present. Carbon exists as surface contaminant (eg. hydrocarbon) at first and then the signal remains constant due to the carbon tape that the powder is mounted on. The progress of the elemental apparent atomic concentration and their plots appear below.

Table 7: Element content (at%) in the surface of the as received and ion etched state of the +106μm fraction of the gas atomized powder

Content[at%]/Element	Fe	O	C	N	Si	Mn	Na
As received	11	40.7	43.6	1.3	2.4	0.3	0.6
Etched 1nm	29.8	57.2	9.9	-	2.4	0.4	0.4
2 nm	30.1	54.3	15.6	-	-	-	-
5 nm	34.3	53	12.7	-	-	-	-
10 nm	42.7	44.8	12.6	-	-	-	-
15 nm	48.9	38.5	12.6	-	-	-	-
20 nm	52.8	34.8	12.4	-	-	-	-
25 nm	55.1	32.6	12.2	-	-	-	-
30 nm	55.7	31	13.3	-	-	-	-
40 nm	60.5	28.8	10.7	-	-	-	-
50 nm	62.2	26.7	11.1	-	-	-	-
70 nm	65.8	22.2	12	-	-	-	-
100 nm	69.9	18.4	11.7	-	-	-	-

Table 8: Element content (at%) in the surface of the as received and ion etched state of the -106/+53μm fraction of the gas atomized powder

Content[at%]/Element	Fe	O	C	N	Si	Mn	Na
As received	12.8	44.1	40.3	0.6	1.4	0.2	0.8
Etched 1nm	25	55.5	17.1	0.2	2	-	0.2
5 nm	32.5	54.7	10.8	-	1.8	-	0.2
10 nm	43	46.4	8.6	-	1.3	-	0.1
15 nm	50.2	40.1	8.4	-	1.8	-	-
20 nm	54.9	35.7	7.6	-	0.5	-	-
25 nm	58.5	34	7	-	1	-	-
30 nm	60.9	31.5	6.6	-	-	-	-
40 nm	64.6	29.6	5.9	-	-	-	-
50 nm	67	26.1	6.9	-	-	-	-
70 nm	71.4	22.4	6.2	-	-	-	-
100 nm	75.6	18.1	6.4	-	-	-	-

Table 9: Element content (at%) in the surface of the as received and ion etched state of the -53µm fraction of the gas atomized powder

Content[at%]/Element	Fe	O	C	N	Si	Mn	Na
As received	13.4	42.5	38	0.3	1.9	0	0.9
Etched 1nm	26.2	54.7	17.4	-	1.2	0.3	0.3
2 nm	31.4	54.5	11.9	-	1.4	0.3	0.5
3 nm	32.3	53.6	10.9	-	2.4	0.3	0.5
4 nm	32.7	53.3	11.2	-	2.1	0.3	0.4
5 nm	33.8	52	11	-	2.8	0.3	0.2
6 nm	35.8	51.3	10.5	-	2.2	0.2	-
10 nm	41.5	46.1	10	-	2.2	0.2	-
15 nm	51	38.8	8.4	-	1.7	0.1	-
20 nm	57.1	32.5	8.8	-	1.6	-	-
25 nm	62.5	28.6	7.5	-	1.5	-	-
30 nm	62.8	25.5	10.3	-	1.3	-	-
40 nm	71.6	21.6	6.8	-	-	-	-
50 nm	73.8	18.4	7.8	-	-	-	-
60 nm	74.9	17.1	8	-	-	-	-

(a)

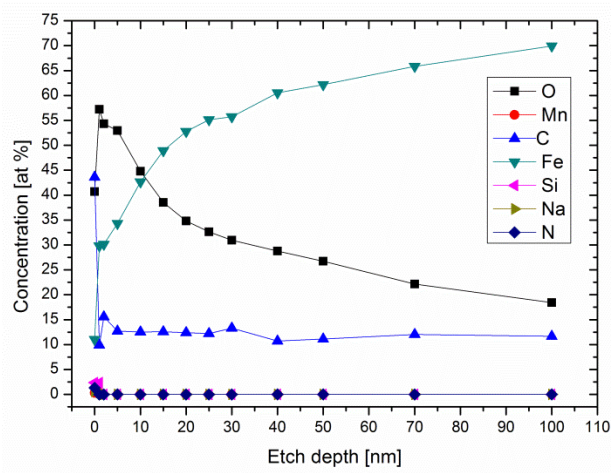

(b)

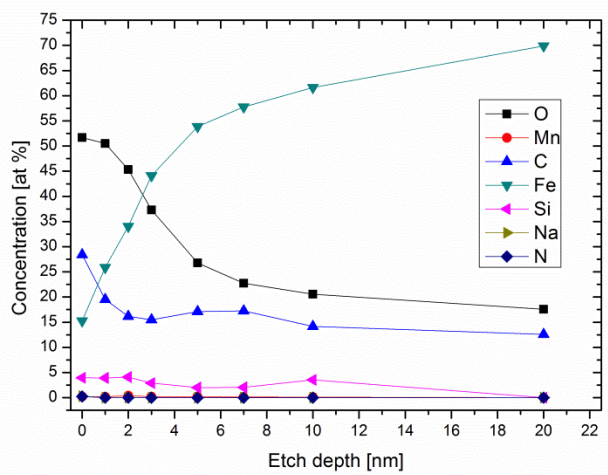

(c)

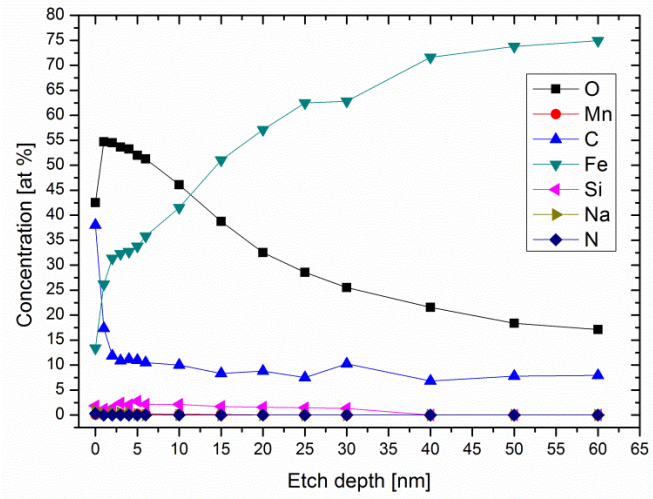

Figure 4.31: The element content over etching depth for the gas atomized powder of the various fractions (a) +106µm (b)106/+53µm(c) -53µm.

For the +106µm fraction iron goes up to almost 70% after extended ion etching whereas in the other two cases it reaches to 75%. From the etching depth it appears that this powder has thicker oxide than the ABC100.30 and more etch steps were needed to get a clear iron signal.

Typical XPS spectra at different etch depths are shown in Figure 4.32. All three fractions appear to have similar behavior.

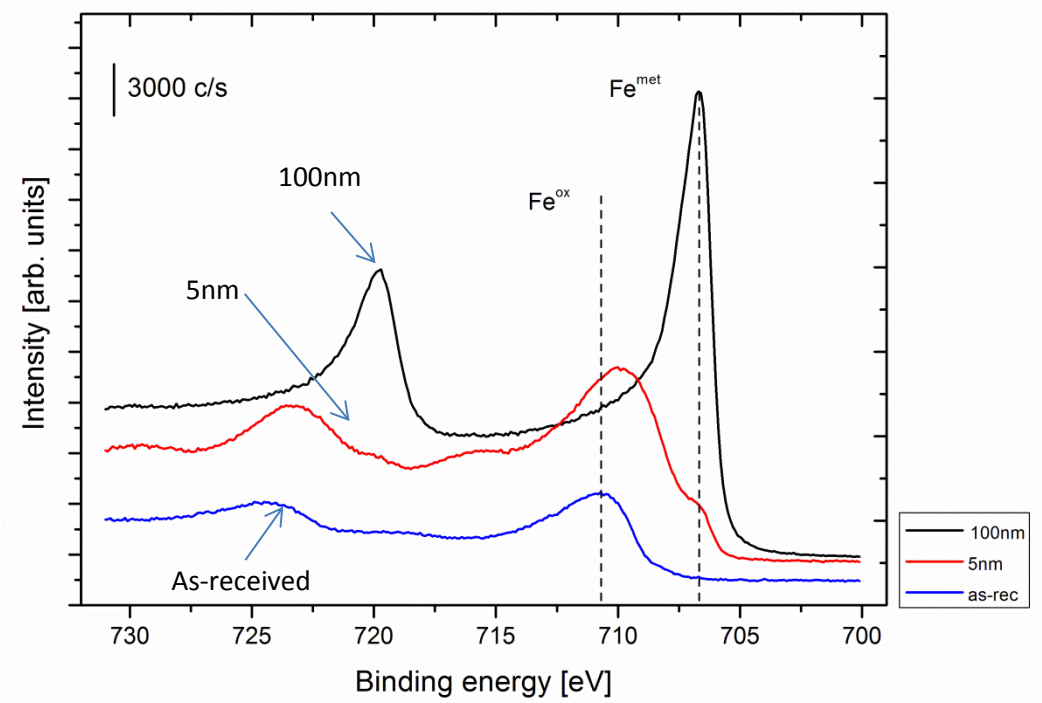

Figure 4.32: XPS spectra in as-received state and etch depths of 5nm and 100nm for the middle fraction (+106/-53µm) of the gas atomized powder. Other fractions exhibit similar behavior when etched.

Using curve fitting the iron signal contributions are determined. The iron peak with a binding energy of 706.6 eV in all fractions is in very good agreement with the iron foil standard along with the signals for the Fe^{3+} contribution and the Fe^{2+} contribution (Fig 4.33).

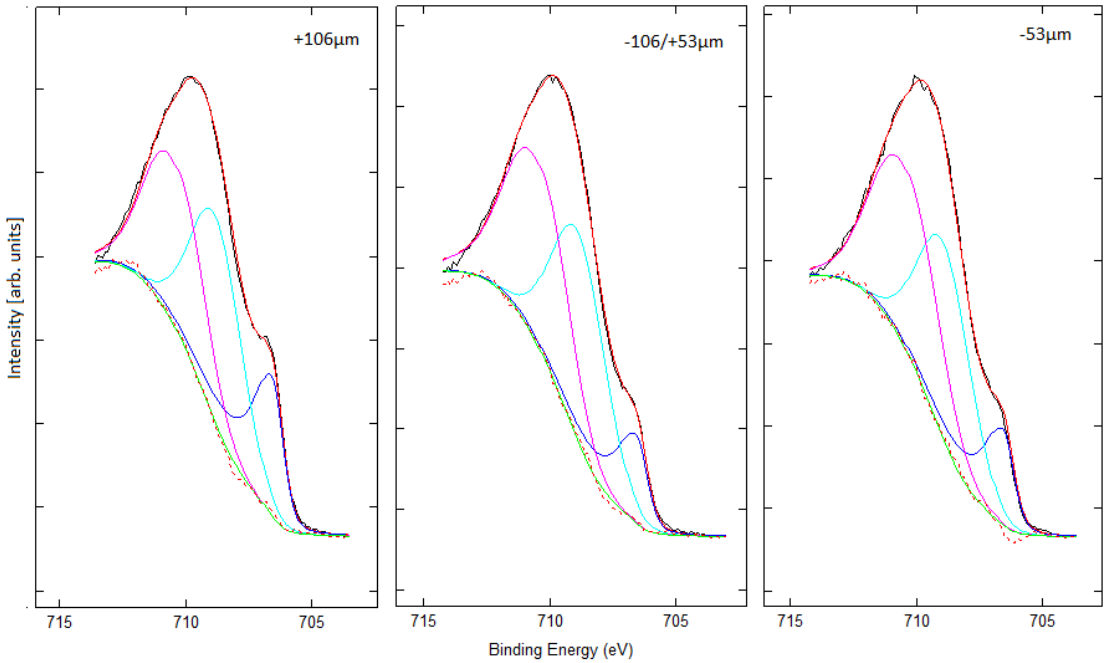

Figure 4.33: Analysis of chemical state of iron with the help of curve fitting for the 5nm etch depth. The metal state is the small peak on the right side of the figures and the rest are peaks for the iron oxides.

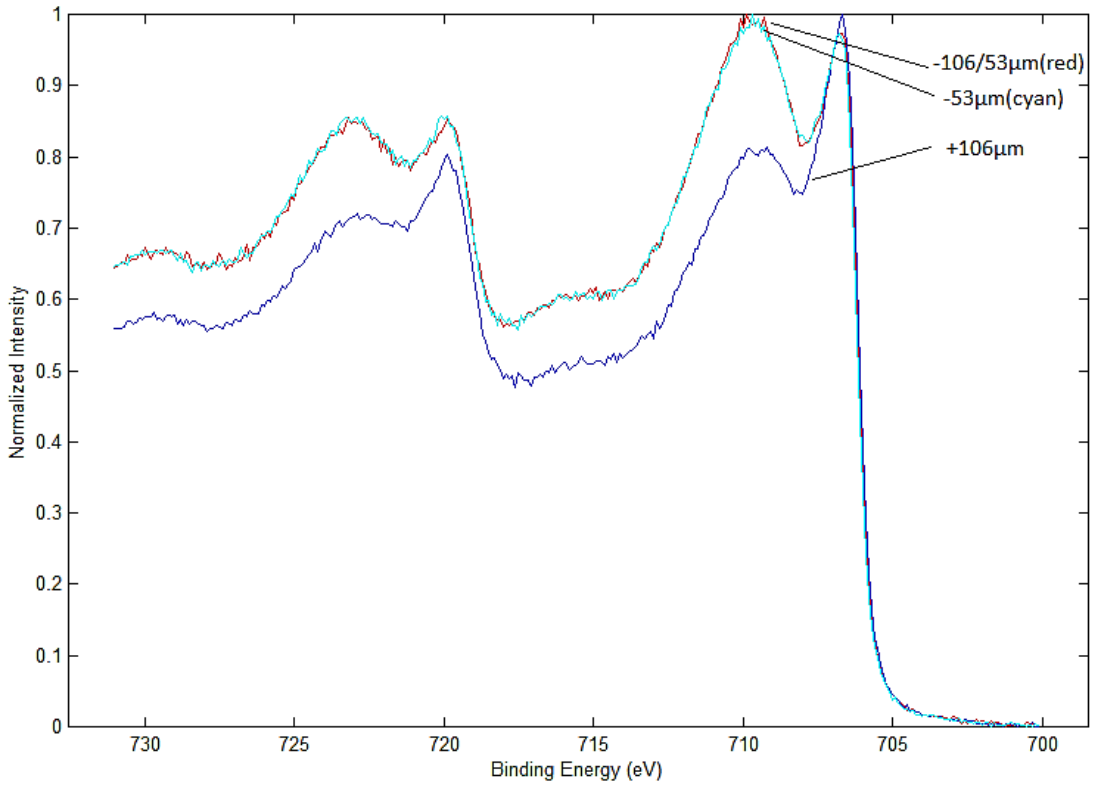

Figure 4.34: XPS high resolution spectra of gas atomized of different as received fractions after 10nm of ion etching.

Figure 4.34 shows a comparison between the three fractions. It is clear from the figures above that the +106µm fraction appears to have a slight higher metallic peak and a lower oxidic one so less oxide thickness is expected. Using the metallic peak intensity the oxide thickness was calculated and is 12.3nm for the +106µm fraction, 14.7nm for the middle fraction and 14nm for the -53µm fraction (figure 4.35).

(a)

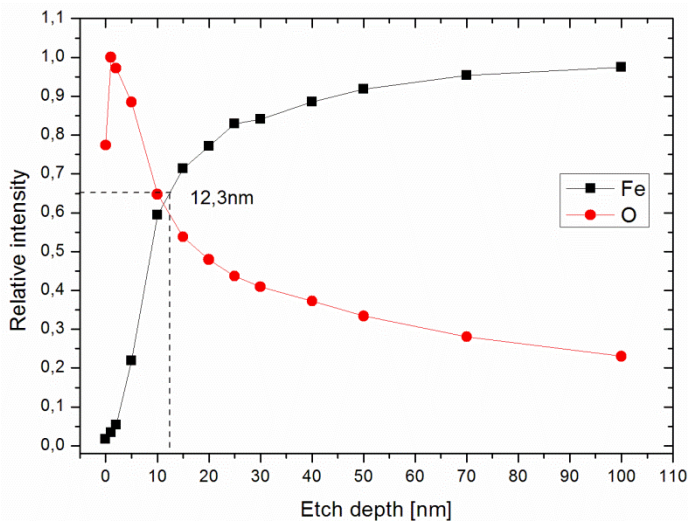

(b)

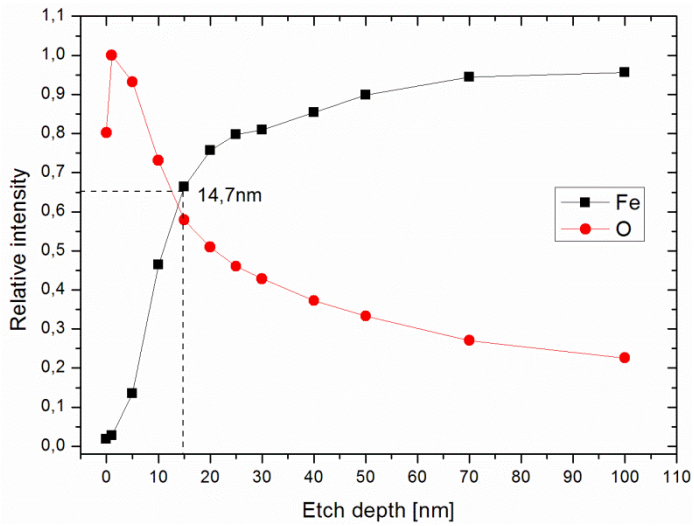

(c)

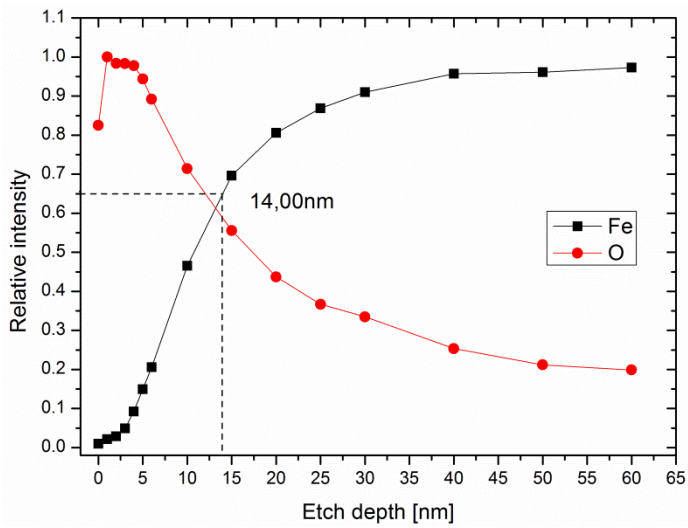

Figure 4.35: Estimation of the surface iron oxide layer using the normalized Fe-metalic (Fe2p peak) and the oxygen (O1s peak) over etching depth for the various fractions of the gas atomized powder (a) +106µm (b)106/+53µm(c) -53µm.

SEM and EDX

Below are shown overview SEM images of the three fractions with specific particles size measured to help determine the quality of the sieving and size distribution of the fractions. The spherical particles are typical for gas atomized powder.

(a)

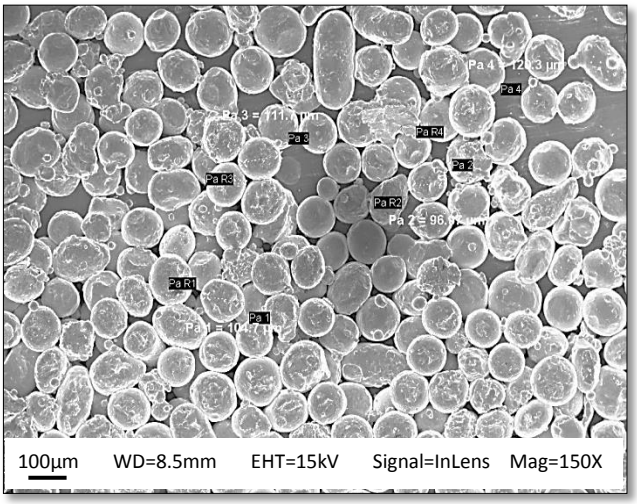

(b)

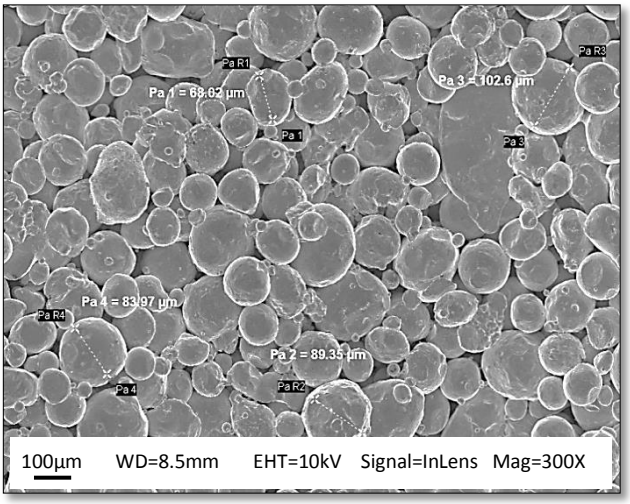

(c)

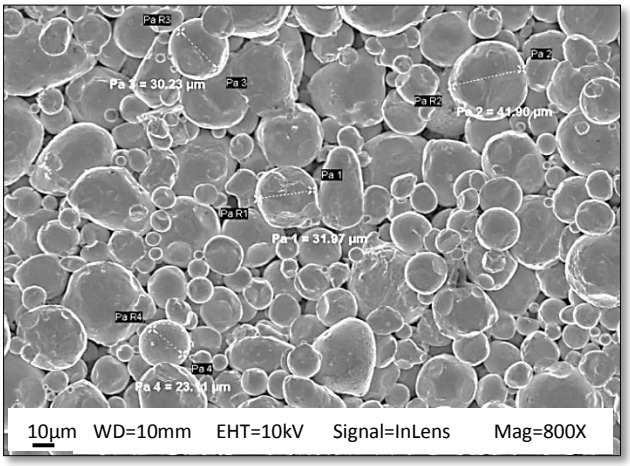

Figure 4.36: SEM overview of the of the as-received gas atomized powder (a) +106µm (b)106/+53µm(c) -53µm.

A first look at this powder revealed a few heavily oxidized particles like the one showing in figure 4.37 at high magnification. The thick oxide layer appears to be fractured and scattered with a clear surface appearing below.

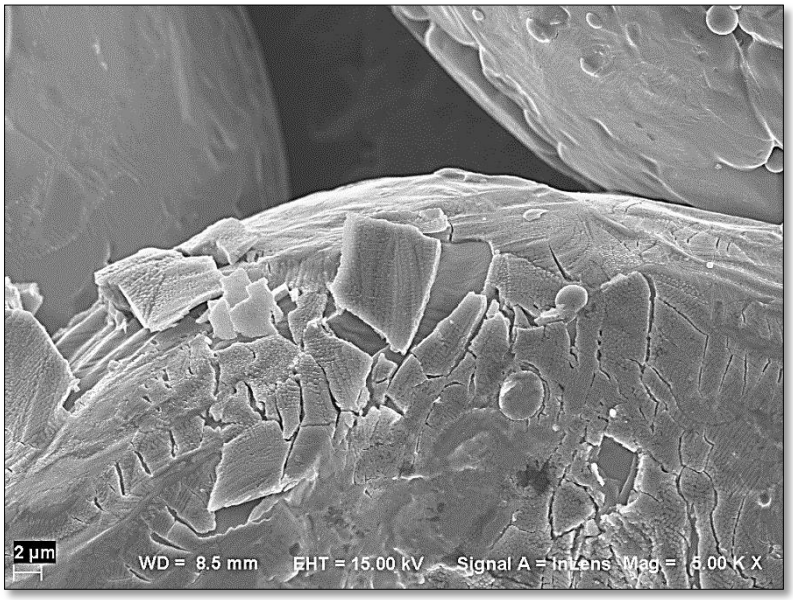

Figure 4.37: Gas atomized powder particle in the as received state.

A more representative appearance of this powder is shown in the SEM images of the various fractions below.

- +106µm

(a) (b)

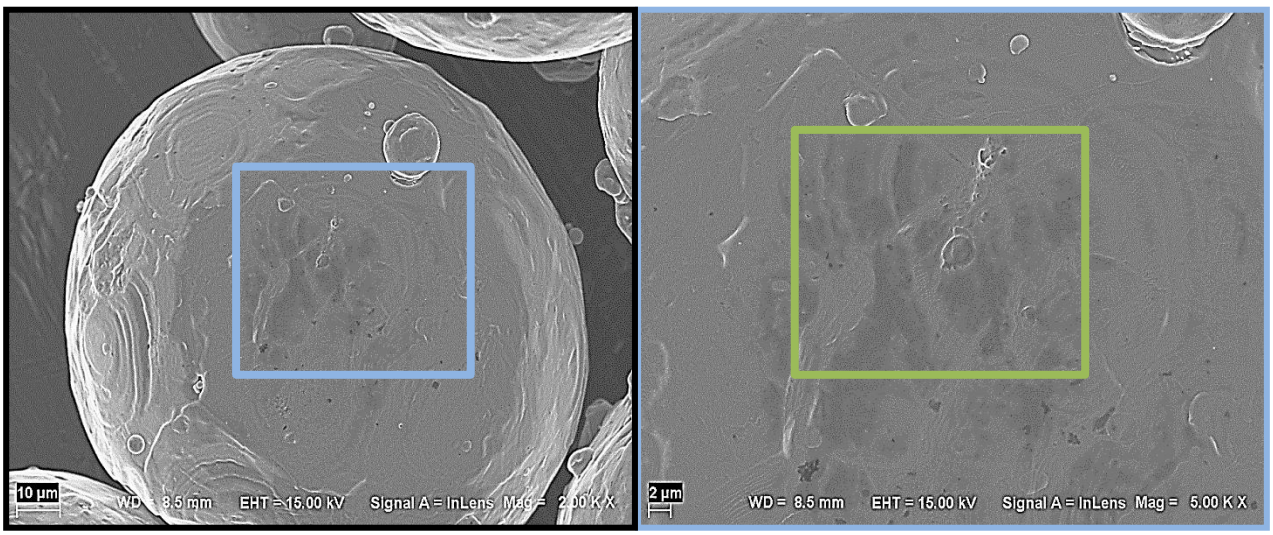

(c) (d)

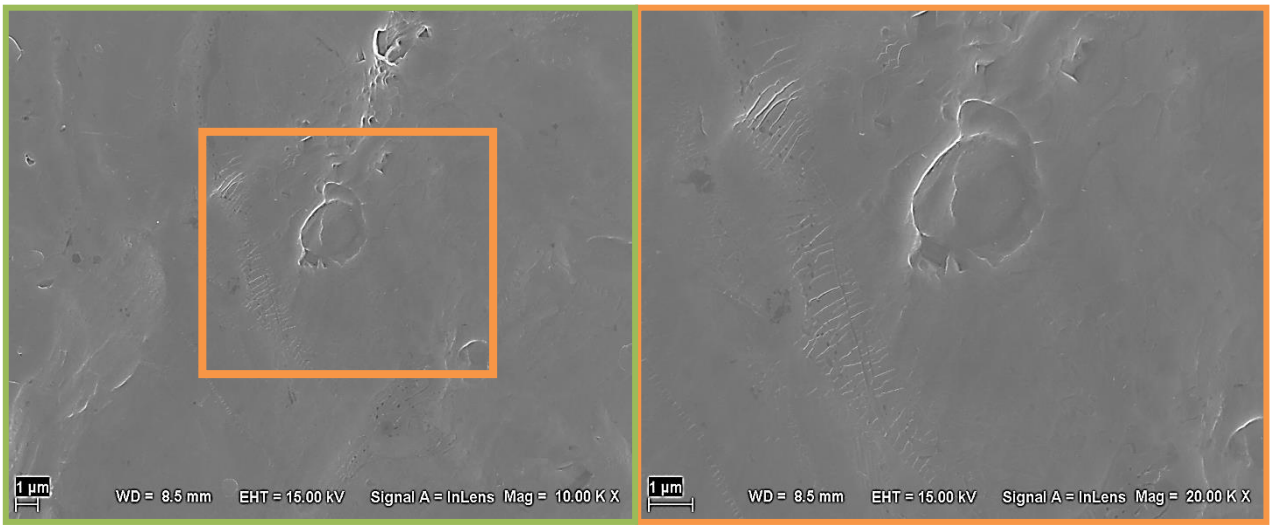

Figure 4.38: Overview of the gas atomized powder in as received state: +106µm fraction.

- -106/+53µm

(a) (b)

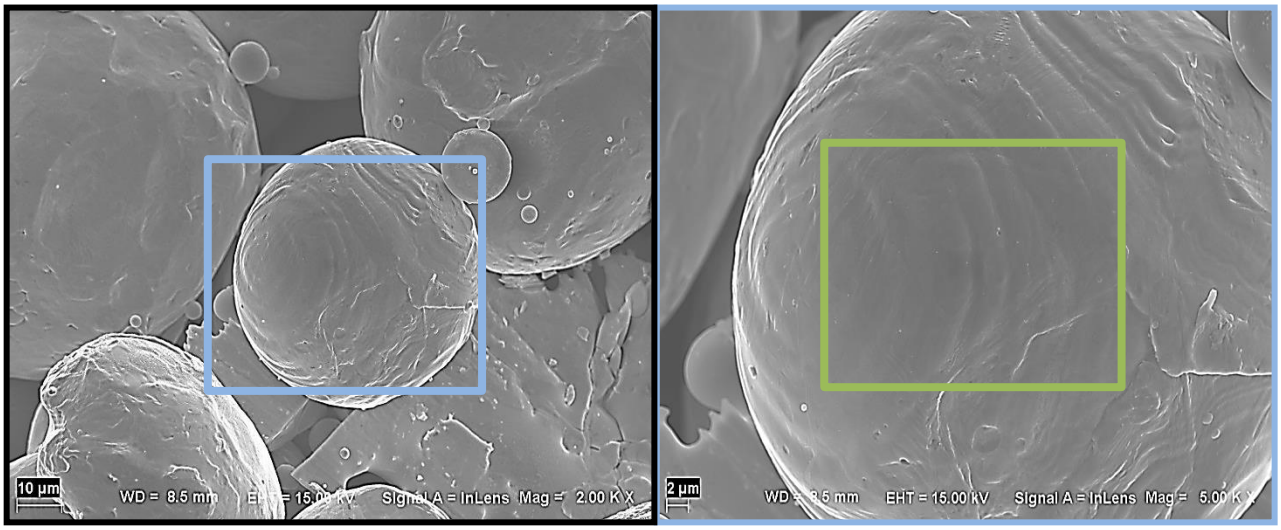

(c) (d)

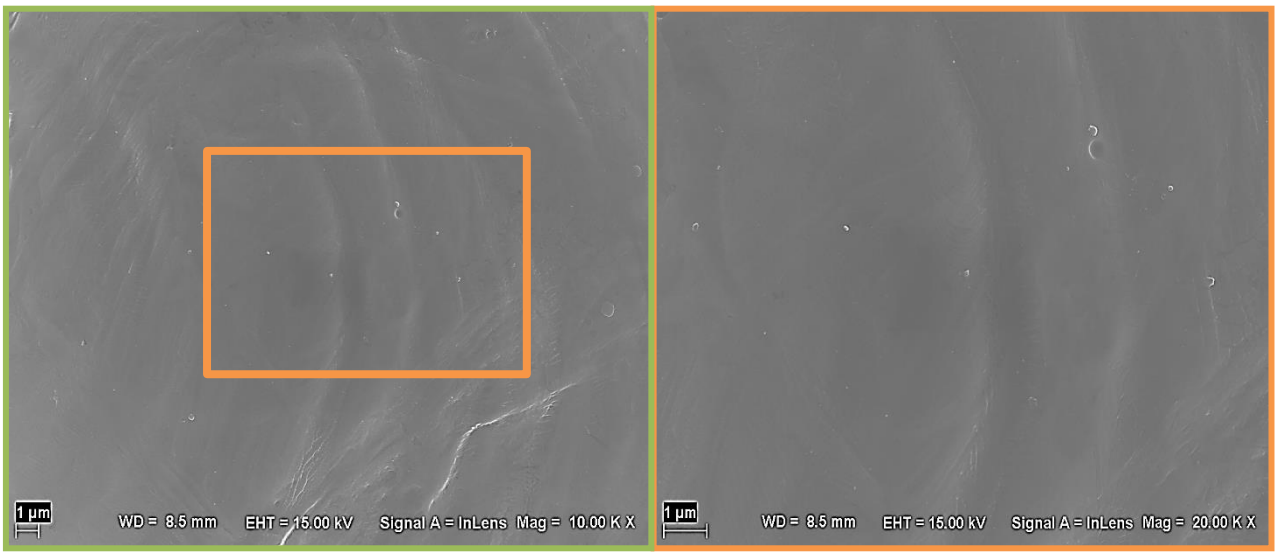

Figure 4.39: Overview of the gas atomized powder in as received state:-106/+53µm fraction.

- -53µm

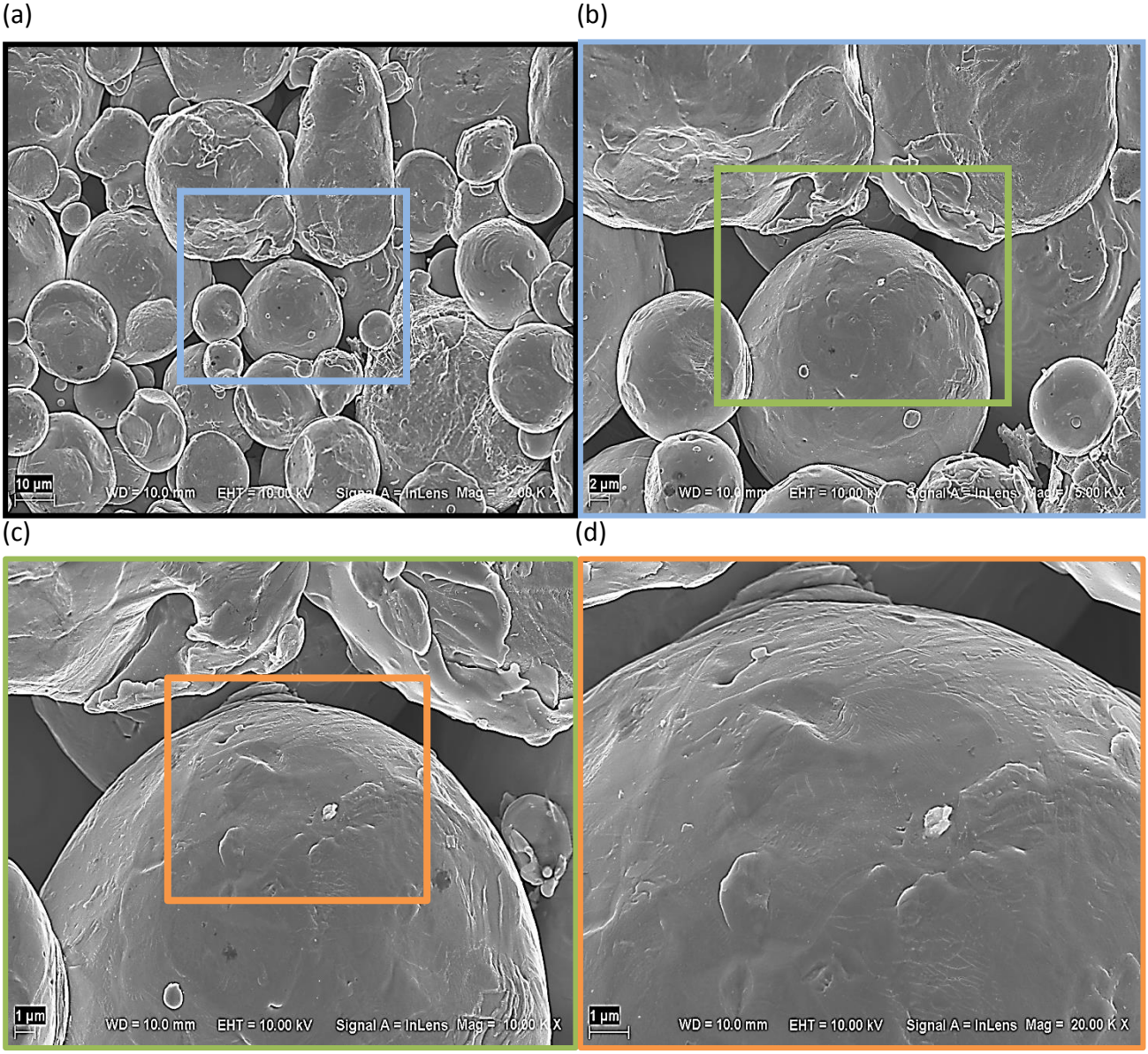

Figure 4.40: Overview of the gas atomized powder in as received state:-53µm fraction.

Figures 4.38, 4.39 and 4.40 show overview (a) and higher magnification image (d) of the three size fractions of the gas atomized powder in as-received state. A smooth surface is obvious for all fractions with some very small particulates also present on the surface. Some of these were examined with EDX, but due to the large interaction volume this was not possible for the really small particulate features.

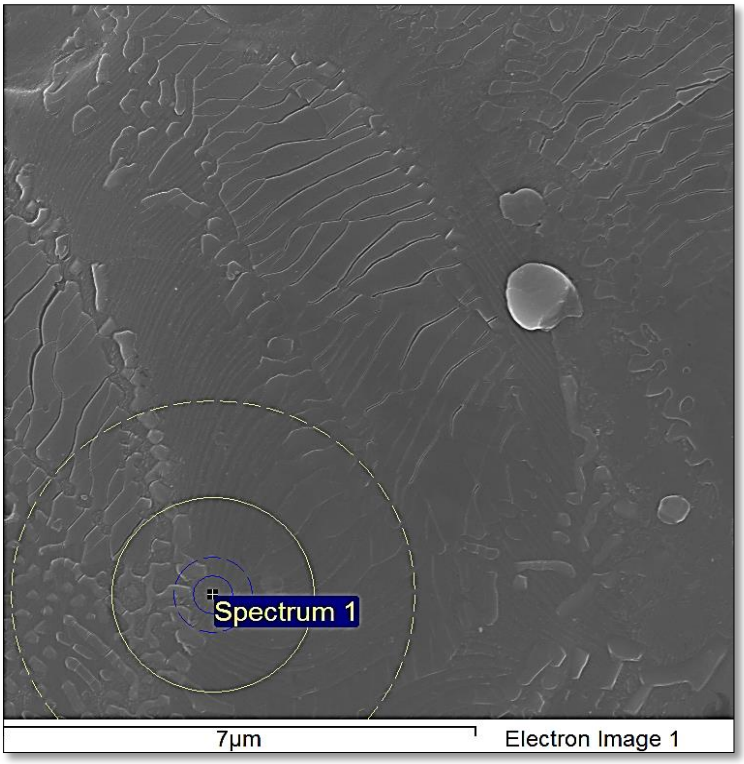

Spectrum[at%]	C	O	Na	Si	Fe
Spectrum 1	24.9	4.8	-	-	70.3

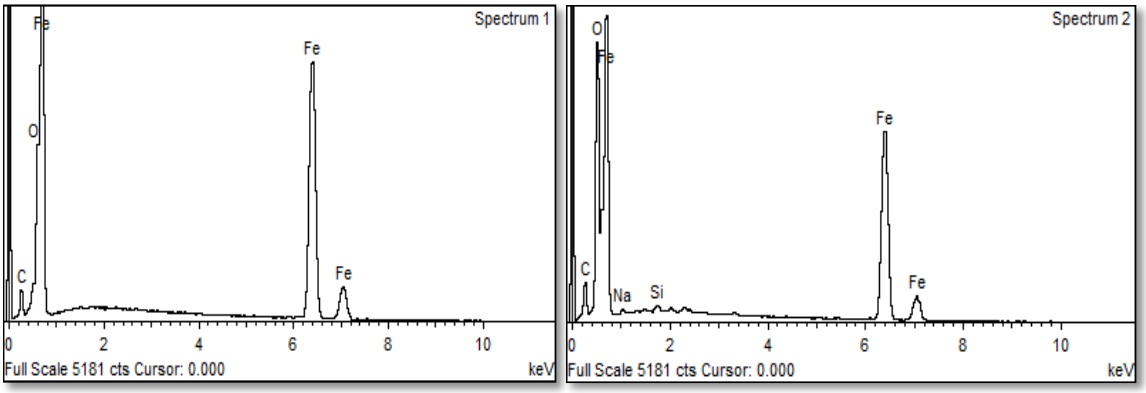

Figure 4.41: SEM image of the powder surface and results of the EDX measurements.

EDX analysis performed on the surface reveals that is pure iron with some line formations visible, possibly an oxide layer that is cracked (figure 4.41). Carbon is also present due to surface contamination.

- Annealed in argon/nitrogen atmosphere

XPS analysis of the powder size fractions

After the gas atomized powder was annealed it was analyzed in the XPS. Below is the progress of the element composition as a function of ion etching for the different samples. It is clear that the oxide layer is reduced in thickness compared to before annealing (cf. Tables 7-9). The impurity elements are also present.

Table 10: Element content (at%) in the surface of the as received and ion etched state of the +106µm fraction of the gas atomized powder

Content[at%]/Element	Fe	O	C	N	Si	Mn	Na
As received	18.2	50.5	28.1	0.1	2.3	0.4	0.4
Etched 1nm	31.3	50.3	15.3	-	2.7	0.3	-
2 nm	42	36.7	19.1	-	2	0.3	-
3 nm	49.7	28.5	19.8	-	1.8	0.2	-
5 nm	54.7	22.9	21.4	-	0.8	0.3	-
10 nm	60.6	20	19.3	-	0.1	0.1	-
20 nm	64.3	17.2	18.5	-	-	-	-

Table 11: Element content (at%) in the surface of the as received and ion etched state of the -106/+53µm fraction of the gas atomized powder

Content[at%]/Element	Fe	O	C	N	Si	Mn	Na
As received	15.3	51.7	28.4	0.2	3.9	0.2	0.3
Etched 1nm	25.9	50.5	19.5	-	3.9	0.2	-
2 nm	34	45.3	16.2	-	4.1	0.4	-
3 nm	44.1	37.3	15.5	-	2.9	0.2	-
5 nm	53.9	26.8	17.1	-	2	0.2	-
7 nm	57.8	22.8	17.3	-	2.1	0.1	-
10 nm	61.6	20.5	14.2	-	3.5	0.1	-
20 nm	69.9	17.6	12.6	-	-	-	-

Table 12: Element content (at%) in the surface of the as received and ion etched state of the -53µm fraction of the gas atomized powder

Content[at%]/Element	Fe	O	C	N	Si	Mn	Na
As received	15.5	44.9	34.9	0.4	3.2	0.6	0.5
Etched 1nm	29.9	49.7	16.5	-	3.3	0.4	0.2
2 nm	40.7	42.7	12.5	-	3.6	0.3	0.1
3 nm	51.1	31.4	14.5	-	2.6	0.4	-
4 nm	57.5	25.1	15.3	-	2.1	0.1	-
5 nm	58.7	22.5	16.01	-	2.6	0.1	-
10 nm	63.1	18.4	16.3	-	2	0.2	-
20 nm	73.7	14.6	11.8	-	-	-	-

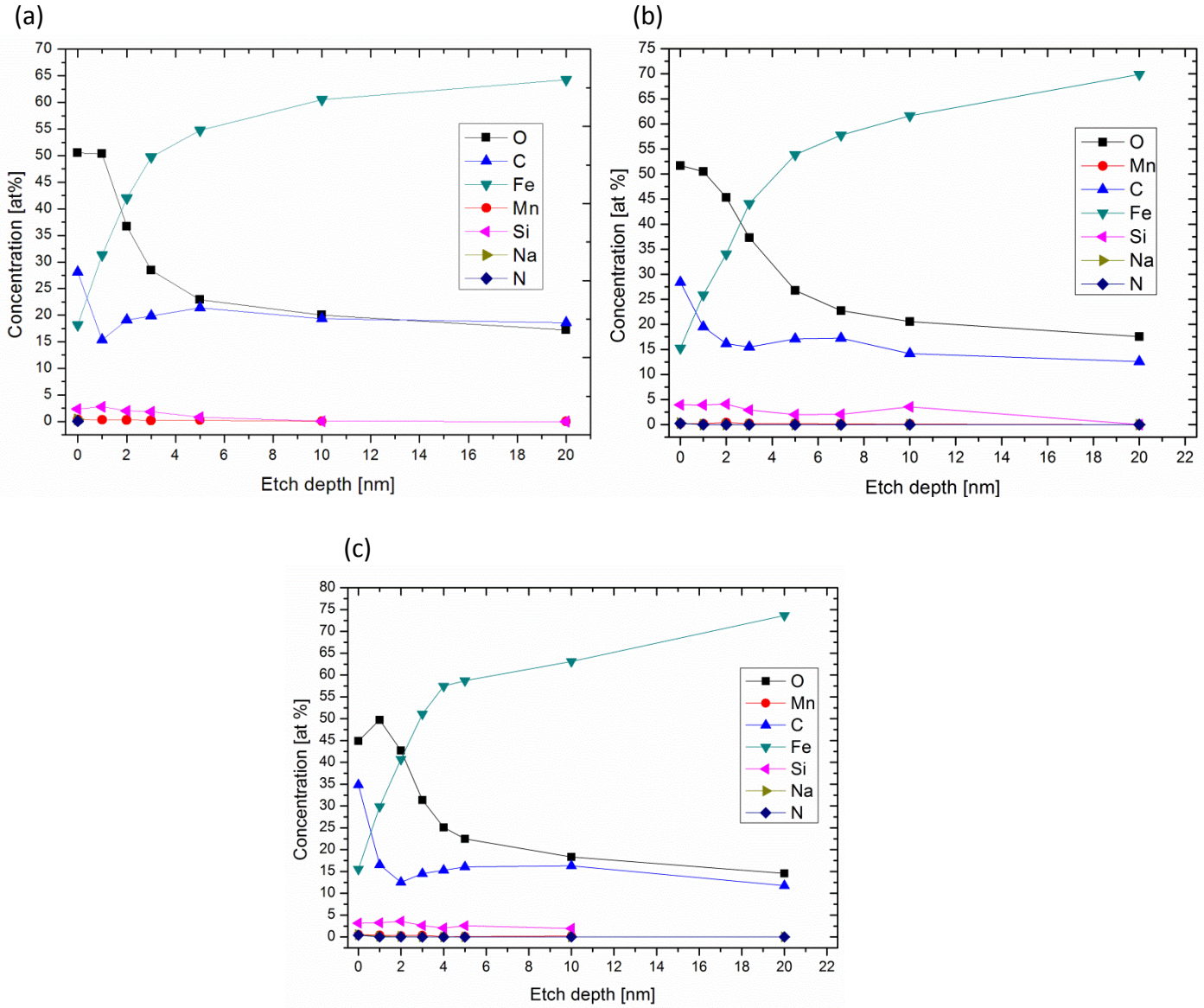

Figure 4.42: The element content over etching depth for the annealed gas atomized powder in the various fractions (a) +106µm (b)106/+53µm(c) -53µm.

Typical XPS spectra of etch depths are shown in Figure 4.43. All three fractions appear to show similar behavior.

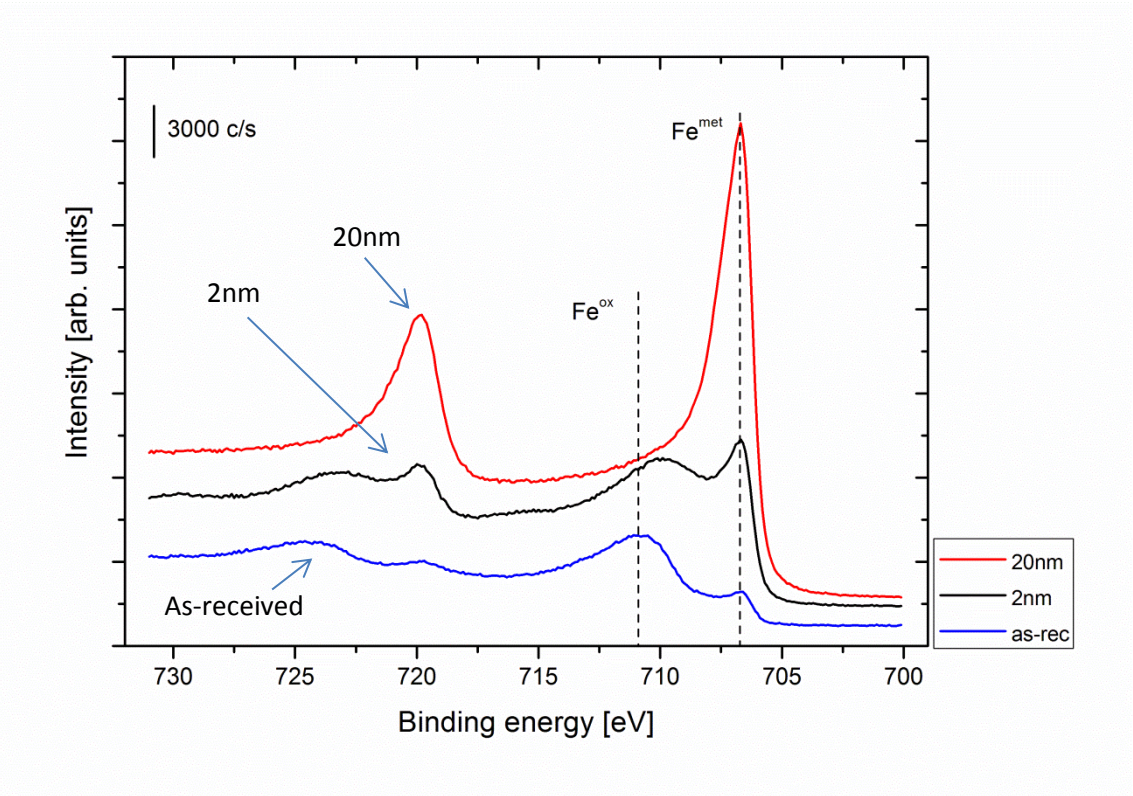

Figure 4.43: XPS spectra in as-received state and etch depths of 5nm and 100nm from the middle fraction (-106/+53µm) of the gas atomized powder. Other fractions exhibit similar behavior.

Using curve fitting the iron signal contributions are determined. The iron peak appears on the right side of the images in Figure 4.44 with a binding energy of 706.6 eV for all fractions, same as the as-received powder fractions and in very good agreement with the iron foil standard. The iron metal peak also appears clearly before ion etching (Fig 4.43-4.44).

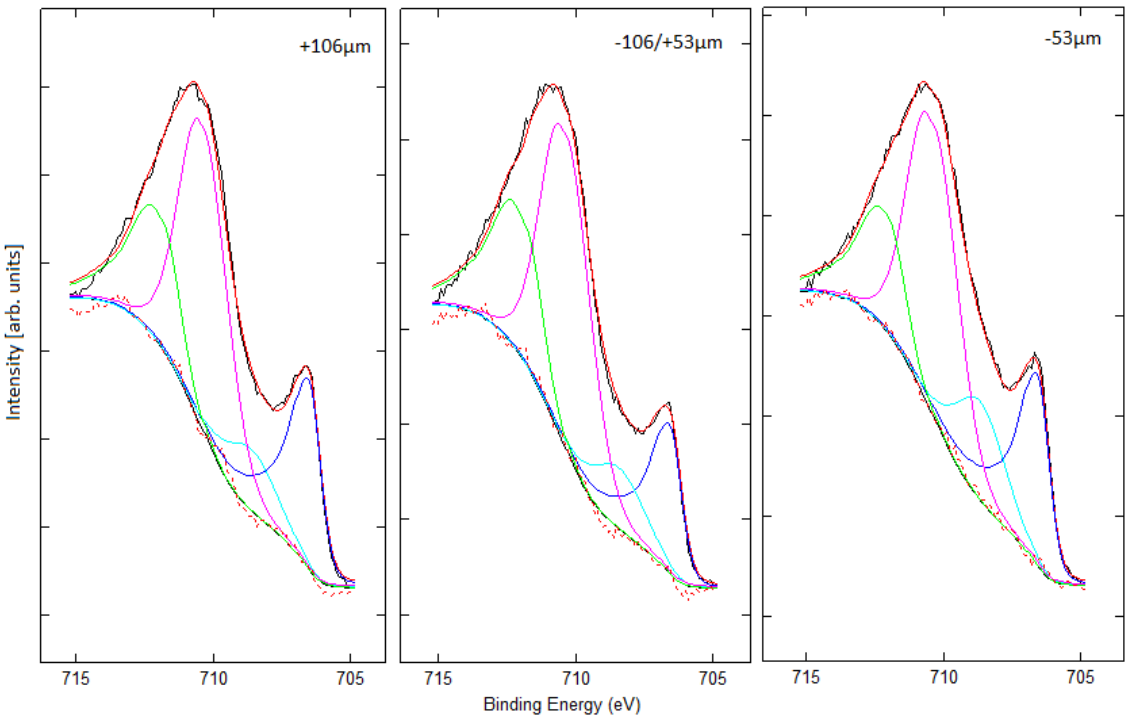

Figure 4.44: Analysis of chemical state of iron with the help of curve fitting before ion etching. The metal state is the peak on the right side of the figures and the rest are peaks for iron oxides.

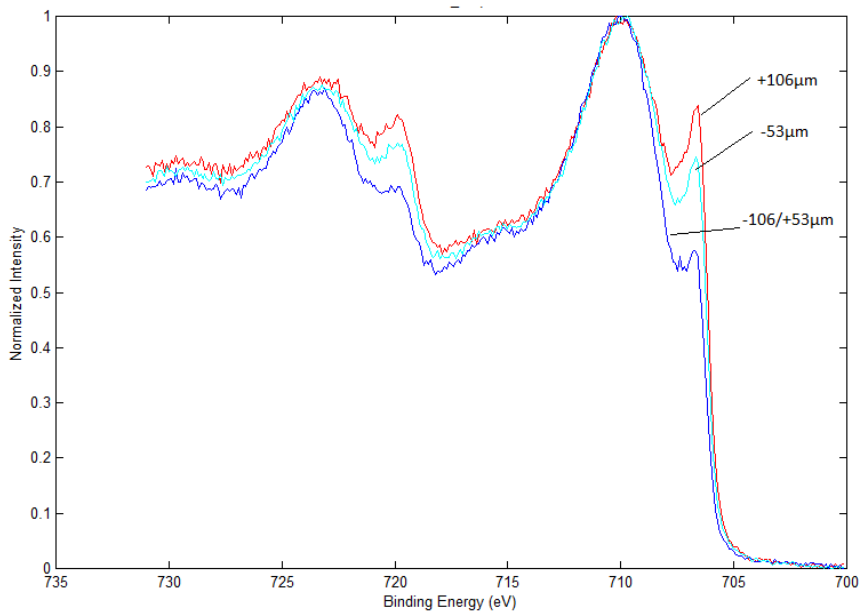

Figure 4.45: XPS high resolution spectra of the Fe signal peak for gas atomized as annealed powder fractions at 1nm etching depth.

The oxide layer thickness was calculated and as indicated by the XPS spectra it is very thin. For the +106µm fraction it is 2.7nm, for the -106/+57µm is 4.2nm and for the -53µm is 2.9nm. The diagrams show the relative intensity of the metallic iron peak and the oxide layer thickness calculation (Fig 4.46). It should however be noted that this represents the thickness estimate related to the Fe-oxide layer. After ion etching to >20nm there is still substantial presence of oxygen (see Tables 10-12). It may therefore be assumed that part of the surface is also covered by thicker oxide products.

(a)

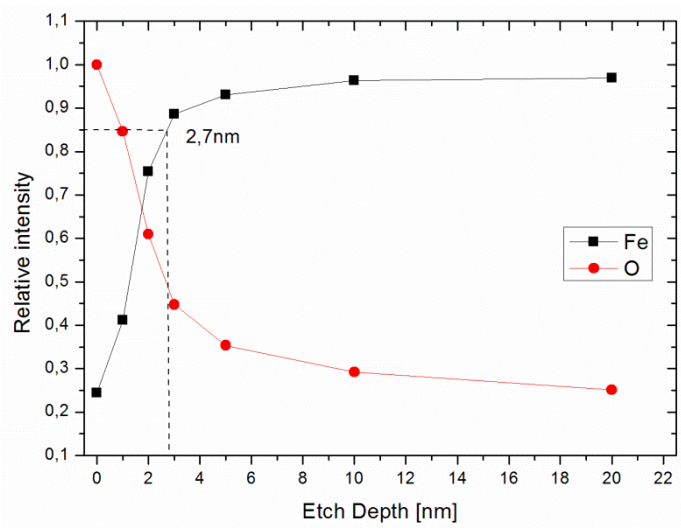

(b)

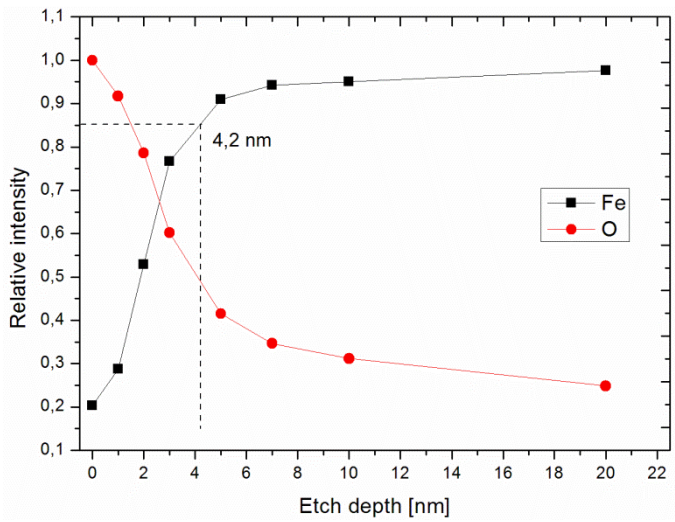

(c)

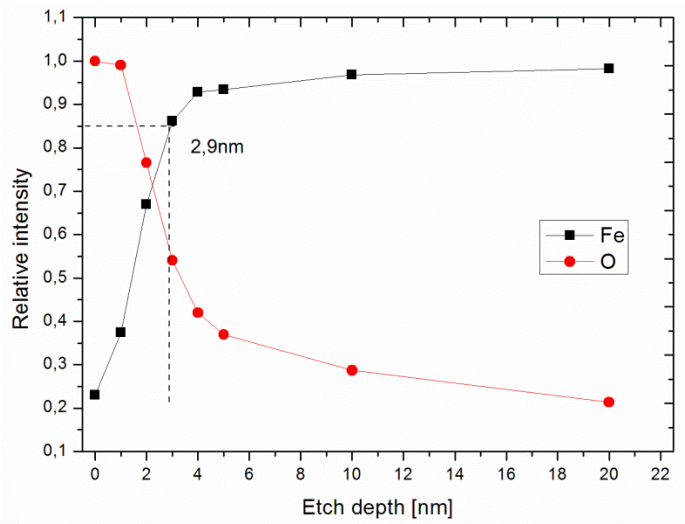

Figur 4.46: Estimation of the surface iron oxide layer using the normalized Fe-metallic (Fe2p peak) and the oxygen (O1s peak) over etching depth for the various fractions of the annealed gas atomized powder (a) +106µm (b)106/+53µm(c) -53µm.

SEM and EDX

Below are then images (Figs 4.47, 4.48, 4.49) of the various fractions of the gas atomized powder in the as-annealed state. After the annealing, smooth, supposedly clean surfaces are observed but there are also particulate features on the surface.

- +106µm

(a) (b)

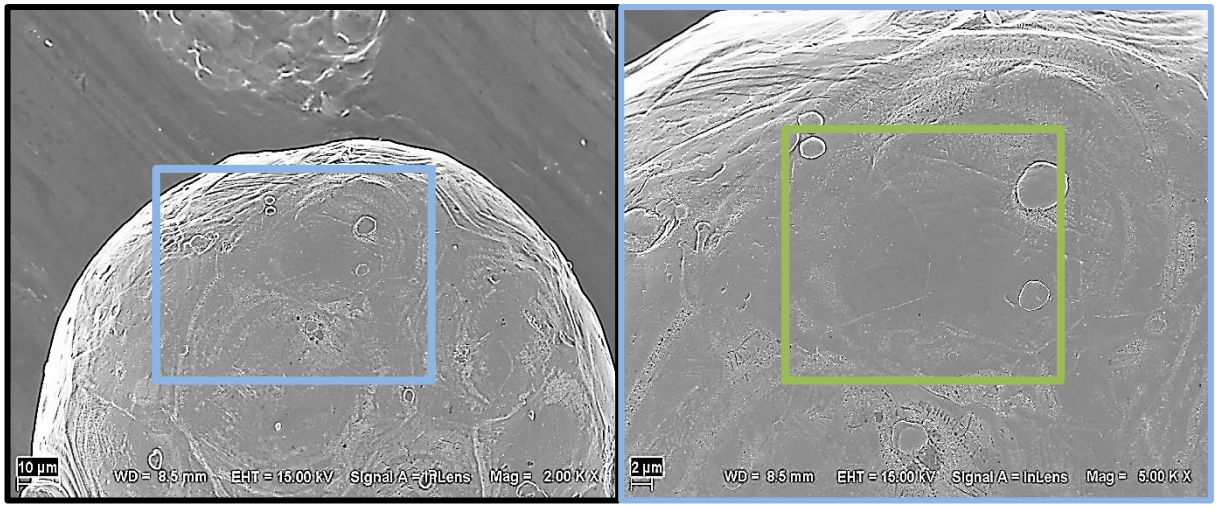

(c) (d)

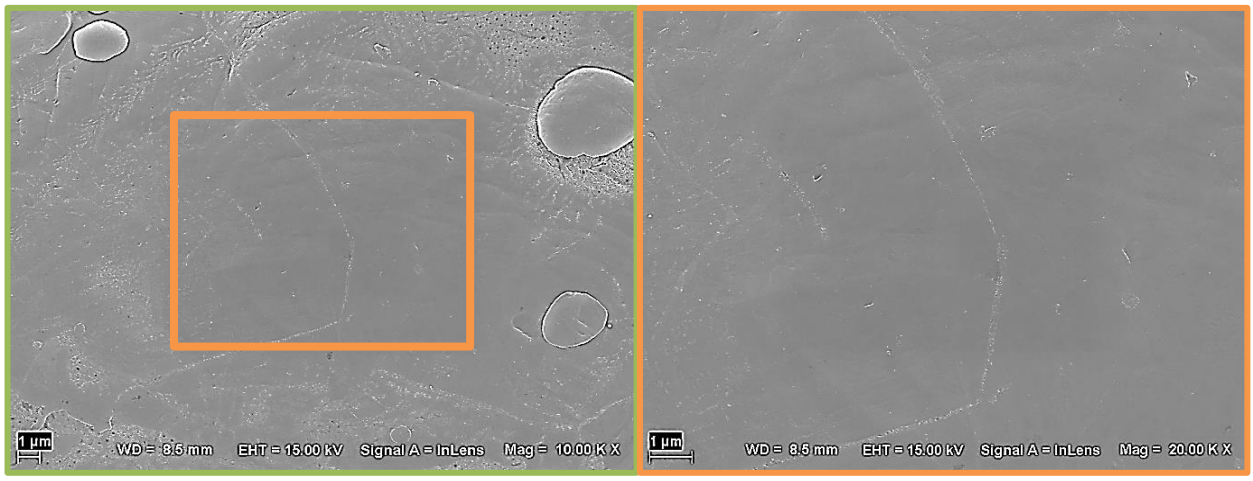

Figure 4.47: Overview of the annealed gas atomized powder +106µm fraction.

- -106/+53µm

(a) (b)

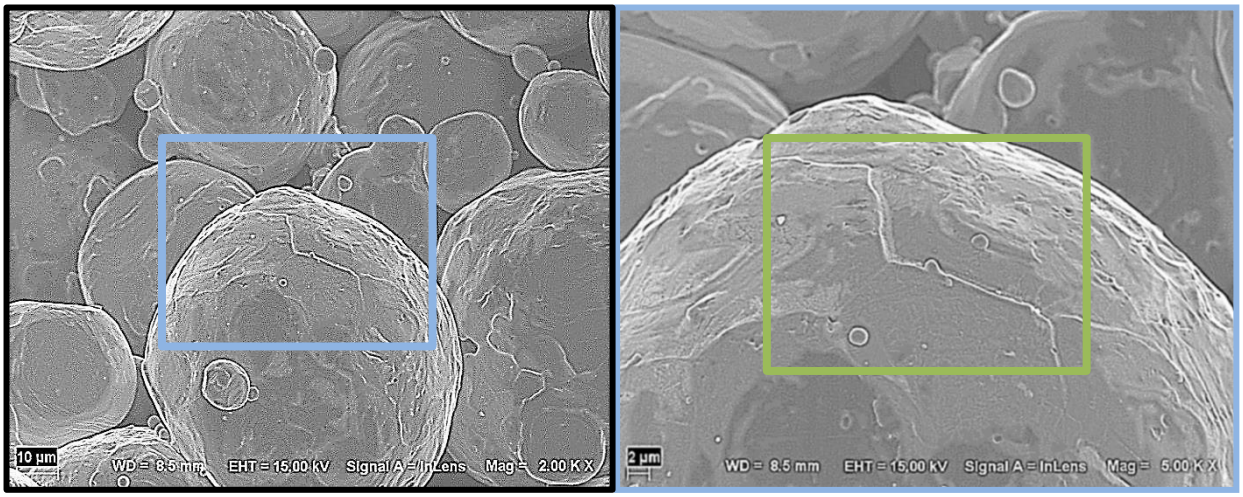

(c) (d)

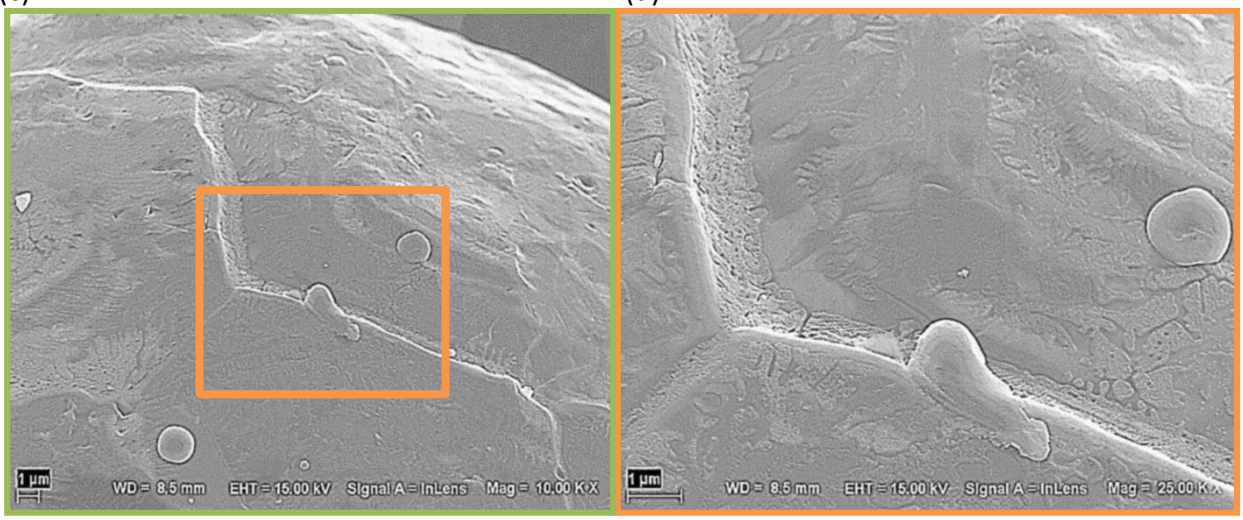

Figure 4.48: Overview of the annealed gas atomized powder -106/+53µm fraction.

- -53µm

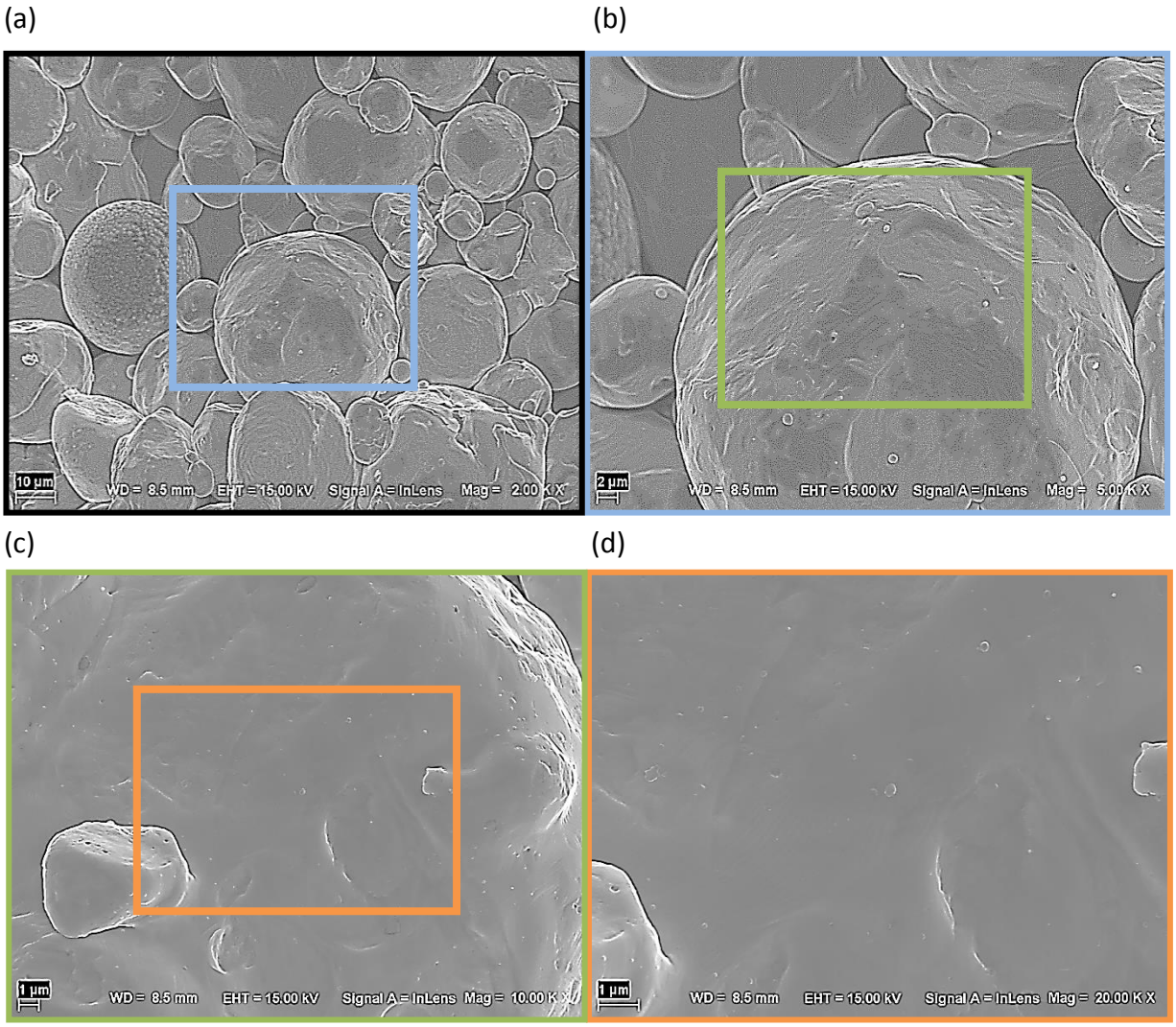

Figure 4.49: Overview of the annealed gas atomized powder -53µm fraction.

EDX analysis (Fig 4.50) showed that these particulates contain manganese, chromium and magnesium together with oxygen (Spectrum 2). The rest of the surface appears to show only iron. As indicated by XPS the oxide layer is thin and thus it cannot be detected with EDX (Spectrum 1). In both cases, carbon is present due to surface contamination.

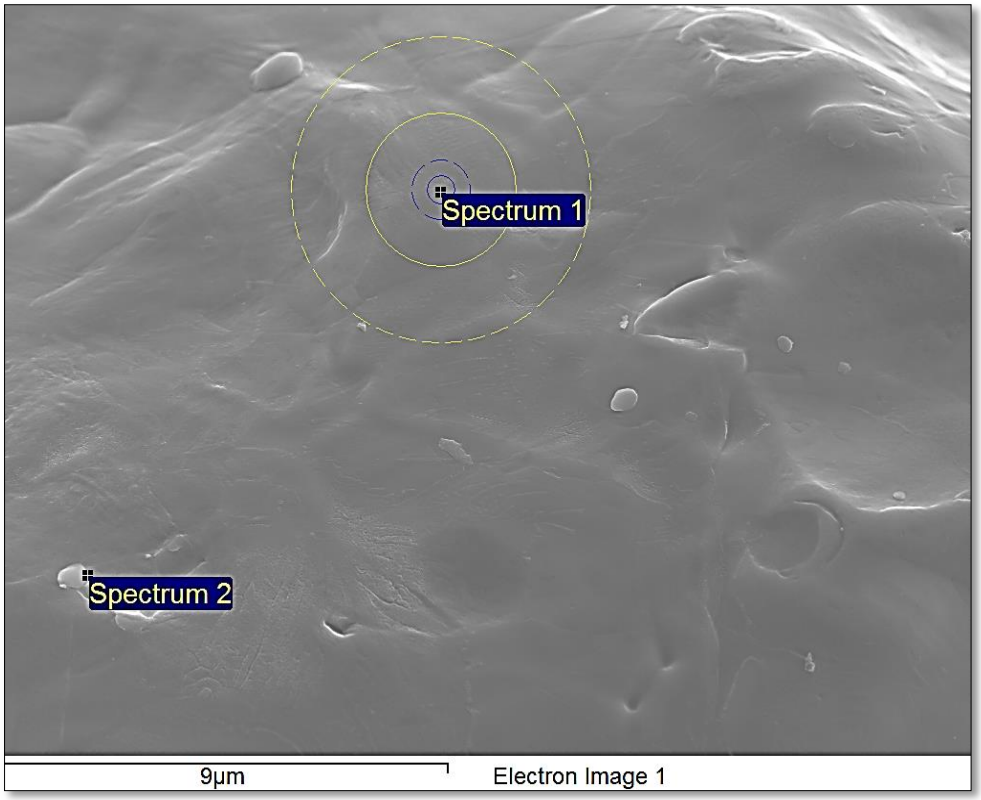

Spectrum[at%]	C	O	Mg	Cr	Mn	Fe
Spectrum 1	55.7	-	-	-	-	44.3
Spectrum 2	22.1	29.3	0.6	5.2	3	39.9

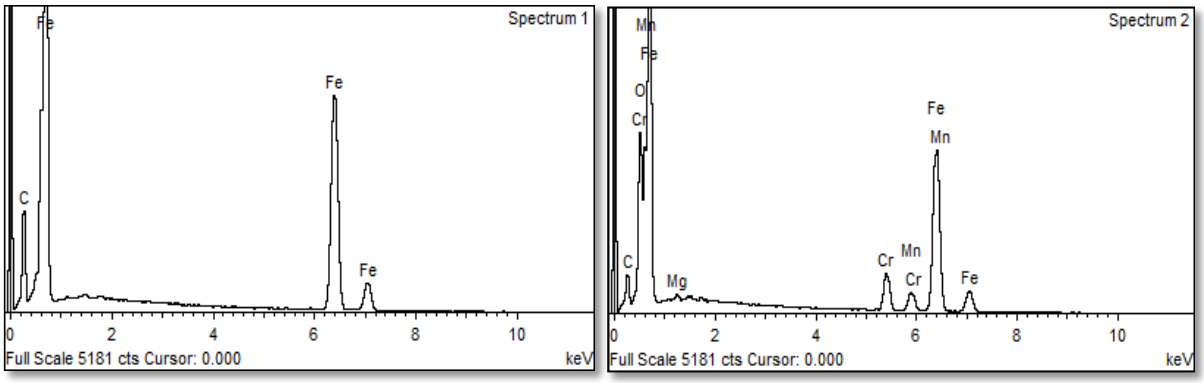

Figure 4.50: SEM image of the powder surface and results of the EDX measurements.

4.4 Analysis of the phosphate standards

- Iron(III) phosphate dihydrate ($FePO_4 2H_2O$)

The iron phosphate dihydrate was examined in the XPS and evaluated in a similar way as the oxides. This time the interest was on the phosphorous peak and curve fitting provided with the binding energy of the phosphate. The binding energy of phosphorous was 133.8 eV that is very close to the values reported in literature [20] and is shown in Figure 4.48. The iron compounds are also visible and as reported in literature they are slightly shifted to higher binding energies compared to the iron oxide standards [26].The Fe2+ is at 709.7 eV and the Fe3+ is at 712 eV. The specimen was also charging so again adventitious carbon charge correction had to be used to position the Fe peaks.

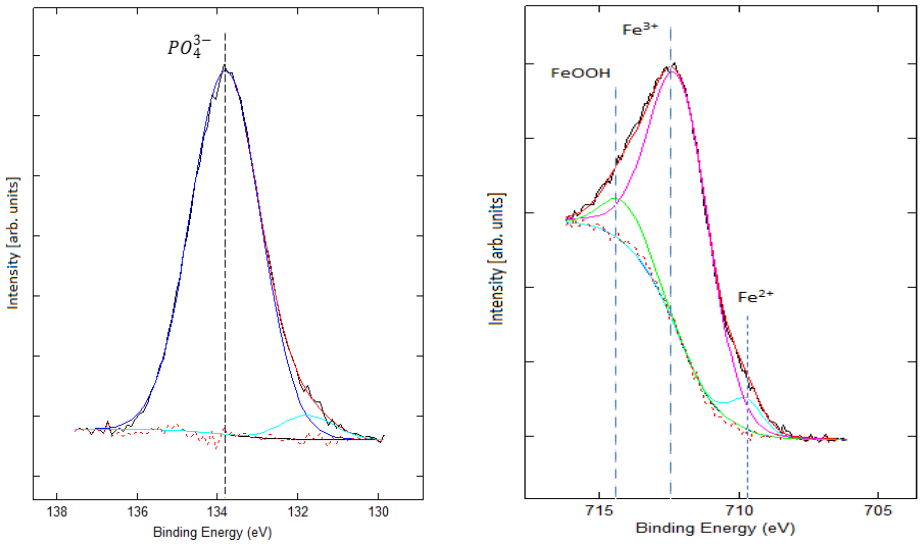

Figure 4.51: Analysis of chemical state of iron phosphate dihydrate with the help of curve fitting in as-received state. Phosphorous left and iron right.

This phosphate powder was found to also contain sodium ($NaPO_4$) hence the small peak on the right side of Figure 4.51(left). The iron phosphate dihydrate sample was analyzed with XRD and this indicated that it was amorphous with no characteristic peaks appearing in the spectrum (Fig. 4.52).

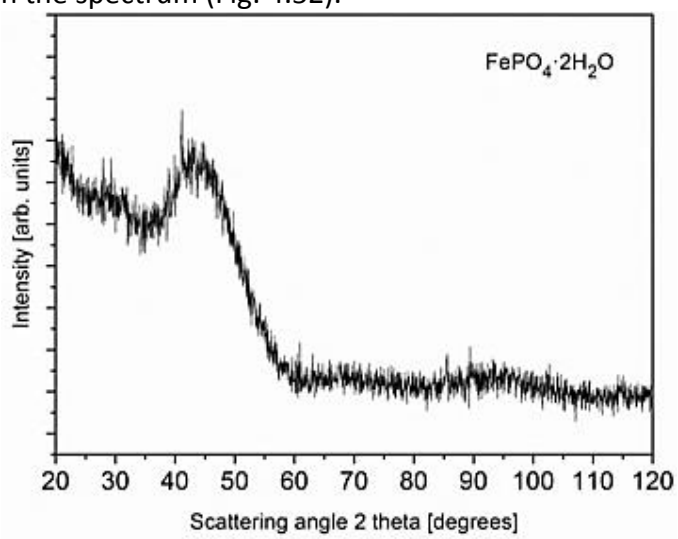

Figure 4.52: XRD spectrum of $FePO_4 2H_2O$.

- Iron(III) phosphate dehydrated ($FePO_4$)

The iron phosphate dihydrate was put in the DSC for the dehydration process. The mass percentage /temperature curve reveals that the sample lost 17.77% of its mass (Fig 4.53) and the onset was observed at 116.2 ^{o}C. Assuming that the weight loss is due to structural water in the compound the percentage that should have been observed is 19.28%. Hence, the dehydration process was almost complete with a very small amount of bound water still remaining.

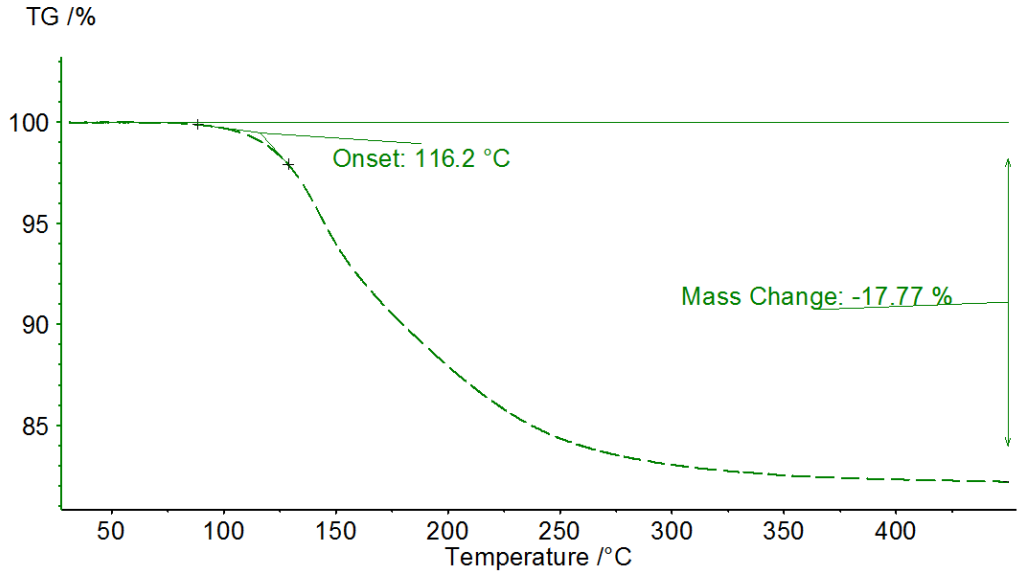

Figure 4.53: Dehydration DSC curve.

After the dehydration the compacted phosphate powder was put to the XPS. The curve fitting applied to the phosphorous signal (Fig 4.54) gave the binding energy of the phosphate at 133.7 eV which is even more close to the literature values as expected. The oxygen peak is also shown with the binding energy for oxygen in the phosphate being 531.6 eV and for O^{2-} in oxide at 529.3 eV. Again the small sodium phosphate contribution on the phosphorous signal is also present.

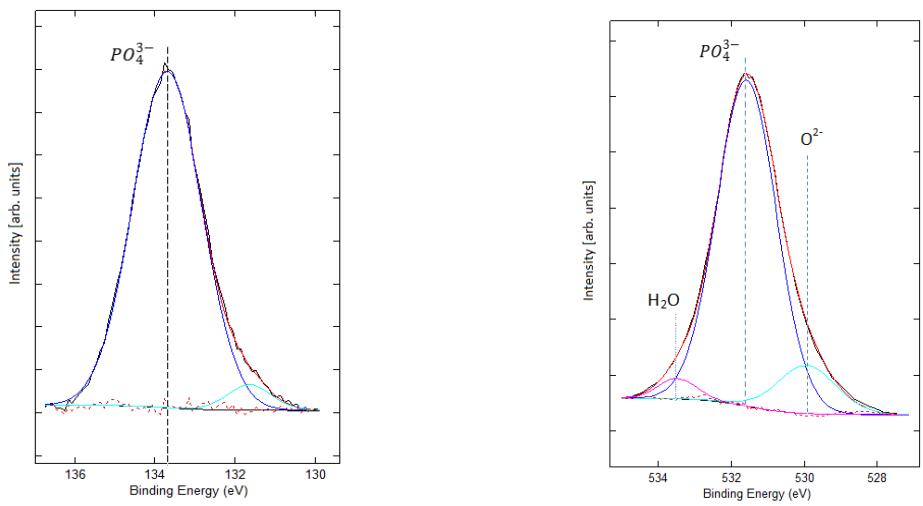

Figure 4.54: Analysis of chemical state of the dehydrated iron phosphate peaks with the help of curve fitting in as-received state. Phosphorous left and oxygen right.

- Phosphated iron foil

XPS measurements was done on the phosphated iron foil with the purpose of obtaining a clear phosphorous peak and use its characteristics for the curve fitting necessary for the Somaloy 500 powder. A survey of this measurement is shown in Figure 4.55.

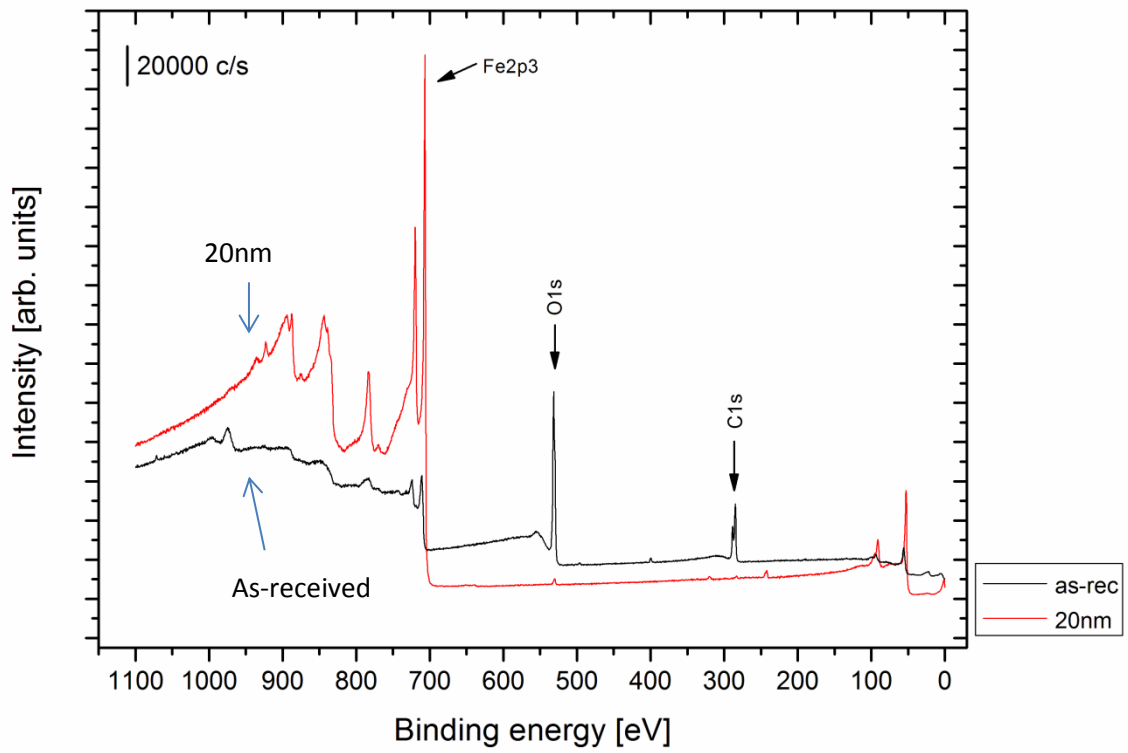

Figure 4.55 XPS survey spectra for the phosphated iron foil in as-received and 20nm etched state.

Main elements that are investigated are iron, oxygen, phosphorous and carbon. The etch steps and the compositions appear in Table 13 below.

Table 13: Element content (at%) in the surface and ion-etched state of the as-polished iron foil

Content[at%]/Element	Fe	O	C	P
As received	8.5	47.5	43.6	0.5
Etched 1nm	31.2	63	3.4	2.4
2 nm	34.7	63	-	2.3
3 nm	38.7	59.4	-	1.9
5 nm	60.6	39.1	-	0.3
7 nm	82.4	13.7	-	-
10 nm	90.2	6.4	-	-
20 nm	88	6.3	-	-

The carbon is immediately removed after the first etch step and disappears after the second. The concentration of iron reaches 88% while oxygen drops to 6.3% after 20nm of etching. Phosphorous is revealed after the removal of the surface contamination and disappears after 5nm. Figure 4.56 shows the progress of the elements apparent concentration with etch depth.

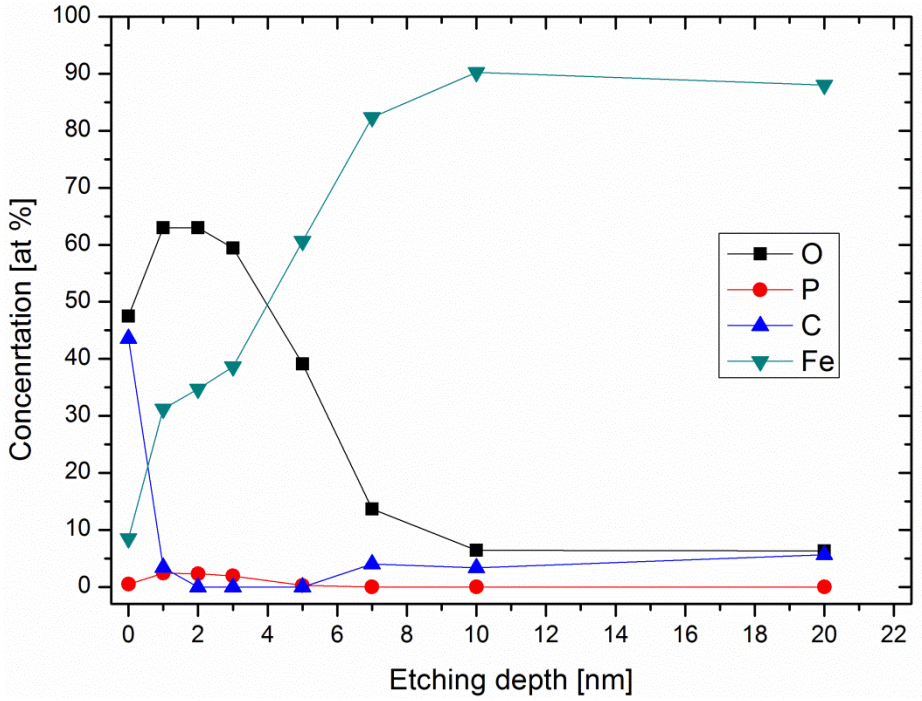

Figure 4.56: The element content over etch depth for the phosphated iron foil in the as-polished state.

The metallic peak of Fe starts to appear after the removal of the surface contamination layer and is very clear at 20nm etch depth. Figure 4.57 shows the XPS spectra for selected etch depths.

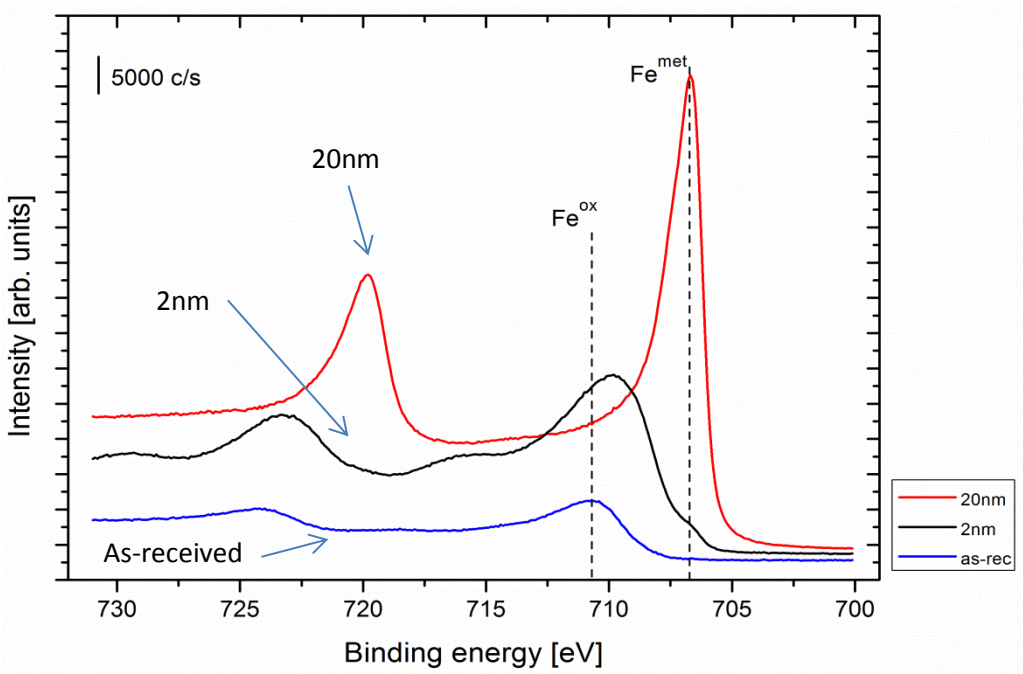

Figure 4.57: XPS spectra of phosphated iron foil before and after ion etching (2nm and 20nm).

After the removal of the surface contamination, curve fitting was used to define the phosphorus peak position. It is at 133.8 eV as shown in Figure 4.58.

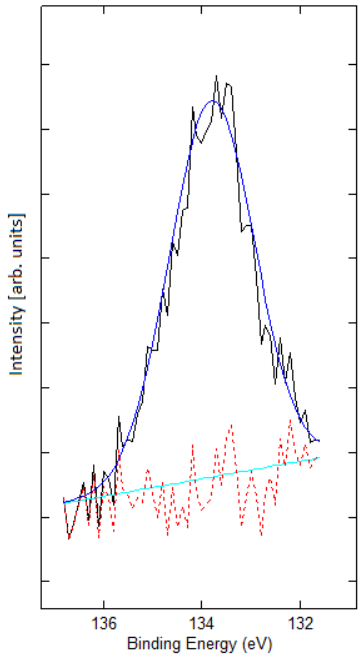

Figure 4.58: Analysis of chemical state for phosphated iron foil phosphorous peak with the help of curve fitting of P2p XPS peak at 1nm etch depth.

The oxide or coating layer thickness for a flat specimen is approximately given by the etch depth at which the coating layer intensity reaches 50% of its maximum value. Considering this for the P intensity the thickness is estimated at 3.7 (Figure 4.59).

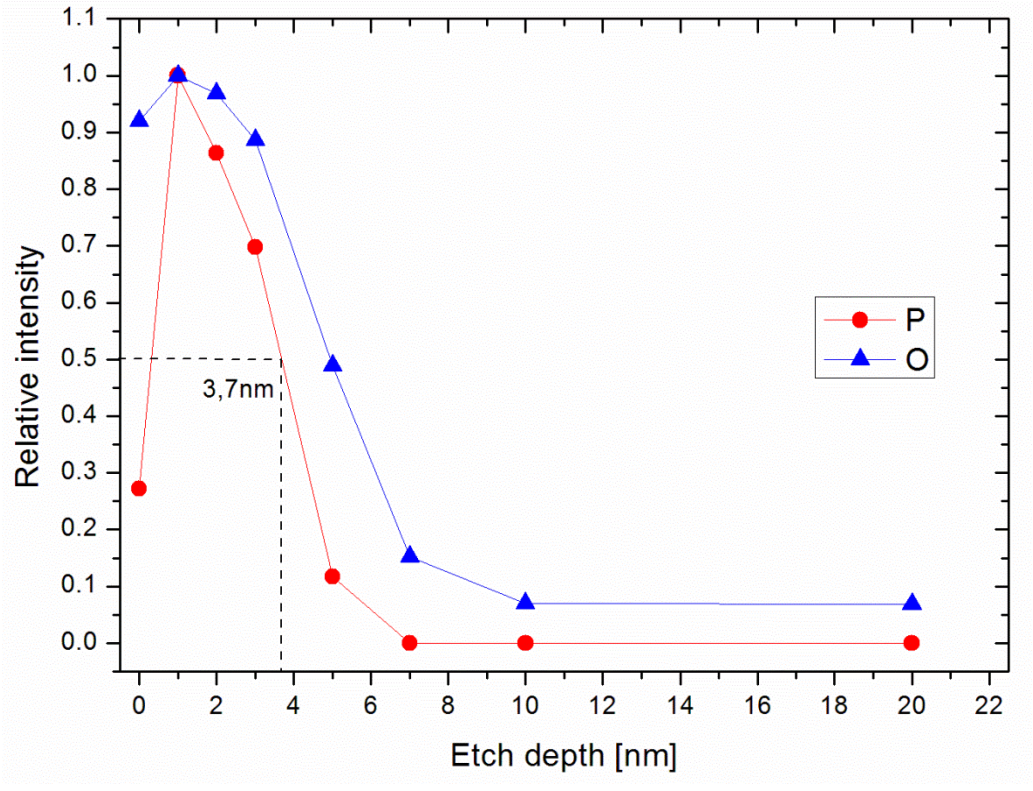

Figure 4.59: Estimation of the surface iron oxide layer using the normalized P peak over etching depth.

4.5 Analysis of the Somaloy 500 powder

XPS analysis of the as-received powder

In the XPS survey spectrum of the Somaloy powder there are four main characteristic peaks. These are from iron, oxygen, carbon and phosphorous.

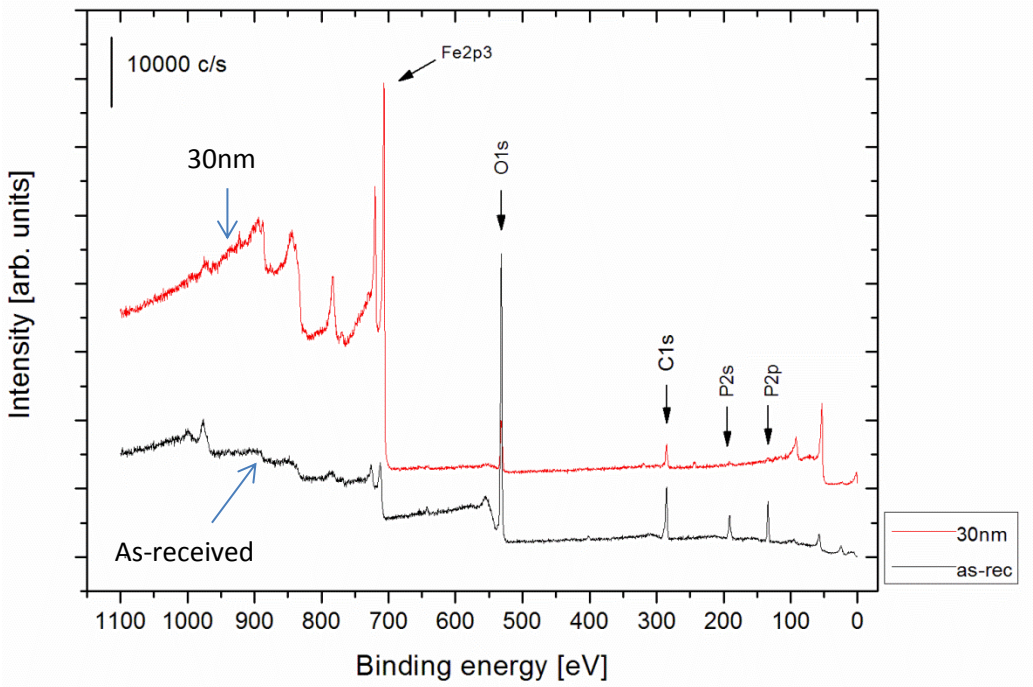

Figure 4.60: XPS survey spectrum for the phosphated iron foil in as-received and 30nm etched state.

The apparent surface composition of this powder in the as received state is shown in Table 14 below.

Table 14: Element content (at%) in the surface of the as received and ion etched state of the Somaloy 500 powder

Content[at%]/Element	Fe	O	C	P	N	Si	Mn
As received	4.6	56.6	24.2	11.7	1.6	0.9	0.5
Etched 1nm	10.9	58.4	15.7	13.3	-	1.2	0.5
2nm	13.2	57.7	15.6	12.2	-	0.8	0.6
5nm	18.5	56.5	15.1	9.3	-	-	0.6
7nm	24.5	53.1	13.7	8.1	-	-	0.7
10nm	32.6	45.6	14.7	6.5	-	-	0.5
12nm	39.4	39.4	15.5	5.2	-	-	0.6
15nm	44.8	33.1	17.2	4.2	-	-	0.7
20nm	54	26.1	15.9	3.5	-	-	0.5
30nm	59	19.9	19	2.2	-	-	-
50nm	64.9	14.4	17.7	-	-	-	-

Carbon is present at all steps due to the carbon tape used for mounting the powder. Iron increases with etch depth up to around 65% while oxygen and phosphorous decrease with increasing etch depth. Phosphorous disappear after 30nm of ion etching

as the coating is etched away. The progress of the element concentration with etch depth is shown in Figure 4.61.

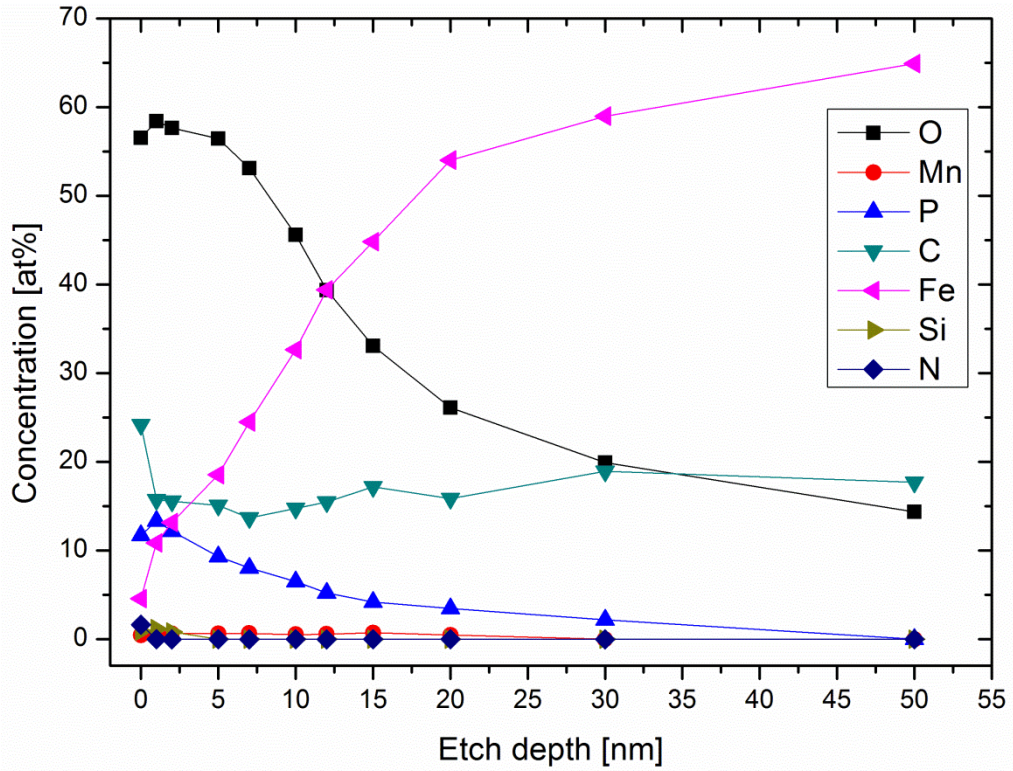

Figure 4.61: The element content over etch depth for the Somaloy 500 powder in the as-received state.

The high resolution XPS spectra at Fe3p region in figure 4.62 show the intensity for different etching depths.

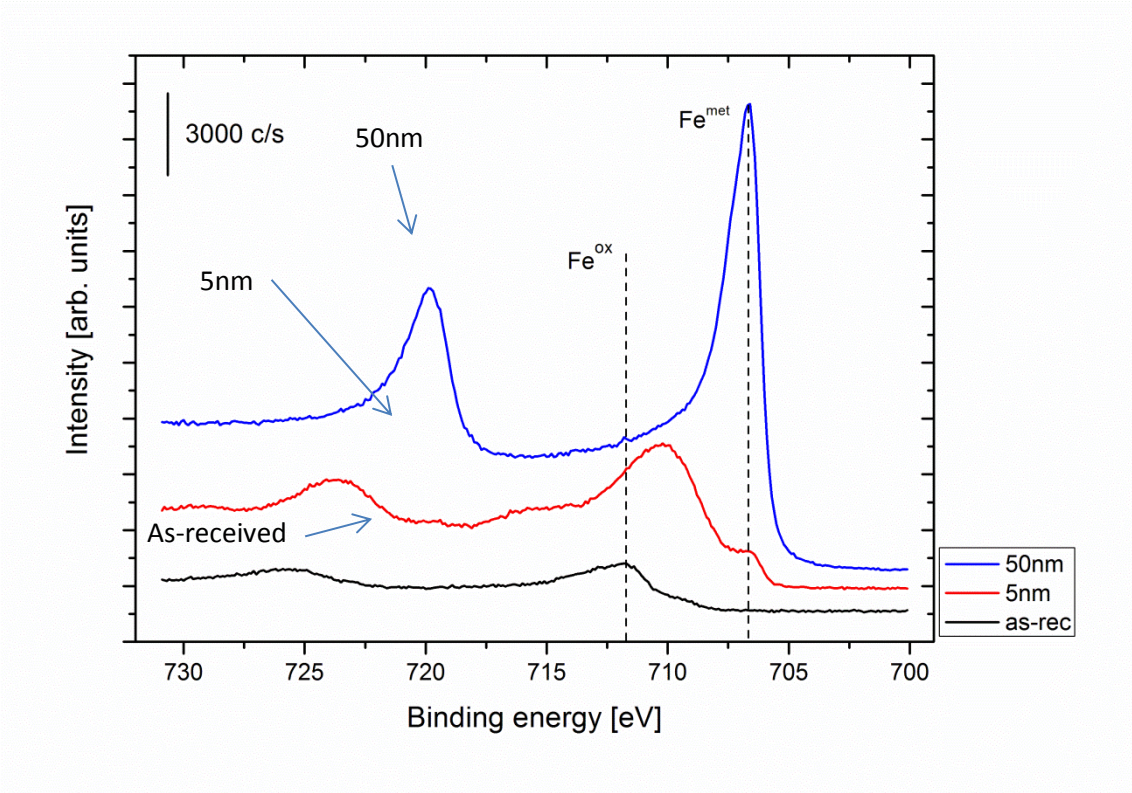

Figure 4.62: XPS spectra in the as-received state and etch depths of 5nm and 50nm.

No metallic peak appears before ion etching. Curve fitting of Fe and P signals shows the contributions before ion etching in Figure 4.63. The left peak component is the hydroxide species on the surface, the middle one is Fe^{3+} and the right is the Fe^{2+} with the binding energies being 712.8, 711.6 and 709.9 eV respectively. The phosphorous peak in the P2p area is at 133.9eV in accordance with previous studies [19].

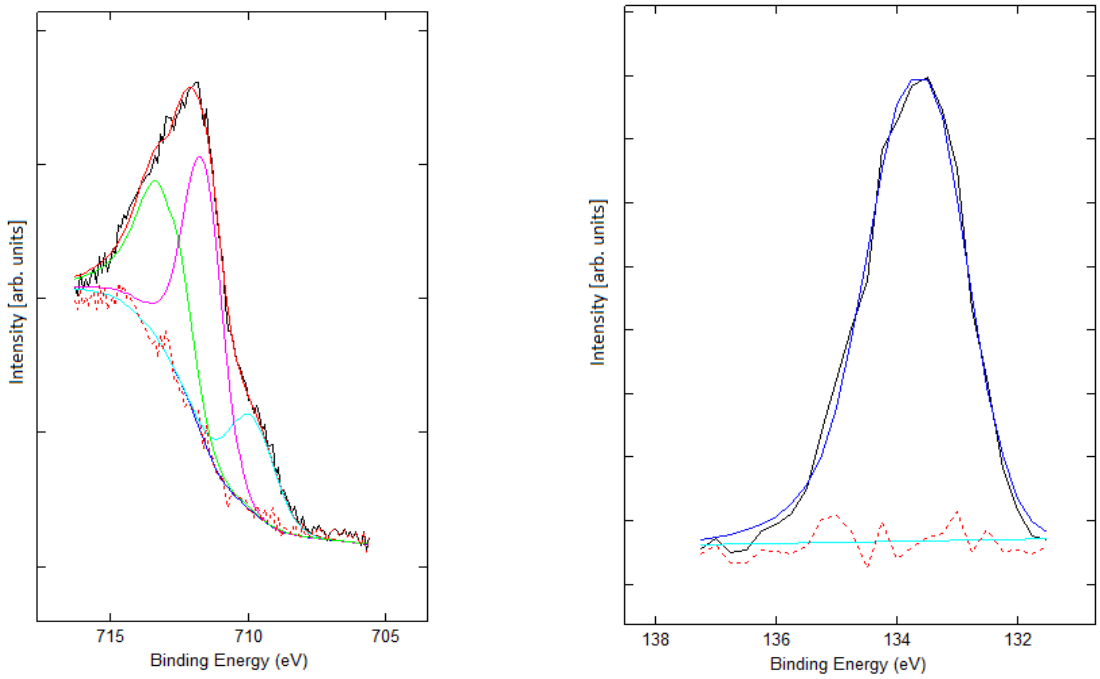

Figure 4.63: Analysis of chemical state of iron (left) and phosphorous (right) with the help of curve fitting in the as received state(0nm).

Curve fitting was also applied for the oxygen peak and the progress of the two contributions with etch depth is shown in Figure 4.64. The phosphate component remains steady while the O^{2-} increases with etch depth and then decreases again. The binding energy of oxygen in phosphate is 531.6 eV and that of O^{2-} in oxide is 530.2 eV

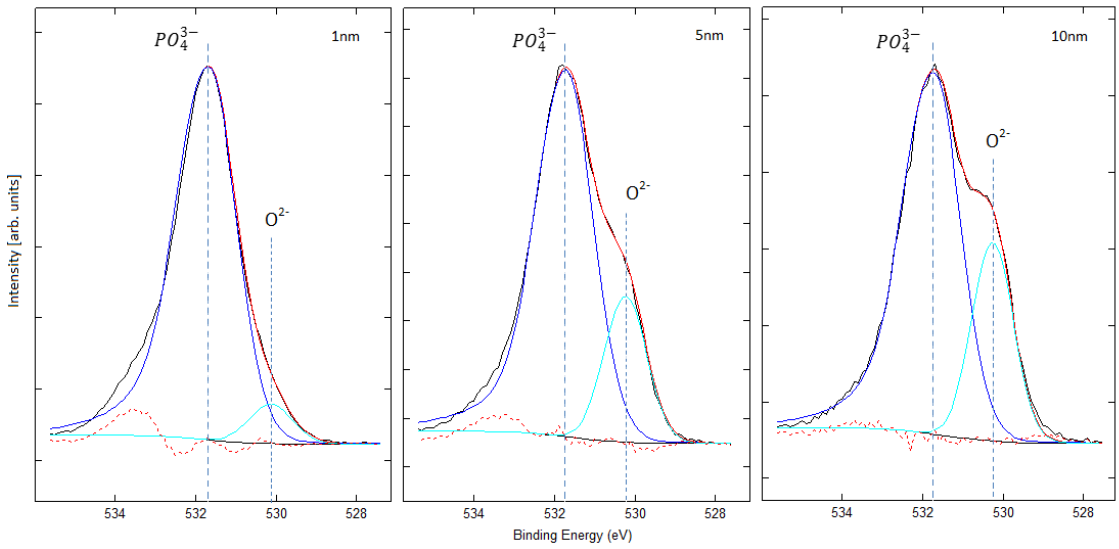

Figure 4.64: Analysis of chemical state of oxygen with the help of curve fitting at three etch depths.

The coating thickness was calculated using two approaches that are shown in figure 4.65.

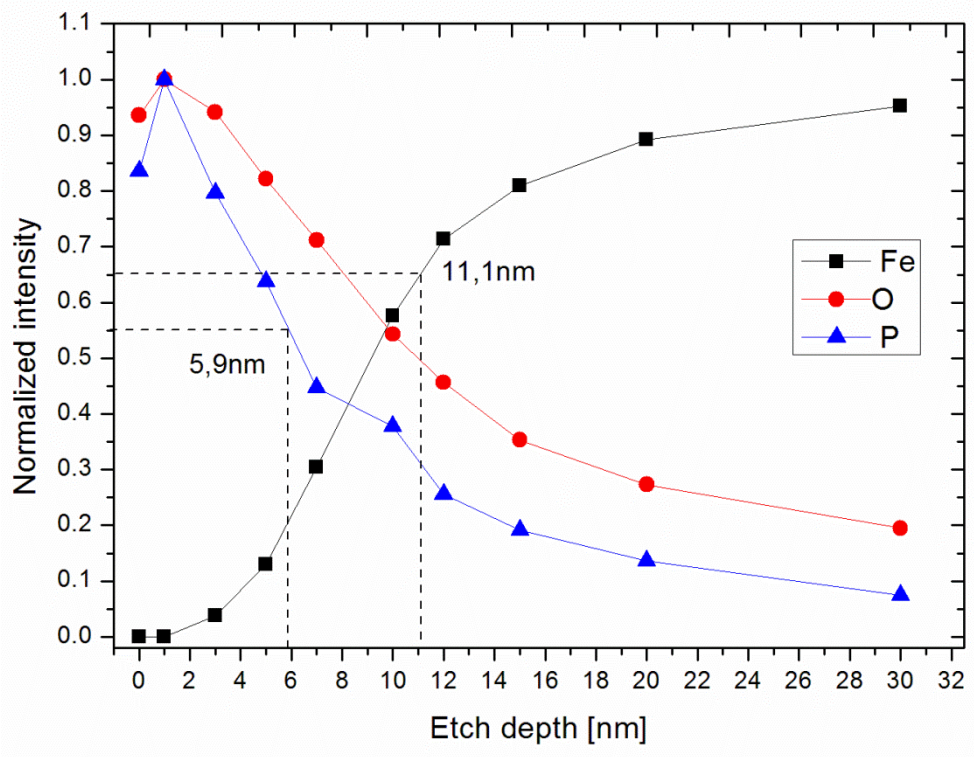

Figure 4.65: Estimation of the phosphate coating using the normalized Fe-metallic (Fe2p peak), the oxygen (O1s peak) and the phosphorous (P2p peak) over etch depth.

The first uses the relative metallic peak intensity as before; here 65% owing to greater thickness, and gives 11.1nm (with the oxide thickness also included) and the second uses the phosphorous peak intensity at 55% relative intensity (due to the fact that P doesn't go to zero) and it gives 5.9nm.

XPS analysis of the powder fractions

The surface coomposition of elements for the sieved fractions of the Somaloy 500 powder are shown in Tables 15-17 below.

Table 15: Element content (at%) in the surface of the as received and ion etched state of the +106μm fraction

Content[at%]/Element	Fe	O	C	P	N	Si	Mn
As received	5	54.4	26.2	11.3	2.3	0.5	0.4
Etched 1nm	12.1	61.4	12.5	12.9	-	1	0.2
2nm	14.4	61.1	10.9	12.3	-	1	0.3
5nm	19.6	57.4	13.6	9.3	-	-	0.1
7nm	25	55	11.3	8.5	-	-	0.1
10nm	31.3	48.1	14.1	6.4	-	-	0.2
12nm	37.4	42.3	14.3	5.8	-	-	0.3
15nm	43.9	36	15.8	4.1	-	-	0.2
20nm	53.7	27.6	14.8	3.8	-	-	0.1
30nm	62.5	21.5	14.2	1.8	-	-	0.1
50nm	66.9	17	16.1	0	-	-	0.4

Table 16 Element content (at%) in the surface of the as received and ion etched state of the -106/+53µm fraction

Content[at%]/Element	Fe	O	C	P	N	Si	Mn
As received	4.8	56.2	24	12.1	1.7	0.8	0.5
Etched 1nm	10.4	59	14.8	14	-	1.2	0.6
2nm	12.8	58.8	12.8	13.1	-	1.9	0.6
5nm	17.8	57.7	12.9	10.9	-	-	0.8
7nm	22.9	53.9	13.9	8.6	-	-	0.7
10nm	29.3	47.4	15.3	7.3	-	-	0.6
12nm	36.6	42.3	14.4	6.2	-	-	0.6
15nm	41.4	35.6	17.4	4.9	-	-	0.8
20nm	53.5	29	14.8	2.4	-	-	0.4
30nm	59.6	21.4	16	2.7	-	-	0.3
50nm	63.5	17.5	17.6	1.4	-	-	0.5

Table 17: Element content (at%) in the surface of the as received and ion etched state of the -53µm fraction

Content[at%]/Element	Fe	O	C	P	N	Si	Mn
As received	4.3	52.6	27.6	11.7	2	1.2	0.5
Etched 1nm	11.2	61.2	11.5	14.8	-	0.8	0.6
2nm	13.7	60.1	10.8	13.5	-	1.3	0.8
5nm	19.1	58.1	11.9	10.3	-	-	0.6
7nm	24.4	54.8	11.5	8.7	-	-	0.7
10nm	32.1	46.8	13.4	7	-	-	0.7
12nm	37.9	41	15.1	5.5	-	-	0.6
15nm	44.5	33.9	16.7	4.5	-	-	0.5
20nm	55.1	27	14.7	2.8	-	-	0.4
30nm	59.3	19.9	18	2	-	-	0.8
50nm	66.4	15.6	16.9	1.1	-	-	0.5

(a)

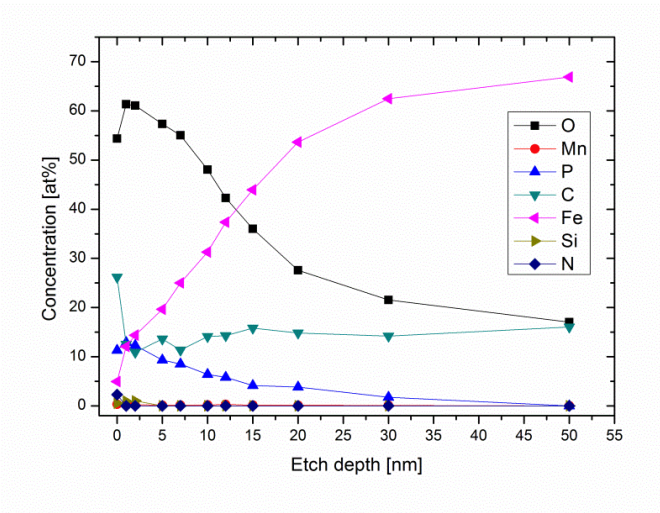

(b)

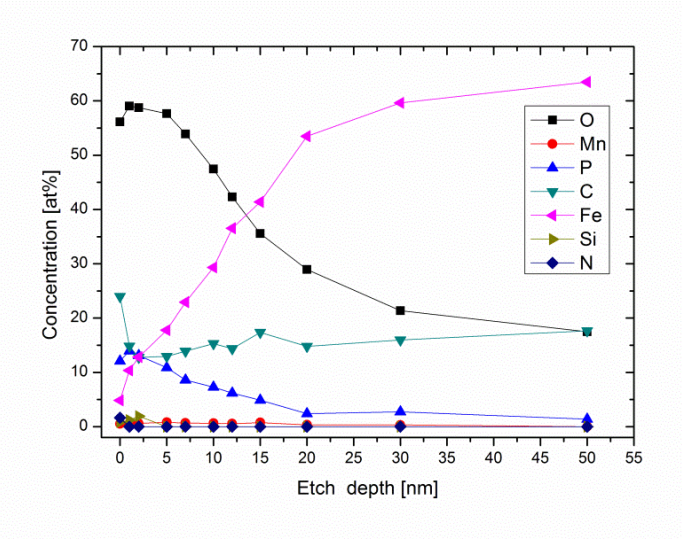

(c)

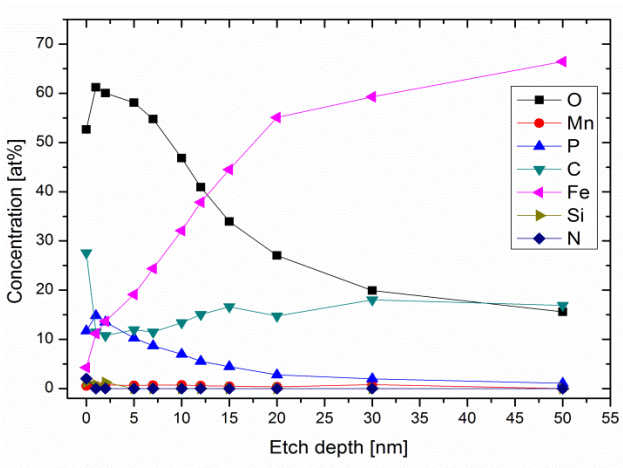

Figure 4.66: The element content over etch depth for the Somaloy 500 powder of the various fractions (a) +106µm (b)106/+53µm(c) -53µm.

The above graphs indicate that the fractions show a similar behavior in the element concentration with the as-received unsieved powder. Here 50% of the P intensity is used. A small difference seems to appear in the phosphate coating thickness with the as-received powder having lower value than the fractions.

(a)

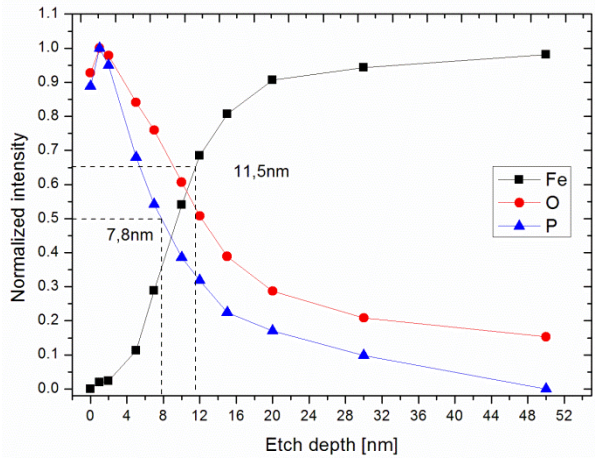

(b)

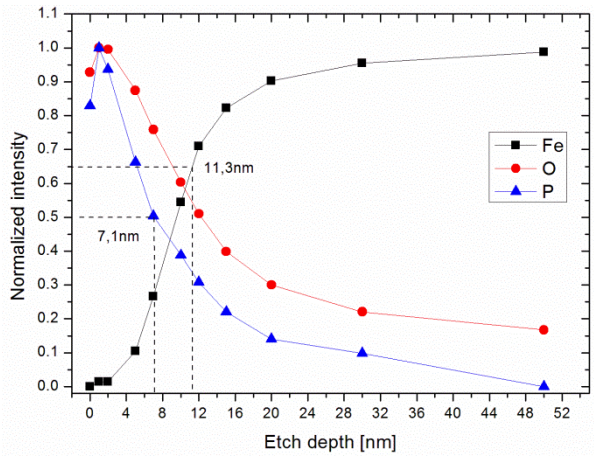

(c)

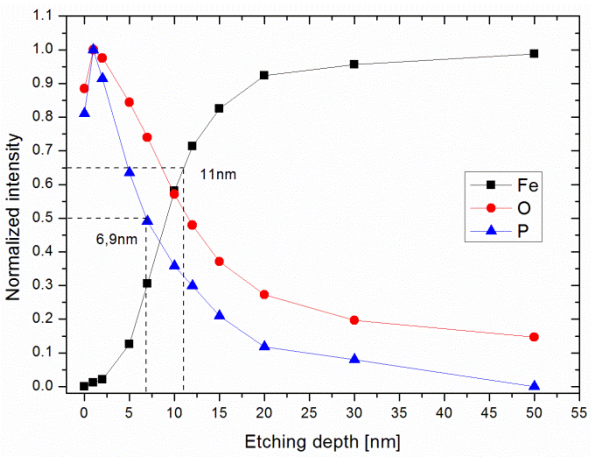

Figure 4.67: Estimation of the phosphate coating using the normalized Fe-metallic(Fe2p peak) ,the oxygen (O1s peak) and the phosphorous (P2p peak)over etch depth for the various fractions (a) +106µm (b)106/+53µm(c) -53µm.

When using the iron metallic peak intensity the thickness starts from 11.5 nm, 11.3 nm for the middle fraction and 11.0 nm for the small one. With the phosphorous intensity these values are 7.8, 7.1 and 6.9 nm respectively following the same trend. Overall the fractions give almost the same contribution in coating thickness as the unsieved powder which was 11.1 nm using the iron peak intensity.

SEM and EDX of the as-received powder

The Somaloy 500 SEM images show a clean surface with some few particulates of around 0,5µm size (fig 4.66). Irregular shape of the particles is visible as a water atomized powder is used as base powder for the Somaloy 500.

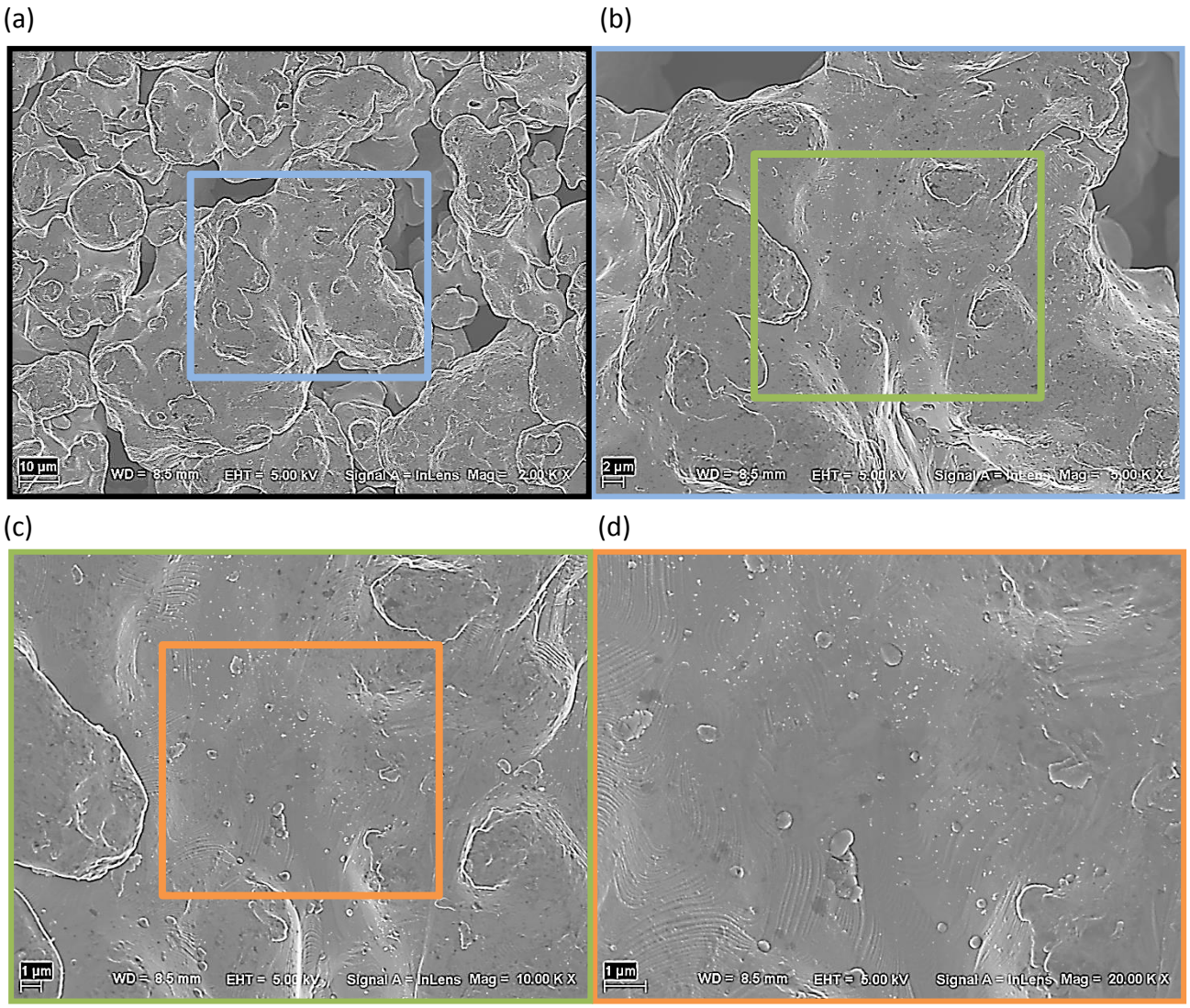

Figure 4.68: Overview of the Somaloy powder.

The EDX examination showed that the particulates on the surface contain aluminum and silicon. The rest of the analysis sites revealed the expected iron, oxygen phosphorous (Fig 4.69). Carbon again is present on the surface as contamination (hydrocarbon species).

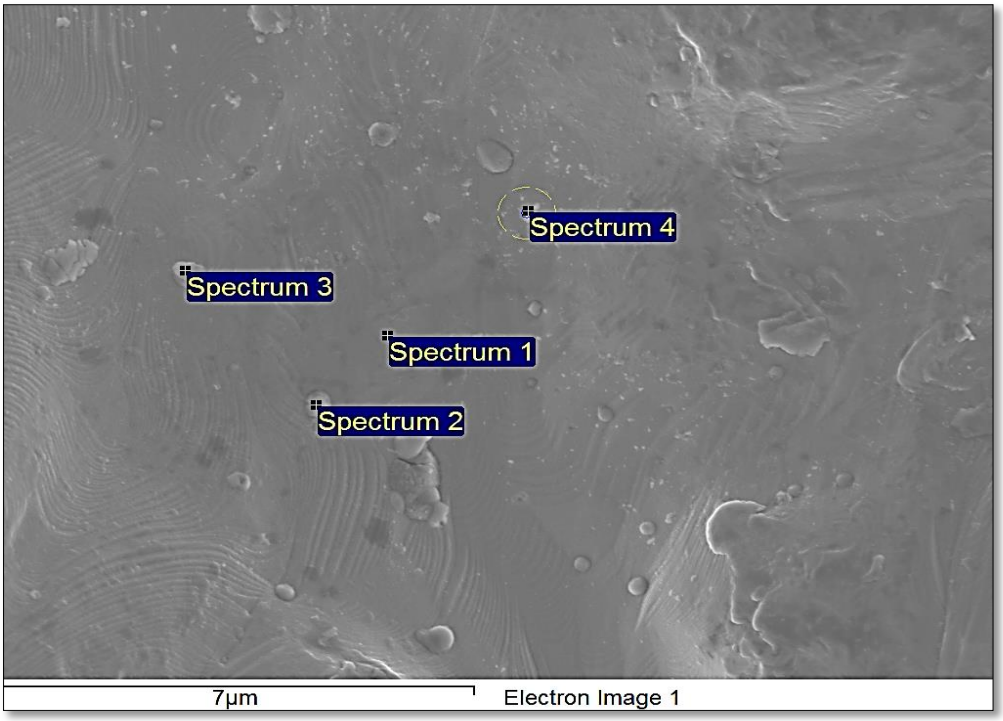

Spectrum[at%]	C	O	Al	Si	P	Fe
Spectrum 1	6.5	7.7	-	-	-	85.8
Spectrum 2	4.2	53.3	1.6	10.6	1.5	29.8
Spectrum 3	6.8	14.5	-	-	1.2	77.5
Spectrum 4	6.8	10	-	--	1.3	81.9

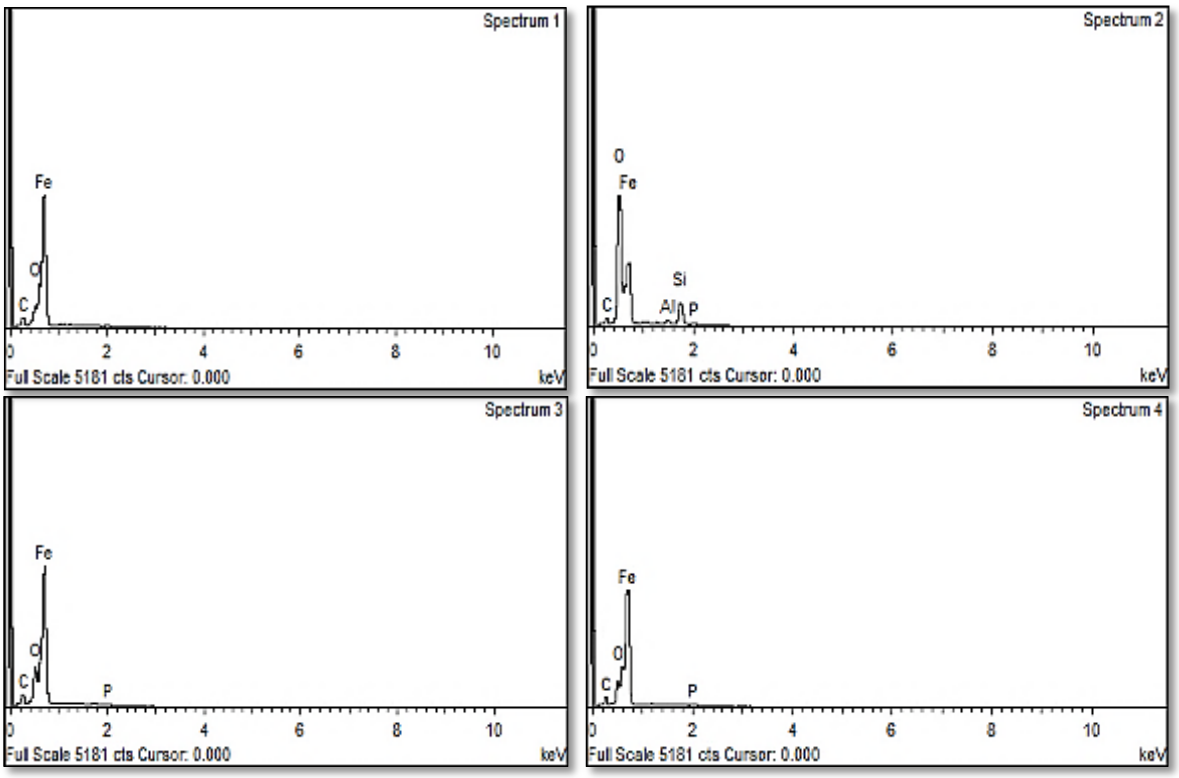

Figure 4.69: SEM image of the powder surface and results of the EDX measurements.

SEM and EDX of the powder fractions

Below appear the SEM images of the Somaloy 500 fractions. Similar surface characteristics are apparent for all fractions. Smooth surface is obvious with only the evaporation lines from the solidification process visible and some few particulates present.

- +106µm

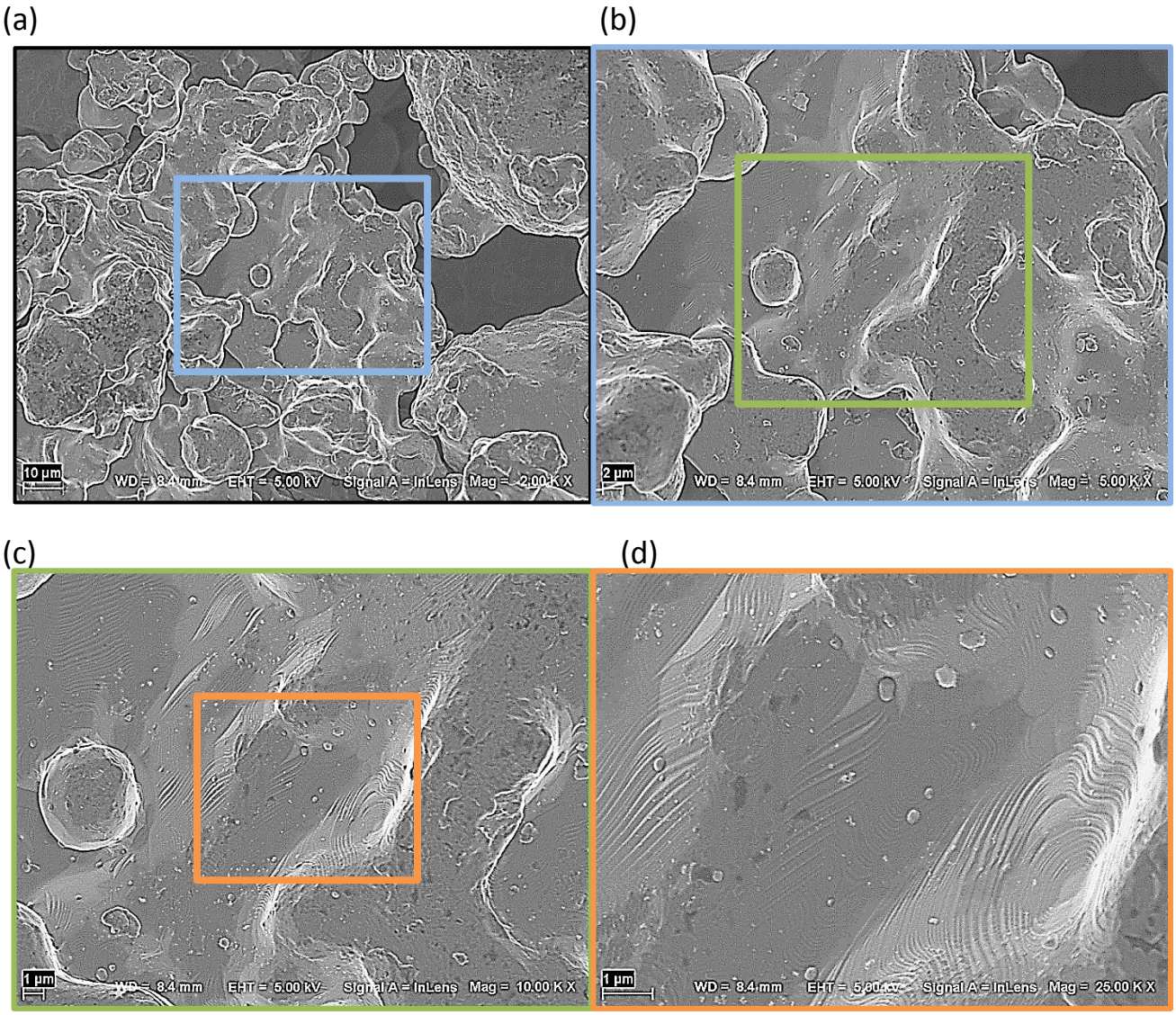

Figure 4.70: Overview of the Somaloy powder, +106µm fraction.

- -106/+53µm

(a) (b)

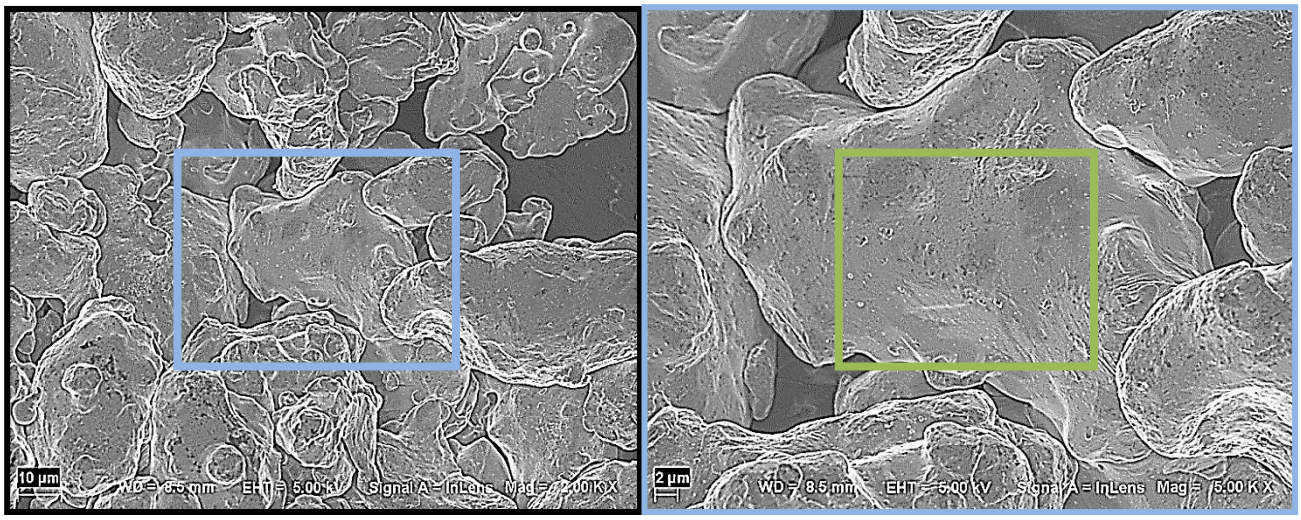

(c) (d)

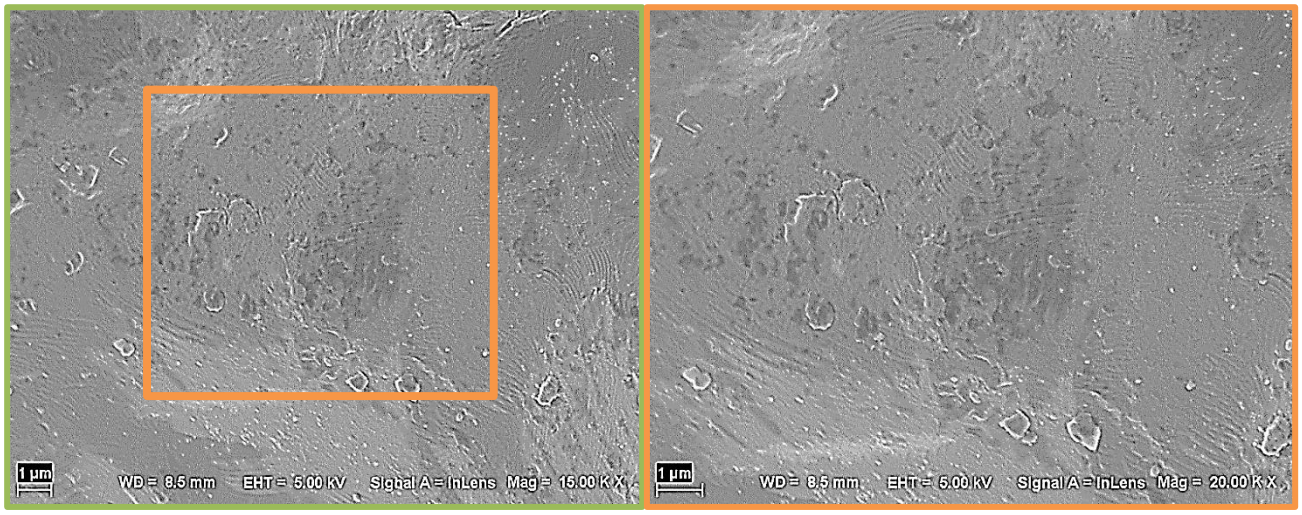

Figure 4.71: Overview of the Somaloy powder, -106/+53µm fraction.

- -53µm

(a) (b)

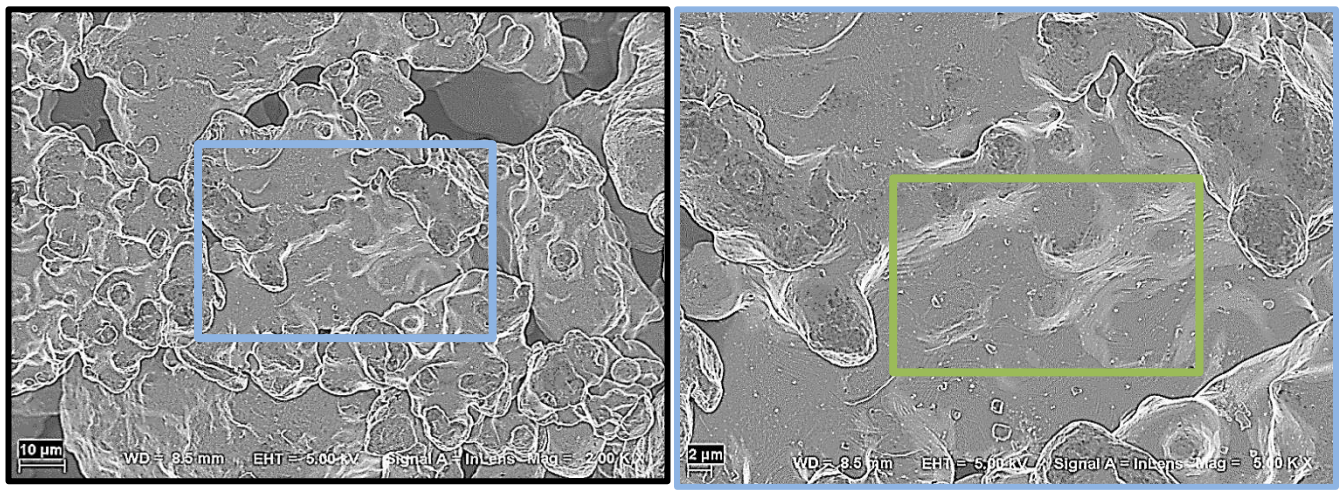

(c) (d)

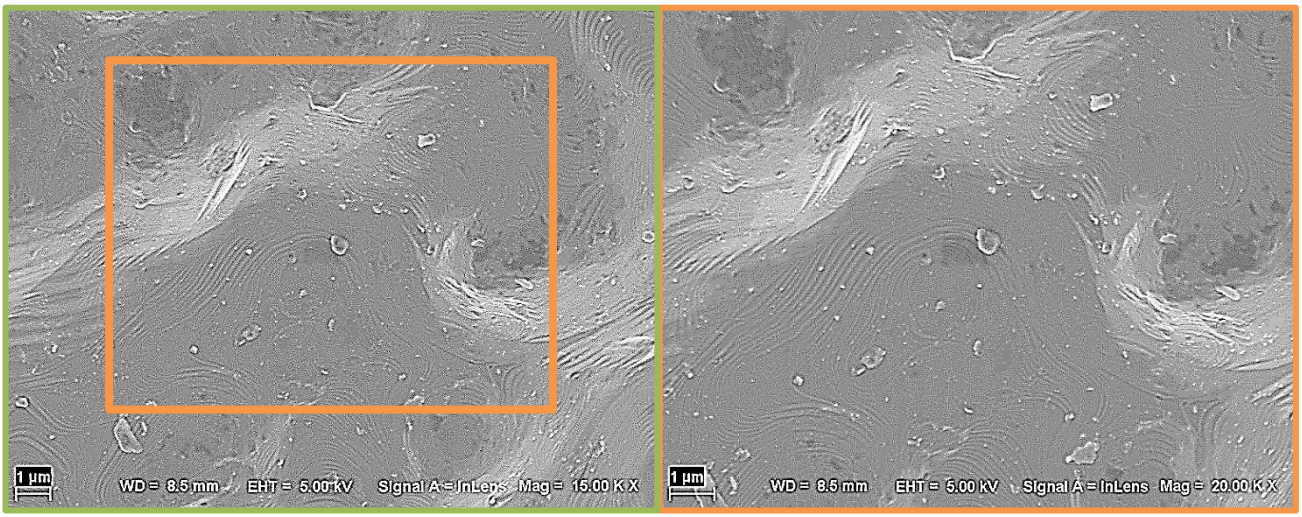

Figure 4.71 Overview of the Somaloy powder, -53µm fraction.

Another feature that appeared in specific sites of this powder is shown in figure 4.72. A high concentration of flaky type particulates is visible.

Figure 4.72: SEM image of Somaloy 500 powder on a flaky particulates site.

EDX analysis on this showed particulates enriched in silicon, aluminum and manganese as well as clear sites with iron, oxygen and phosphorous concentration (fig 4.74).the signal in the spectra appear low due to the low accelerating voltage used but voltage is enough to excite the X-rays from the elements expected.

Examination of the flaky particulates is shown on fig 4.73. Phosphorous signal is much higher than areas around this spot so it is assumed that these particulates are part of the phosphate coating.

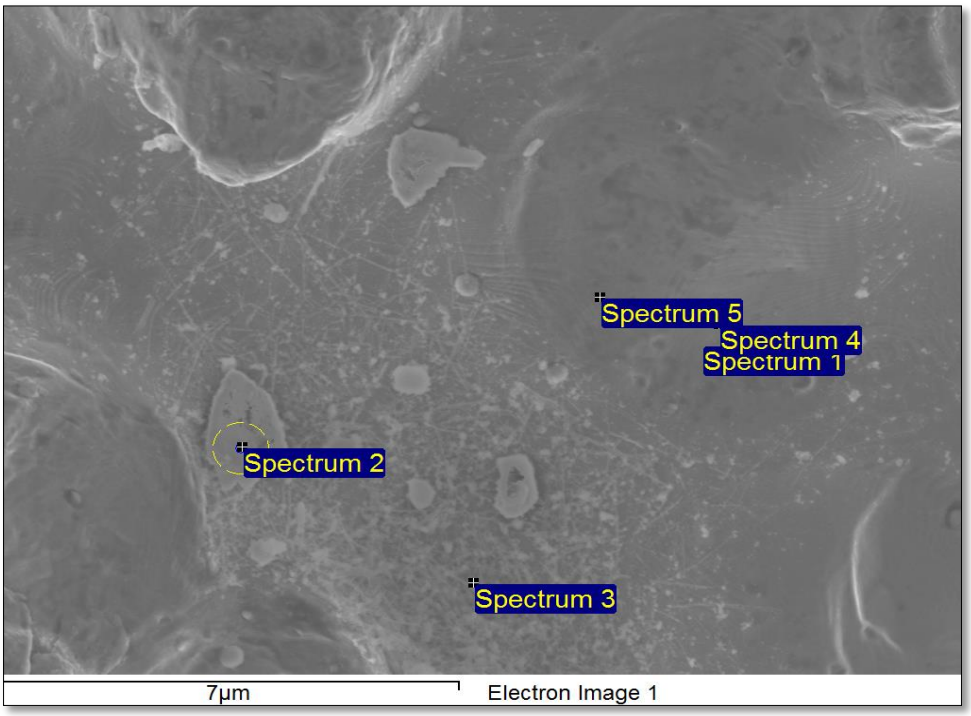

Spectrum[at%]	C	O	Mg	Si	P	Ca	Mn	Fe
Spectrum 1	2.1	60.3	3.4	10.5	0.6	10	13.1	-
Spectrum 2	5	21	-	-	1.7	-	-	72.3
Spectrum 3	4.6	18.1	-	-	3.7	-	-	73.4
Spectrum 4	21.5	25.3	-	-	5.1	-	-	48.1
Spectrum 5	18.2	8.8	-	-	1.8	-	-	71.20

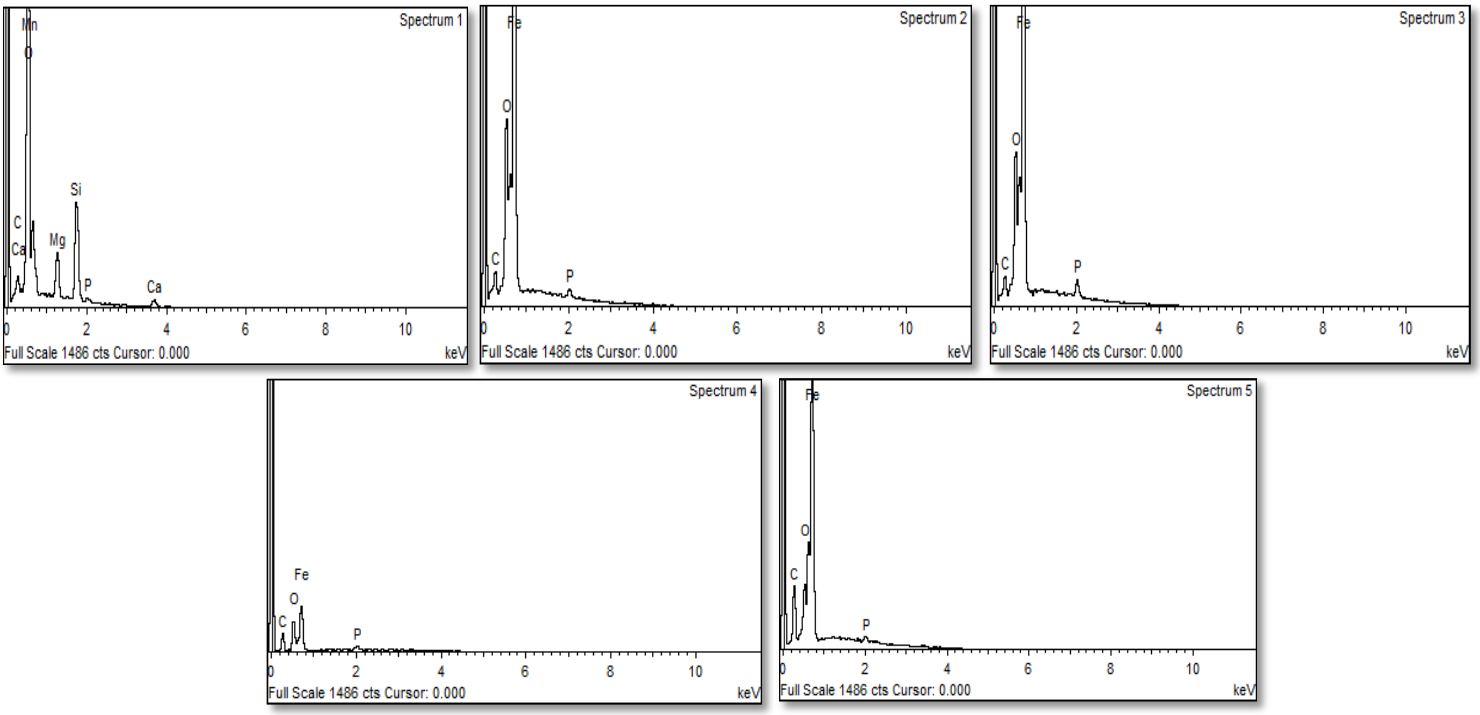

Figure 4.73 SEM image of the powder surface and results of the EDX measurements.

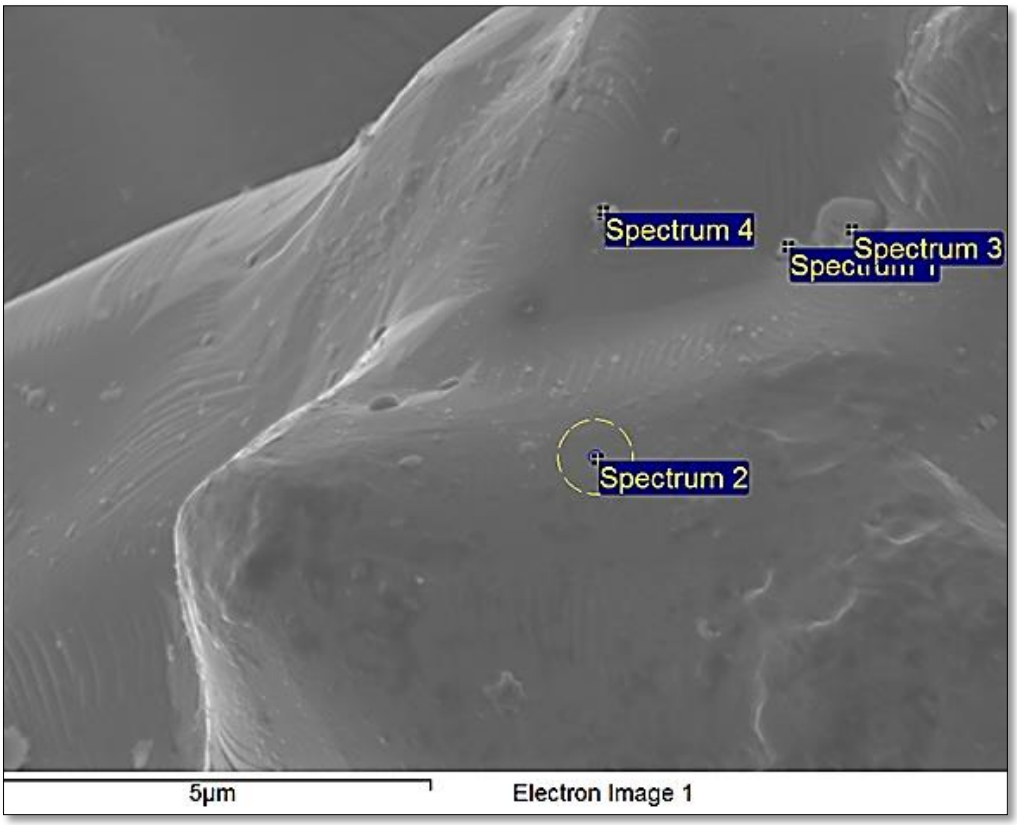

Spectrum[at%]	C	O	Al	Si	P	Mn	Fe
Spectrum 1	7.8	71	1.6	-	1.5	-	18.1
Spectrum 2	33.4	5.8	-	-	-	-	60.9
Spectrum 3	8	49.2	-	6.5	3.3	22.4	10.6
Spectrum 4	7	23	-	-	4.5	-	65.7

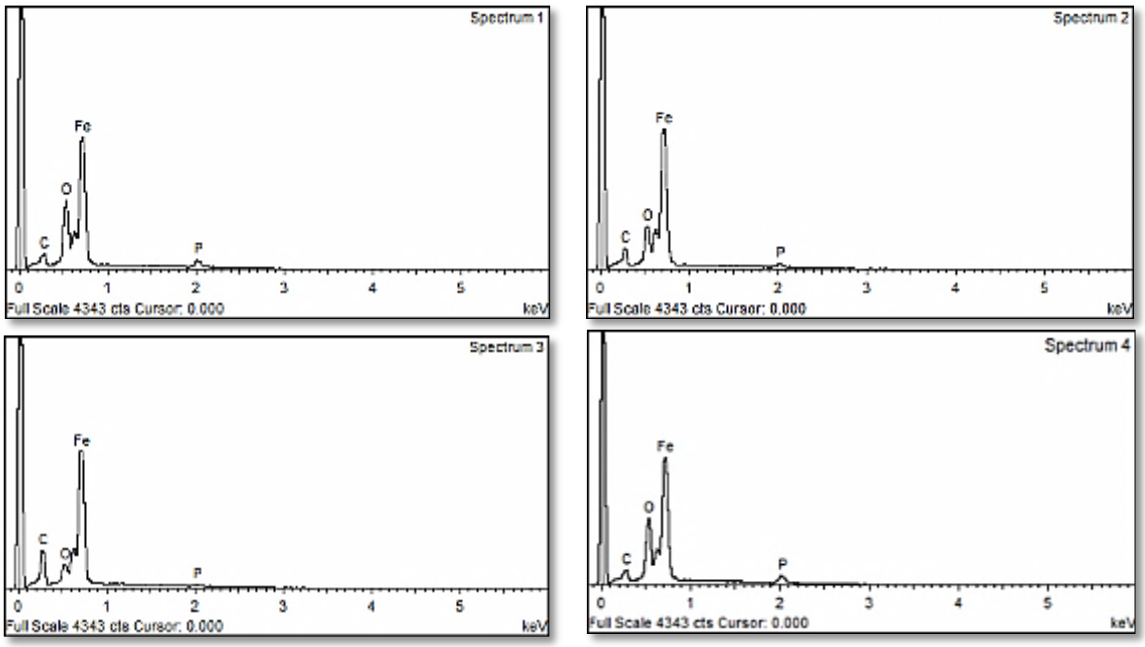

Figure 4.74: SEM image of the powder surface and results of the EDX measurements.

Chapter 5

Discussion

5.1 Pure iron powders and standards

For a valid characterization of a material using XPS, good reference values for peak positions are necessary. Such can be obtained from analyses of chemical standards fabricated with well characterized and known techniques. For this purpose, the oxides and phosphates were examined during this thesis work in order to establish the peak positions and peak characteristics such as peak width and peak shape asymmetry of the XPS signals by compounds of interest. Furthermore, the ion etching technique is used in order to acquire compositional depth profiles, and by means of which the surface layer thickness is also estimated. Here, the analysis of the chemical standards also provides information on their behavior under etching. Additionally, from the flat foil samples that were prepared accordingly to match the elemental composition for given surfaces of interest it is also possible to acquire the precise etch rate for specific compounds provided their thickness is controlled and pre-known.
The results from the analyses showed that the two types of iron oxides that were examined are in agreement with reference values in literature (Figures 4.2 and 4.6)[24,27]. Although there was prominent charging for the case of Fe_2O_3 standard, the charge correction was correct as the oxide peak value was similar to the one obtained from the Fe_3O_4 which was not charging and according to the XRD analyses both of these standards had expected compounds as major constituents (Figures 4.4 and 4.7). From the analyses on the chemical iron standards it was also shown that after extensive ion etching a progression of the initial oxidized state of iron to lower state is taking place and signal on the metallic iron position is also emerging and stabilizing at a fixed ratio with respect to the oxide state (Figures 5.1 and 4.3). This result is an artifact of the ion etching and should not be considered as actual presence of pure metallic iron in the oxide sample.

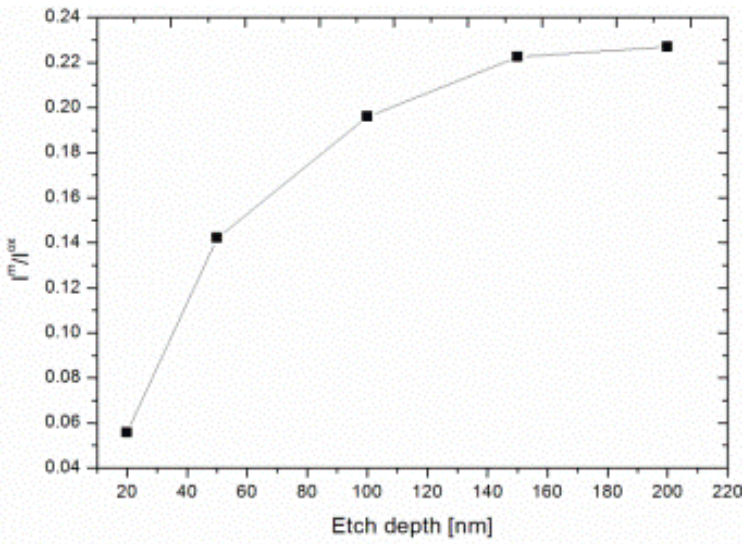

$$\frac{I^m}{I^{ox}} \approx 0.22$$

Figure 5.1: Oxidized vs metallic state of iron with etch depth.

Analysis on the iron foil showed that the iron oxide surface layer is 2.54 nm thick, taking into account the etch rate calibration with Ta_2O_5, (Figure 4.12) based on the iron metal normalized signal. This layer thickness is in the range expected for Fe-oxide formed at room temperature. The chemical compositional profile indicated the presence of manganese thick oxide particles (Figure 4.9) which were not removed entirely by the etching process, assuming that they are thicker and distributed within a uniform iron oxide layer.

The analysis of the ABC100.30 water atomized powder showed that the surface and its compositional depth profiles resemble the ones acquired from the heat treated iron foil. This is implies that all information extracted from the analysis of the latter can be used for the characterization of the water atomized powder as well. The estimation of the surface oxide layer thickness was given by the iron relative signal. Under the annealing treatment of the powder to reduce the oxide layer from its production, the impurity elements such as manganese diffuse on the surface and form oxide particulates as shown in the SEM and EDX analysis. These particulates contribute to the total oxide on the surface.

The XPS analysis of the ABC100.30 showed that in the as-received state there is a slightly greater oxide thickness shown from the depth profiling compared to that for fractioned powder samples. This could be due to the fact that the unsieved powder has a great difference in the particle size distribution which ranges from a few microns to 200 µm. This can cause shading effects during the XPS analysis because of the geometry of the experimental arrangement, since the ion beam cannot etch the entire oxide layer and thus more oxide contribution is obtained after ion etching (Fig 5.2).

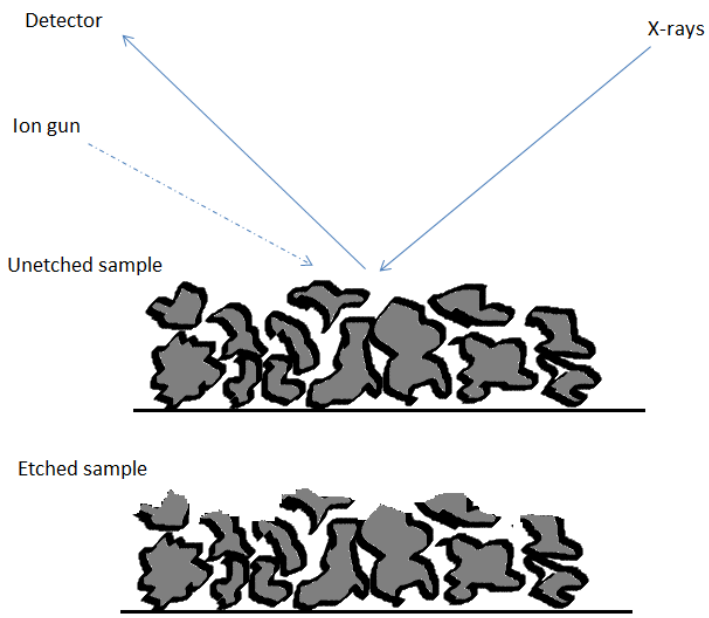

Figure 5.2: XPS geometry and possible shadowing effect.

Results from the analyses on the sieved fractions for this powder are very close to one another, indicating that when a narrower particle size distribution is examined the deviation is minimal. Furthermore, it is shown that the surface layer thickness is independent of the particle size, which is in accordance to the theoretical model [17], while the degree of shape irregularity and surface roughness of the ABC100.30 is also consistent along its size fractions.

XPS analysis of the gas atomized powder in the as-received state showed thicker oxide layer. The large size particles (+106µm) appear to have thinner oxide (12.32nm) than the other two with the middle fraction having the thickest (14.65nm).
The SEM and EDX analysis of the pure iron gas atomized powder in the as received state showed the presence of inhomogeneous surface characteristics. The presence of certain amount of more oxidized powder particles (Figure 4.37) is expected to give an overestimation of the oxide layer thickness for all samples. For this reason an annealing treatment was performed and as shown later from subsequent imaging and chemical microanalysis on the annealed gas atomized powder, this gave a much more homogeneous surface which mainly consists of only an iron oxide layer and some dispersed particulates of silicon and manganese oxides (Figure 4.50).
The XPS analysis of the annealed gas atomized powder, as seen from the normalized iron intensities and from the thickness determination method, has shown that the large size particles (+106µm) appear to have thinner oxide layer as compared to the other two fractions (Figure 4.44 and 4.45). This could be explained using the previous argument from the un-sieved ABC100.30 powder as compared to its sieved fractions. A wider particle size distribution on the sample can lead to overestimation of the true layer thickness. This can also be seen in Figure 4.36 that for the large size fraction the sample has a more homogeneous surface while for the other two fractions a rougher surface is evident with a wider particle size distribution available for analysis. This concept is also portrayed in Figure 5.3 where a theoretical narrow distribution of spherical particles is compared against a wider one. The line above the particles indicates the surface roughness profile and the dashed line the theoretical flat surface

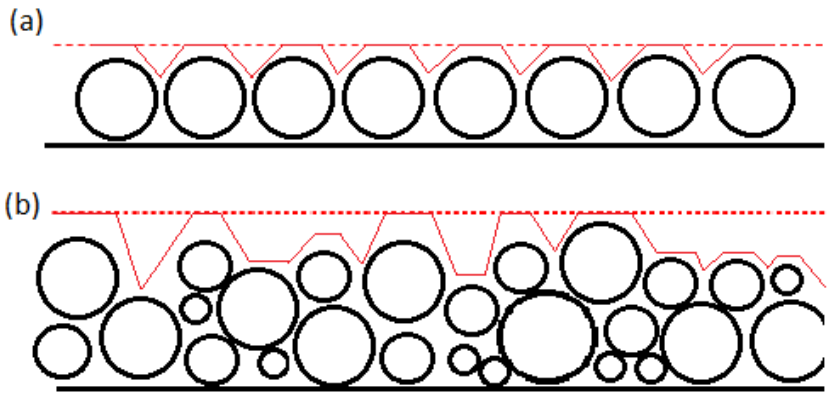

Figure 5.3: Particle size distribution in the large size fraction of the annealed gas atomized (a) and in the other two (b).

The middle fraction appears to have the thickest oxide layer compared to the other two. This could be explained with the above argument as the middle size fraction has a wider particle size distribution than the other two and thus shading effects are more prone to occur for this fraction

5.2 Somaloy powder and phosphate standards

The XPS analysis of the phosphated iron foil showed that the surface layer consists of an iron phosphate compound which shows a sharp substrate interface when examining the relative intensities of the iron and phosphorus signal. The chemical state of the surface layer of the phosphated iron foil, based on the peak values of iron and phosphorus, is in agreement with the iron phosphate dihydrate chemical standard (Figure 4.51) and close to the dehydrated phosphate (Figure 4.54) and literature data [11]. Here, it is shown that it consists of a XRD amorphous or very fine crystallized iron

phosphate compound and the iron is present in a mixture of ferrous and ferric states. The thickness of the surface layer was determined at the 50% of the relative P intensity 3.7 nm

From the SMC powder XPS analysis the chemical state and thickness of the surface insulating layer were determined for both un-sieved and sieved fractions. As for the case of the phosphated plate the peak position values for phosphorus and iron are in agreement with the standards tested showing again the presence of XRD amorphous iron phosphate in ferric and ferrous states. Additionally, the chemical compositional profile for this grade in combination with the chemical microanalysis of the EDX layer showed similarities with the ABC100.30 (Table 13) indicating the presence of a thin iron based oxide layer and dispersed oxide particulates. Furthermore, the oxygen signals from the SMC powder indicate the presence of more than one compound in the surface layer (Figure 4.64). From the curve fittings of the oxygen signals for different etch depths using reference values from the analyzed standards it can be concluded that the layer is a complex mixture of iron phosphate and iron oxide in ferrous and ferric states. These results indicate that the relative intensity of the phosphorous signal should be used in order to determine the thickness of the phosphate coating at the 50-55% of its value. Moreover, the metallic iron relative intensity at 65%, according to the theoretical model, and oxygen relative intensity at 50% are in agreement and determine the whole complex surface layer thickness.

Based on these results, the phosphate coating is in the range of 7 to 8 nm for all sieved fractions of the SMC powder, much more than the one on the iron plate as expected due to the difference in specific surface area between those two samples. Based on the arguments though created earlier for the thickness of the homogeneous surface layers for the water atomized iron powder fractions, one would expect that surface layer on the SMC fractions would all follow the same trend and have similar values if they were coated in a homogeneous manner. Conversely, the smaller size fraction has the lowest thickness and the coarsest one the highest estimated both by phosphorus or iron signal (Figure 4.67). Also, the un-sieved SMC sample shows lower thickness value only to the coarsest size fractions when taking into account the phosphorus signal while it shows higher values only for the smaller size fraction based on the iron signal (Figure 4.65).These findings can be interpreted based on the effect of the phosphating process. Shorter of time of the phosphating process would mean that the oxide layer cannot be totally reduced as is suggested from the phosphating theory kinetics and would form a thin amorphous type of compound. With that in mind the phosphoric acid removes some of the oxide layer but then the coating starts to grow on top of it.

If it is assumed that the SMC base powder is a similar to ABC100.30 then the values of the oxide thickness match the above suggestion. For example the oxide thickness calculated for the ABC100.30 powder was ~ 6 nm. A small part of this oxide layer is removed during the phosphating process and then the coating grows on top of what is left which is given from the phosphorous intensity (~ 6-7 nm again). Thus the total layer thickness given from the iron intensity should be around 10-12 nm (in this case 11nm). The above can be also explained by the phosphating process factors that cause the powder to oxidize.

The SEM and EDX analysis of the SMC grade showed highest intensity of the phosphate coating at places of high degree of irregularity on a powder particle at regions with concave surface (Figure 4.72) while in more convex type of regions the coating thickness is smaller (Figure 4.74, spectrum 5). Additionally, the larger size particles exhibit a more irregular shape than the finer ones. Hence, difference in the coating

thickness with increasing particle size can be expected as well as the intermediate value of the un-sieved fraction between the finer size and the rest (Figure 5.4)

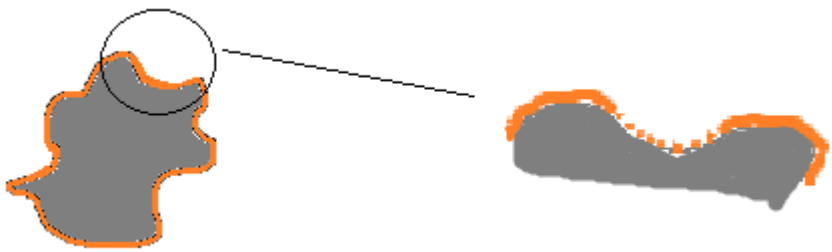

Figure 5.4: Schematic of phosphate concentration in different areas of a particle.

Moreover, with the SEM and EDX analyses it was observed that high concentration of the iron phosphate compounds in the concave regions appear as flaky particulates or small crystals in the nanometer scale (Figure 4.72). This can be explained by the fact that during the phosphating process the solution has a better flow in convex areas than concave ones where it is formed as flaky particulates.

Another explanation could be that these particulates are a result of the handling process of the powder during sample preparation and thus a more thorough investigation of this effect should be performed

Overall the present work compliments the theoretical model for calculating this type of layers with experimental data. It also provides with a good basis for characterizing such types of powder and estimating the coating thickness.

Chapter 6

Conclusions and future work

In the present study a standard and robust analysis method was developed for characterizing insulating layers on metal powder, SMC powder by means of X-ray photoelectron spectroscopy(XPS). For a valid and accurate analysis of such surfaces, chemical standards were acquired and analyzed. Iron oxides were examined and their main peak contributions were identified. An interesting observation here was the fact that after excessive ion etching a signal on the metallic iron position is emerging and stabilizes at a fixed ratio with respect to the oxide state. This result is an artifact of the ion etching technique and should not be considered as actual presence of pure metallic iron. Examination of an annealed pure iron foil provided the necessary data for the metallic iron peak determination.

The analysis of the water atomized iron powder showed that the surface and its depth compositional profiles resemble the ones acquired for the heat treated iron foil. The powder has a clean surface with only some small particulates on the surface. The XPS analysis showed that in the as-received state there is a higher apparent contribution of oxide thickness than when it is fractioned due to the fact that the unsieved powder has a great difference in the particle size and this can cause a lot of shading effects during the XPS analysis because of the geometrical characteristics of the experimental arrangement.

The XPS analysis of the gas atomized powder in as-received state showed a thick oxide layer due to the presence of heavily oxidized powder particles and for this reason an annealing treatment was performed. For the annealed gas atomized powder the normalized iron intensities versus etch depth gave the thicknesses of the oxide layer. The results show that the large size particles (+106µm) appear to have somewhat thinner oxide layer as compared to the other two fractions. This could be explained using the previous argument from the un-sieved water atomized powder as compared to its sieved fractions. A wider particle size distribution of the sample can lead to overestimation of the oxide layer thickness.

Phosphate standards and a phosphated iron foil were examined in order to establish references to compare with the elements of the coating of the metal powder. The chemical state of the surface layer of the phosphated iron foil, based on the peak values of iron and phosphorous, is in agreement with the iron phosphate dihydrate chemical standard and close to the dehydrated phosphate.

From the SMC powder XPS analysis, the chemical state and thickness of the surface layer were determined for both un-sieved and sieved powder fractions whereby the contribution to thickness from the phosphate layer and the Fe-oxide could be shown. These findings can be interpreted as the effect of the phosphating process or the sample preparation of the powder samples.

Future work

- Auger electron spectroscopy (AES)

The interest here is to determine the homogeneity of the coating and its thickness using point analysis. Also etch rate of the iron oxide for fixed as well as varying angle of ion incidence could be achieved and thus provide more accurate thickness calculation in XPS.

- Narrower particle size distribution in fractions

By choosing more sieve sizes a more narrow size distribution in each fraction could be achieved and thus more accurate determination of the effect of surface roughness could be obtained.

- Ion etching angle dependence in XPS

The theoretical model of calculating oxide and layer coatings is also affected by the angle between the normal to the surface under consideration and the ion incident beam. By measuring a flat sample in XPS and progressively changing the angle this dependence could be estimated experimentally as well.

References

[1] **German, Randall M.** *Powder Metallurgy Science.* New Jersey : Metal Powder Industries Federation, 1984.

[2] **Association, European Powder Mettalurgy.** *EPMA.* [Online] http://www.epma.com/New_non_members/intro-home.htm.

[3] **AB, Hoganas.** *hoganas.* [Online] http://hoganas.com/en/Segments/PM-Components/Downloads/Handbooks/.

[4] **Werner Schatt,Klaus-Peter Wieters.** *Powder Metallurgy-Processing and Materials.* Shrewsberry : European Powder Mettalurgy Association, 1997.

[5] **Aerospace, GKN.** *gkn.* [Online] http://www.gkn.com/hoeganaes/media/Pages/product_data_sheets.aspx.

[6] *Soft magnetic composite materials (SMCs).* **H. Shokrollahi, K. Janghorban.** Shiraz,Iran : Journal of Materials Processing Technology, 2007, Vol. 189.

[7] **Wagner, Johanna M.** *X-ray Photoelectron Spectroscopy.* New York : Nova science publishers, 2011.

[8] **D Briggs, M.P. Seah.** *Practical surface analysis,Vol 1,Auger and X-ray photoelectron spectroscopy.* West Sussex,England : John willey & sons Ltd, 1983.

[9] **John F Watts, John Wolstenholme.** *An introduction to surface analysis by XPS and AES.* West Sussex,England : John Wiley & Sons Ltd, 2003.

[10] **Olefjord, I.** *Surface characterization by XPS.* Goteborg : Department of Engineering Metals,Chalmers Univeristy of Technology.

[11] *Phosphating of bulk a-iron and its oxidation resistance at 400 C.* **S. Rebeyrat, J.L. Grosseau-Poussara, J.F. Silvain, B. Panicaud, J.F. Dinhut.** Bordeaux : Applied Surface Science, 2002, Vol. 199.

[12] **Dr. Dmitri Kopeliovich .** Substances and technologies. *SubsTech.* [Online] http://www.substech.com/dokuwiki/doku.php?id=phosphate_coating.

[13] *Properties of iron-based soft magnetic composite with iron phosphate–silane insulation coating.* **A.H. Taghvaei, H. Shokrollahi, K. Janghorbana.** Department of Materials Science and Engineering, Engineering School, Shiraz University, Shiraz, Iran : Journal of Alloys and Compounds, 2009, Vol. 481.

[14] *Surface pretreatment.* [Online] http://www.surfacepretreatment.com/default.asp?id=2.

[15] *Effect of Zinc Phosphating on Corrosion Control for Carbon.* **Dr. Mohammed Hliyil Hafiz,Junan Sttar Kashan,Ali Shaker Kani.** 5, s.l. : Engineering and technology, 2008, Vol. 26.

[16] **Joseph I. Goldstein, Charles E. Lyman, Dale E. Newbury, Eric Lifshin, Patrick Echlin, Linda sawyer, David C. Joy, Joseph R. Michael.** *Scanning electron microscopy and X-ray microanalysis.* New York : LKluwer Academic/ Plenum publishers, 2003.

[17] *Thickness determination of oxide layers on Spherically-shaped metal powders by ESCA.* **L. Nyborg, A. Nulund, I. Olefjord.** 110-114, Göteborg : Surface and interface analysis, 1988, Vol. 12.

[18] *The influence of phosphate on repassivation of 304 stainless steel in neutral chloride solution.* **M.Lakatos-Varsanyi, F. Falkenberg, I. Olefjord.** 1-2, s.l. : Elsevier Science Ltd., 1997, Vol. 43.

[19] *Characterization of surface oxides on water-atomized steel powder By XPS/AES depth profiling and nano-scale lateral surface analysis.* **D.Chasoglou,E. Hryha, M. Norell, L. Nyborg.** Gothenburg : Elsevier, 2013, Vol. 218.

[20] **Barbaux Y., Dekiouk M., Le Maguer D., Gengembre L., Huchette D., and Grimblot J.** s.l. : Appl. Catalysis A 90, 1992, Vol. 51.

[21] *Phosphate Conversion Coatings, Corrosion Fundamentals, Testing, and Protection.* **K. Ogle, M. Wolpers.** p 712–719, s.l. : ASM Handbook, ASM International, 2003, Vol. 13A.
[22] *Kinetics of the phosphatizing reaction on carbonyl powders.* **Yu. G. Kir'yanov, T. A. Zavina,V.G Syrkin.**
[23] **Ewald, P. P.** *Fifty Years of X-Ray Diffraction.* Utrecht : s.n., 1962
[24] **Seyama H., Soma M.** 97 , s.l. : J. Electron Spectrosc. Relat. Phemon, 1987, Vol. 42.
[25] An XPS study of phosphate glasses. ***P.K Brow, C.M Arens, X. Yu, E.Day.*** *3, s.l. : Physics and chemistry of glasses, 1993, Vol. 35.*
[26] **Heal, G. R.** *Principles of Thermal Analysis and Calorimetry.* Salford : Peter Haines, 2002.
[27] *Studies of the oxidation of iron by air after being exposed to water vapour using angle-resolved x-ray photoelectron spectroscopy and QUASES.* **A. P. Grosvenor,B. A. Kobe, N. S. McIntyre.** London : SURFACE AND INTERFACE ANALYSIS, 2004, Vol. 36.
[28] *Investigation of multiplet splitting of Fe 2p XPS spectra and bonding in iron compounds.* **A. P. Grosvenor,B. A. Kobe, M. C. Biesinger and N. S. McIntyre.** London : SURFACE AND INTERFACE ANALYSIS, 2004, Vol. 36.